



**(1) Understanding the molecular role of NKG2D ligands in
lymphoid stress recognition in cancer**

**(2) Investigating neuroblastoma mediated
immunosuppression**

STUART HUNTER

A thesis submitted to the University of Birmingham
for the degree of
Master of Research (Molecular and Cellular Biology)

School of Biosciences

UNIVERSITY OF
BIRMINGHAM

University of Birmingham Research Archive

e-theses repository

This unpublished thesis/dissertation is copyright of the author and/or third parties. The intellectual property rights of the author or third parties in respect of this work are as defined by The Copyright Designs and Patents Act 1988 or as modified by any successor legislation.

Any use made of information contained in this thesis/dissertation must be in accordance with that legislation and must be properly acknowledged. Further distribution or reproduction in any format is prohibited without the permission of the copyright holder.



**Understanding the molecular role of NKG2D ligands in
lymphoid stress recognition in cancer**

STUART HUNTER

A thesis submitted to the University of Birmingham

for the degree of

Master of Research (Molecular and Cellular Biology)

**Supervisors: Prof. B. E. Willcox; Dr. F. Mohammed, School of Cancer
Sciences**

Understanding the molecular role of NKG2D ligands in lymphoid stress recognition in cancer

NKG2D is an activating immune receptor expressed on the surface of many lymphocytic cells. Upon binding of “stress ligands” that are expressed on the surface of transformed or infected cells, NKG2D can trigger destruction of the target cell. ULBP6 is one such stress ligand, and has been implicated in the variation in survival rates of patients that have undergone stem cell transplant (SCT) to treat haematopoietic malignancy. Patient genotype for the two most common ULBP6 alleles (*01 and *02) is associated with significantly different survival rates. To understand the molecular mechanism behind this difference, this study has conducted binding and structural investigation of the NKG2D-ULBP6 interaction. Firstly, binding affinities of NKG2D with ULBP6*01, ULBP6*02, and mutants that share one of the two amino acid variations between the two alleles were calculated using surface plasmon resonance experiments. Variation in the ULBP6-NKG2D binding affinity was attributed to a polymorphism in residue 86 of ULBP6. ULBP6*02, possessing a leucine at this position displayed a 13-fold increase in affinity. Secondly, crystallisation of the NKG2D-ULBP6*02 complex was performed in order to derive the structure from X-ray crystallography. This study has furthered understanding of the NKG2D-ULBP6 interaction and may lead to improvements in SCT protocols.

CONTENTS

INTRODUCTION	1
NK cells are part of the innate immune response.....	1
NK cell activation is dependent on inhibitory “missing self” and activating “stressed self” recognition.....	2
NKG2D is an activating receptor that mediates the “stressed self” response	5
The stressed-self response relies on the interaction of NKG2D with a family of MHC-like molecules.....	6
A number of challenges have been shown to upregulate NKG2D ligands, including DNA damage and other indicators of transformation.....	8
The clinical importance of NKG2D and its ligands.....	10
The NKG2D/ NKG2D ligand interaction is thought to affect the outcome of haematopoietic stem cell transplants conducted as a therapy of haematological malignancies.....	12
ULBP6 has been demonstrated to be of particular significance in this scenario, with some single nucleotide polymorphism alleles showing significantly improved RFS and OS over others.....	14
PROJECT AIMS	17
MATERIALS AND METHODS.....	18
ULBP6-NKG2D binding affinity experiments.....	18
Site directed mutagenesis (SDM) and analysis	18
Primer details	19
Transfection and culture of S2 Drosophila cells.....	20
Induction of protein expression and collection of supernatant.....	21
Purification of target proteins.....	22
Biotinylation of target proteins.....	22
Protein analysis (Western blot).....	23
Surface Plasmon Resonance.....	24
X-Ray Crystallography	24
Bacteria transformation	25
Protein expression.....	25

Inclusion body preparation	26
Inclusion body re-folding.....	27
Size exclusion chromatography.....	27
Anion-exchange chromatography	28
Protein analysis (SDS PAGE)	28
Protein crystallisation.....	29
X-ray diffraction data collection	29
RESULTS	31
Investigating the molecular mechanism for enhanced survival in patients with	
RAET1L*02 allele	31
Analysis of binding data for ULBP6*01 and ULBP6*02 with NKG2D	31
Identification of ULBP6*02 SDMs	33
Expression and purification of ULBP6*02 SDMs	34
Binding affinity studies of ULBP6 isoforms and mutants with NKG2D	37
Kinetic analysis of NKG2D-ULBP6 interaction	43
Solving the NKG2D-ULBP*02 complex structure using X-ray Crystallography	45
X-ray diffraction studies of NKG2D-ULBP6*02.....	45
Expression and purification of NKG2D	48
Expression and purification of ULBP6	50
NKG2D-ULBP6*02 crystallisation trials	53
DISCUSSION.....	55
REFERENCES	62

INTRODUCTION

1.1 NK cells are part of the innate immune response.

The innate immune response forms one layer of an elaborate system that has evolved to protect the body from invading pathogens and toxins. The first of these layers is the physical barrier, such as the skin and mucosal tissues that protect vulnerable interior tissue from harm. The second layer is formed by a non-specific innate line of defence. This includes anti-microbial enzymes such as lysozyme, anti-microbial peptides such as the defensins, and the action of the complement system, which helps to trigger the third layer, the induced innate immune response. Complement binding to a pathogen will “flag” it for destruction by phagocytes, which in turn initiate an inflammatory response. Inflammation recruits monocytes and dendritic cells, which through activation of their Toll-like receptors (TLRs) recruit a range of cytotoxic effector cells such as neutrophils, lymphocytes and natural killer (NK) cells. If the infection has not been cleared by this stage, these recruited cells will illicit the fourth and final layer of defence, the adaptive immune response, by generating cells capable of targeting specific pathogen and forming an immunological memory to the pathogen in case of repeat infection.

Both the innate and adaptive responses have the key ability to distinguish between self and non-self. In the innate response, this distinction is made by macrophage TLRs which bind to molecular patterns found in a wide range of common pathogen, including bacteria, viruses and fungi. These patterns are usually repeated structures found in components of the microbe not found in vertebrate cells, such as the bacterial cell wall or double-stranded RNA in viruses. In the adaptive response, B-cells and T-cells express receptors for a huge variety of specific antigens from many pathogens, and it is clonal selection and expansion of these

activated lymphocytes that drives the adaptive immune response upon antigen recognition. The extensive polymorphism in antigen-recognising receptors is generated by gene rearrangement, a somatic recombination event that occurs in developing lymphocytes.

NK cells are derived from the same progenitor cells as the B-cells and T-cells, and function in a similar manner to the cytotoxic T cell, releasing lytic enzymes that destroy target cells. However, antigen recognition in NK cells does not occur through receptors generated by gene rearrangement, but instead is performed by invariant, germ-line encoded receptors that recognise molecules expressed on the surface of damaged or infected cells. NK cells are recruited to the site of infection by IL-12 secreted by activated macrophages, and interferons such as IFN- α and IFN- β which are secreted by virally-infected cells. In this way, they form an innate immune response to intracellular pathogens in the same way that macrophages form part of the innate response to extracellular pathogens.

1.2 NK cell activation is dependent on inhibitory “missing self” and activating “stressed self” recognition.

Because NK cells target infected or damaged cells of the host organism and lack the fine specificity of lymphocyte antigen receptors, they need a method to distinguish between normal cells and infected cells to prevent unnecessary killing of healthy cells.

To prevent the targeting of healthy cells, NK cells are able to recognise naturally-expressed cell surface markers of the major-histocompatibility complex (MHC) class I molecule family, normally with a cytolytically inhibitory receptor, such as the killer cell immunoglobulin-like receptors (KIRs) (Borrego *et al*, 2002). MHC class I molecules are expressed on nearly all

healthy tissues, with the exception of erythrocytes. If a sufficient inhibitory signal is generated through the binding of inhibitory receptors to MHC class I molecules, the NK cell will not kill the target cell. However, if cell surface MHC molecule expression is reduced through the action of intracellular pathogens in an attempt to evade the T-cell mediated immune response, the cell is more likely to be eliminated by NK cell action – the so-called “missing self” paradigm (Cerwenka & Lanier, 2001).

NK cells (as well as other cells with similar roles, such as natural killer T cells, cytotoxic T cells and $\gamma\delta$ T cells) also display, to a varying degree, cell surface receptors that recognise ligands that tend to be up-regulated on the surface of infected or transformed cells (Diefenbach & Raulet, 2002). Binding of these ligands to the activating receptors triggers cytolytic activity and cytokine release which scales up the immune response towards the infected or damaged cells, and confers the ability of NK cells to recognise and eliminate “stressed-self”. Activating receptors in NK cells include immunoglobulin-like natural cytotoxicity receptors, e.g. Nkp44 and Nkp46, and the C-type lectin family member NKG2D.

In this way, a combination of activating signals from stress-generated ligand binding, balanced by the inhibitory signals from MHC molecule binding, determines whether the NK cell exhibits cytotoxic effector activity towards the target cell.

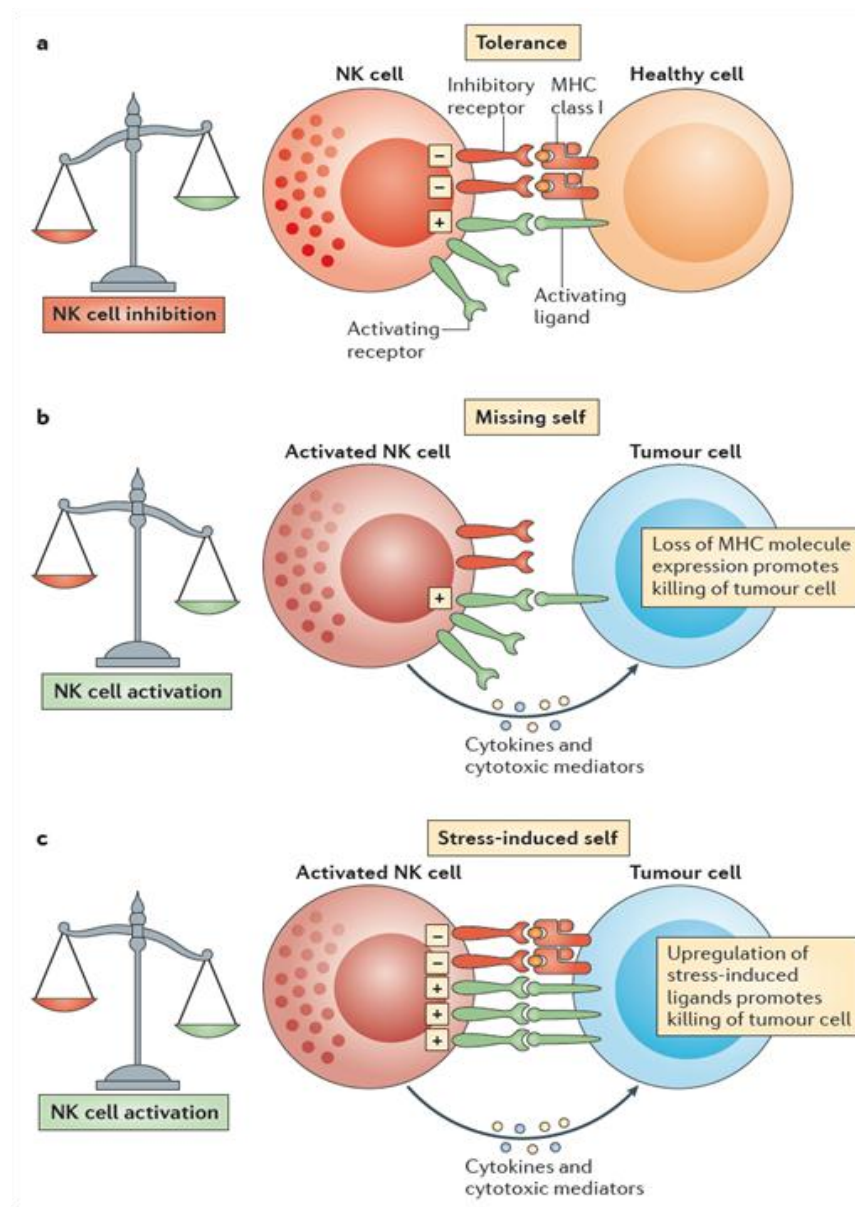


Figure 1.1: Tumour cell recognition by Natural Killer (NK) cells. (a) Engagement of inhibitory NK receptors by MHC class 1 molecules on the surface of healthy cells prevents NK activation. (b) Reduction in surface expression of MHC class 1 molecules in tumour cells triggers activation of NK cells – the “missing self” paradigm. (c) Over-expression of “stress ligands” on tumour cell surface leads to activation of NK cells through stimulation of activating receptors, such as NKG2D – the “stressed self” paradigm. (Taken from Vivier *et al*, 2012).

1.3 NKG2D is an activating receptor that mediates the “stressed self” response.

A prominent example of an activating receptor expressed in a variety of lymphocytes, including NKs (Bauer *et al*, 1999), CD8⁺ cytotoxic T cells (Upshaw & Leibsen, 2006) and $\gamma\delta$ T cells (Rincon-Orozco *et al*, 2005), is Natural Killer group 2, member D (NKG2D). This receptor is formed from a homodimer of proteins belonging to the C-type lectin-like family (Houchins *et al*, 1991). It is a transmembrane type II protein forming a hexameric structure consisting of the NKG2D dimer and four DAP10 adaptor proteins that associate with the transmembrane domain of the NKG2D monomers, in a similar manner to the T cell receptor (TCR)-CD3 complex (Gilfillan *et al*, 2002; Garrity *et al*, 2005). On activation of NKG2D by binding a complementary ligand, the intracellular YINM motif of DAP10 is phosphorylated, coupling the receptor/ ligand complex to the phosphatidylinositol-3-kinase (PI3K)/ Grb2 signalling pathway that in NK cells triggers cytotoxicity and IFN- γ production to instigate an inflammatory response (Wu *et al*, 1999; Chang *et al*, 1999; Upshaw *et al*, 2006). In cytotoxic CD8⁺ T cells, this mechanism provides a co-stimulatory effect (Groh *et al*, 2001), stimulating cytokine production but is insufficient to induce cytotoxicity without TCR engagement (Jamieson *et al*, 2002).

The cell surface expression of NKG2D depends on the external concentrations of numerous cytokines. IL-2 (Park *et al*, 2011), IL-12 (Zhang *et al*, 2008a), IL-15 (Becknell *et al*, 2005) and IFN α (Zhang *et al*, 2008b) have all been demonstrated to upregulate transcription of NKG2D, while transforming growth factor β (TGF β) (Espinoza *et al*, 2012) and INF γ (Zhang *et al*, 2008b) have been shown to reduce transcription of NKG2D and DAP10. A key element to the cell-surface regulation of NKG2D is the effect of chronic stimulation of the NKG2D receptor, either by cell surface-expressed ligand or soluble ligand in the extracellular matrix. Chronic stimulation leads to reduced expression of NKG2D through retention and

degradation within the cell, a mechanism exploited by tumour cells to avoid immunosurveillance by NK cells (Groh *et al*, 2002), which will be discussed further later.

1.4 The stressed-self response relies on the interaction of NKG2D with a family of MHC-like molecules.

The binding site of NKG2D displays remarkable flexibility and binds to a number of MHC molecule-like ligands (Radaev *et al*, 2001; Culpepper *et al*, 2011). In mice these ligands include the histocompatibility antigen 60 (H60) and the Rae1 family of proteins (Diefenbach *et al*, 2000; Cerwenka *et al*, 2000), encoded by the retinoic acid inducible early transcript gene family (*Rae1*). In humans, the NKG2D ligands discovered to date are the two MHC-class 1-polypeptide-related sequence A and B, and 6 cytomegalovirus UL-16-binding proteins (ULBP1-6), encoded by the human orthologue of the murine *Rae1* genes, RAET1 (Cosman *et al*, 2001) (Figure 1.2). MICA shares only 20-25% sequence homology with the ULBPs (Radosavljevic *et al*, 2002), and the structure of each varies fairly significantly from ligand to ligand, with some exhibiting transmembrane domains and others being anchored with a glycosylphosphatidylinositol domain. All exhibit an MHC-class-1-like $\alpha\beta$ extracellular domain that binds the NKG2D receptor (Groh *et al*, 1996). The genes encoding the NKG2D ligands are highly polymorphic, particularly MIC genes (Kasahara & Yoshida, 2012).

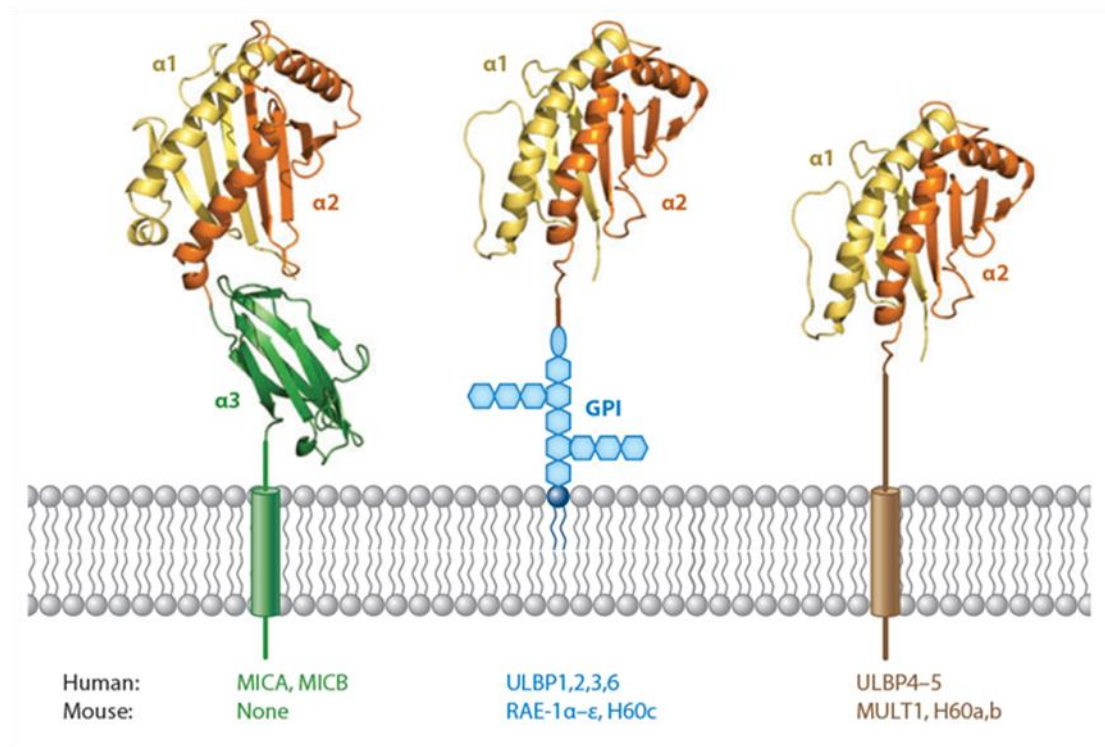


Figure 1.2: Structure of known NKG2D ligands. Cartoon diagram showing the structure of human and orthologous mouse NKG2D ligands (taken from Raulet *et al*, 2013).

It is likely that this diverse array of ligands has evolved as a defensive mechanism, allowing the host to counter viral immune evasion strategies, relying on the conformational plasticity of the NKG2D receptor to allow induced-fit binding of multiple ligands and propagate the cytotoxic immune response (Eagle & Trowsdale, 2007). The human cytomegalovirus (hCMV) produces a protein that binds to at least 3 of the known NKG2D ligands (Muller *et al*, 2010), sequestering them within the cell, preventing trafficking and cell surface expression which in turn renders the infected cell invisible to the activating receptors on circulating lymphocytes (Dunn *et al*, 2003; Bennett *et al*, 2010). This is an essential component of hCMV, as it also prevents cell surface expression of MHC Class I and II molecules on infected cells, which would protect the infected cells from T-cell mediated lysis, but not from NK-cell mediated attack, where “missing-self” will trigger the KIR to induce an immune response. The high

level of polymorphism found in some of the human NKG2D ligands, particularly MICA and ULBP 3, 4 and 6, may be a further mechanism employed in the arms race against viral infection (Fernandez-Messina *et al*, 2012).

1.5 A number of challenges have been shown to upregulate NKG2D ligands, including DNA damage and other indicators of transformation.

NKG2D ligand expression is regulated at many cellular levels, including transcription, mRNA degradation and post-translational sequestration, shedding and protein modifications (Champsaur & Lanier, 2010). Unsurprisingly, this regulation occurs through many pathways, which vary in importance depending on the ligand concerned (Raulet *et al*, 2013). Several transcription factors, including the E2F family (Jung *et al*, 2012), p53 (Textor *et al*, 2011) and NF- κ B (Molinero *et al*, 2004) have been demonstrated to affect NKG2D ligand transcription, as well as the heat shock pathway (Groh *et al*, 1996), indicating cell proliferation and the heat shock stress pathway has an effect of NKG2D ligand expression.

The DNA damage pathway regulates NKG2D ligands via the Ataxia telangiectasia mutated (ATM)/ Ataxia telangiectasia and Rad3 related (ATR) response (Gasser *et al*, 2005), which promotes stabilisation of NKG2D ligand mRNA, via a mechanism that is poorly understood. This is important, as it is believed that lymphocytes expressing NKG2D have a key role in the immunosurveillance of tumour cells, and DNA damage is often a critical step of tumour formation.

Oncogenes and tumour suppressor genes have been demonstrated to affect NKG2D ligand production in the case of MICA (Liu *et al*, 2012), but expression of oncogenes such as *K-Ras* and *c-myc* is insufficient to induce significant NKG2D ligand expression in ovarian epithelial

cells (REFS). Therefore it is likely that transformation in and of itself is not sufficient to induce the “stressed self” NKG2D-mediated response. One study has shown that expression of an adenovirus oncogene, E1A, upregulates NKG2D ligands in mice (Routes *et al*, 2005).

An additional mechanism by which stress responses lead to increased NKG2D ligand expression is through decreasing the amount of ubiquitination of transmembrane ligands such as MICA or the murine MULT1, leading to decreased intracellular degradation of the protein (Nice *et al*, 2009).

Several micro-RNAs have also been demonstrated to affect NKG2D ligand expression through enhanced degradation of ligand mRNA (Stern-Ginossar *et al*, 2008), although it is likely that these contribute to the regulation of NKG2D ligand expression in healthy cells. NKG2D ligands have been shown to be displayed on the surface of healthy cells, including T-cells and macrophages, where it is hypothesised they have a role in down-modulating an immune response (Eagle *et al*, 2009a). Indeed, NKG2D ligands are expressed in a wide variety of different tissues, suggesting NKG2D has a role beyond simply recognising stressed self. The precise nature of these roles is likely to be defined by a combination of signals in the tissue microenvironment.

Taken as a whole, these findings suggest that cells are likely to express NKG2D ligands when undergoing hyper-proliferation, heat shock stress pathway induction and/ or the DNA damage repair pathway, in addition to the presence of oncogenes within the cell. All of these events occur to greater or lesser in extent in cells undergoing transformation.

Research has indeed found that a large variety of primary tumours and tumour-derived cell lines express NKG2D ligands (Nausch & Cerwenka, 2008), although the actual ligands

expressed depends on the location of the tissue/ tumour, the pathway of cellular stress involved and the cytokine cocktail present in the microenvironment.

These findings suggest a mechanism by which the immune system surveys and eliminates nascent malignancies, thereby preventing the development of a significant number of tumours. The system is far from perfect however, as cancers can avoid detection and elimination by NKG2D-mediated NK or T-cell attack by several mechanisms. Shedding of soluble NKG2D ligands from the cell surface of transformed cells into the blood serves to downregulate the expression of NKG2D on NK and T-cells surfaces (Song *et al*, 2006; Cao *et al*, 2007), as well as reducing the likelihood that the tumour cell will be targeted by these cells. Cancer cells have been shown to upregulate matrix metalloproteinases (MMPs) (Waldhauer *et al*, 2008), as well as endoplasmic reticulum protein 5 (ERP5) (Jinushi *et al*, 2008), which both serve to increase proteolytic cleavage of ligand extracellular domains. In addition, transformed cells can also secrete TGF, which, as mentioned earlier, downregulates lymphocyte expression of NKG2D (Lee *et al*, 2004).

Different types of cancer tend to exhibit altered patterns of NKG2D ligand expression, potentially due to either differential immunoediting or variation in stress-response pathways triggered by different cancers. It is hypothesised that having multiple NKG2D ligands may help prevent cancer immunoediting and loss of the NKG2D-mediated anti-tumour response.

1.6 The clinical importance of NKG2D and its ligands.

It has long been established that immunocompromised individuals have a higher than usual incidence of developing malignancies (Gatti & Good, 1971), and although a large proportion of these malignancies are virally-associated, the evidence presented above has seen a re-

emergence of the once marginalised tumour immunosurveillance theory (Raulet & Guerra, 2008). Studies over the last 15 years have gone a long way to defining the role of the NKG2D receptor in tumour immunosurveillance (Nausch & Cerwenka, 2008).

Early studies showed that NKG2D/ NKG2D-ligand engagement stimulates NK, CD8⁺ T cells and $\gamma\delta$ T cell cytotoxicity towards transfectant and epithelial tumour cells (Bauer *et al*, 1999). Tumour cells expressing murine RAE-1 ligands are still eliminated by NK cells, despite tumour expression of MHC class I self antigens (Cerwenka *et al*, 2001). This demonstrates the potential role of NK cells in the immune response to transformed self-tissue and confirmed that NKG2D-expressing lymphocytes have the capability of destroying tumour cells.

NKG2D⁺ KLRG1⁺ CD11c⁺ CD8⁺ T cells preferentially infiltrate into tumour tissue and inhibit tumour growth (Choi *et al*, 2007). In addition, upregulation of NKG2D ligands is seen in mice transfected with an oncogenic adenovirus, which subsequently enhances tumour rejection *in vivo* (Routes *et al*, 2005).

NKG2D deficiency results in a higher incidence of malignant prostate adenocarcinomas in transgenic model of prostate adenocarcinoma (TRAMP) model *Klrk1*^{-/-} knockout mice, as well as accelerating the progression of E μ -myc-induced lymphomas in E μ -myc transgenic mice (Guerra *et al*, 2008). This study provided evidence of NKG2D action in the formation of primary tumours.

NKG2D ligand expression is heterogenous and combinations of ligands can be used as a prognostic marker in colorectal cancer patients, with those expressing high levels of certain ligands showing a significant improvement in survival rates following surgery (McGilvray *et*

al, 2009). This suggests that the action of NKG2D-bearing cells is important in controlling tumour progression. The same study demonstrated that tumour expression of NKG2D ligands decreases as tumour stage increases, indicating that late stage tumours have been driven toward lower expression of NKG2D ligands.

This research demonstrates the clinical relevance of the NKG2D/ NKG2D-ligand interaction. Work is on-going into determining whether this interaction can be targeted for therapy in the treatment of cancers (Vivier *et al*, 2012) and autoimmune diseases (Van Belle & von Herrath, 2009), but there is another high profile clinical scenario where the NKG2D receptor may play an important role.

1.7 The NKG2D/ NKG2D ligand interaction is thought to affect the outcome of haematopoietic stem cell transplants conducted as a therapy of haematological malignancies.

Haematopoietic stem cell transplants (HSCT) represent a significant development in the treatment of haematological malignancies such as leukemia and lymphoma. HSCTs were first developed to combat the toxicity to bone marrow caused by aggressive chemo- and radio-therapy of haematological malignancies (Thomas *et al*, 1959). It was soon found that SCTs also trigger immune reactions, both toward the host malignancy (graft versus leukaemia, or GvL) and towards host tissues, particularly gut, skin and liver (graft versus host disease, or GvHD) (Goker *et al*, 2001). These immune responses are mediated by the human leukocyte antigen (HLA) molecules, class I in the case of CD8⁺ T cells, class II in the case of CD4⁺ T cells (Bleakley & Riddell, 2004).

By ablating the host immune system through chemo-and radiotherapy, the introduction of haematopoietic cells from an HLA-matched donor allows targeting of the malignant cells by donor T-cells (GvL) and reconstitution of the recipient immune system. However, the donor T-cells can also mediate an immune response against host tissue (GvHD), necessitating T-cell depletion from the graft, which negatively impacts the GvL potential, increasing chances of relapse.

The GvHD effect is worst in HLA-mismatched SCTs but still occurs in HLA-matched transplants due to the minor histocompatibility antigens displayed by HLA molecules of recipient cells. The GvL effect has been shown to significantly reduce the chance of relapse, so separating the beneficial GvL and harmful GvHD effects is one of the prime focuses of SCT research (Blazar *et al*, 2012).

Discovery of the GvL effect has led to switching the pre-transplant condition away from the very harsh chemo- and radio-therapies and towards the so called “non-myeloablative” conditioning, thereby allowing treatment of those for which myeloablative therapy may have proved fatal. The objective of non-myeloablative conditioning is immunosuppression with insufficient strength to cause irreversible damage to the patient’s bone marrow (McSweeney *et al*, 2001).

Due to the unique combination of receptors that recognise both MHC molecules and stress ligands, NK cells, and by inference their activating receptors such as NKG2D, have been shown to have a positive effect on HSCTs. Alloreactive NK cells have been shown to be associated with improved GvHD effects in acute myeloid leukaemia (AML) patients (Ruggieri *et al*, 2002). This is thought to be due to alloreactive NK donor cells attacking the recipient antigen presenting cells (APCs) that mediate GvHD. In addition, HSCTs from a donor that

shares only one HLA haplotype with the recipient show improved GvL by NK cells uninhibited by HLA-recognition on leukemic cells, which don't target healthy recipient cells because of the lack of activating ligands (Moretta *et al*, 2011). In this scenario, the T cell population can be almost entirely removed from the graft, which reduces GvHD effects.

There is evidence to suggest that NKG2D is important in the HSCT scenario, with a recent clinical trial demonstrating that an engraftment of T cells expressing NKG2D demonstrated significantly increased killing of autologous myeloma cells compared with T cells that did not express the receptor (Meehan *et al*, 2012).

1.8 ULBP6 has been demonstrated to be of particular significance in this scenario, with some single nucleotide polymorphism alleles showing significantly improved RFS and OS over others.

As mentioned earlier, the ULBP/ RAET1 gene family exhibits extensive polymorphism, existing as a cluster of functionally and structurally related genes, likely due to evolutionary attempts to maintain viral resistance, and perhaps prevent cancer immunoediting. Each ULBP locus exhibits between 10 and 28 single nucleotide polymorphisms (*inter alia* Hubbard *et al* 2007), but these polymorphisms occur in a wide variety of locations, including promoter regions and non-coding regions. Importantly, they also occur in binding site regions, notably in the RAET1L (ULBP6) gene (Eagle *et al*, 2009b). However, only three of the known NKG2D ligands have been demonstrated to have undergone preferential selection in discrete global populations (Antoun *et al*, 2010), while the ligands that also bind UL-16 (ULBP1, 2 and 3) seem to be far more conserved.

In MHC-matched HSCTs, allelic variation of the recipient's RAET1L (ULBP6) gene has been shown to strongly contribute to relapse free survival (RFS) and overall survival (OS) (Antoun *et al*, 2012). Improved RFS and OS were observed in patients carrying at least one copy of the second most common RAET1L allele, RAET1L*02, and patients homozygous for the RAET1L*02 allele had improved OS and RFS over heterozygotes. Patients heterozygous for RAET1L*02 displayed a 14% better OS at 8 years than those without a copy of the allele, and patients homozygous for the RAET1L*02 gene displayed a 33% improvement in RFS relative to those without a copy of the RAET1L*02 gene. Notably, this data was obtained from HLA-identical transplantations between siblings, which removed the influence of the strongly immunogenic MHC-mismatch scenario.

It is also important to note that it is the recipient's expression of ULBP6 that has the effect. It is possible that ULBP6 is expressed on the malignant haematopoietic cells, which induces killing by NKG2D-expressing NK cells, $\gamma\delta$ T-cells or CD8⁺ CTCs. Alternatively ULBP6 could be mediating the killing of recipient APCs by the donor leukocytes.

There is little evidence to show whether the improved OS of patients carrying at least one copy of the RAET1L*02 gene is due to enhanced GvL or reduced GvHD, or a combination of both effects. The data suggests a much higher RFS in homozygotes and insignificant improvement in death in remission due to infection, GvHD and other causes in RAET1L*02 carriers, which implies the improvement in OS is likely due to enhanced GvL. Based on these observations, it is the ULBP6 on malignant cells, rather than APCs, that most likely contributes to a beneficial transplant outcome.

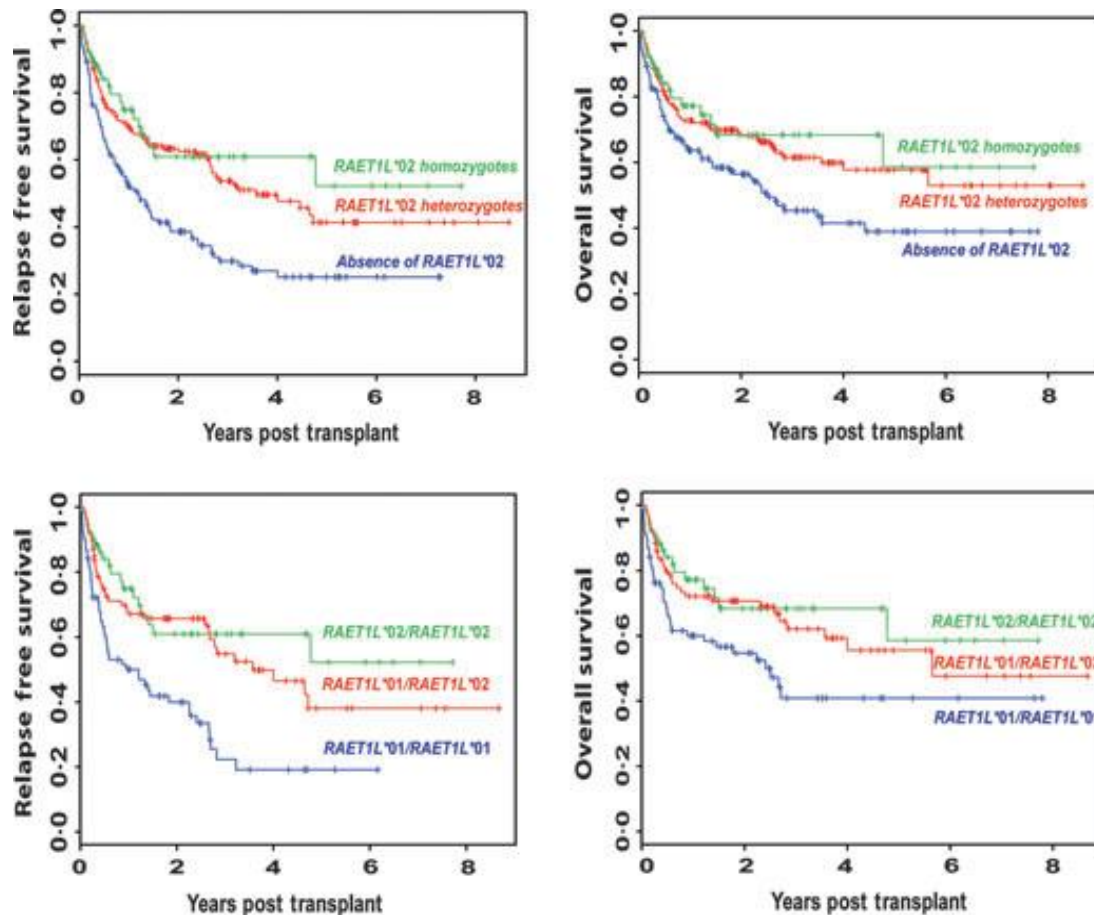


Figure 1.3: Effect of RAET1L*02 gene possession on relapse free survival (RFS) and overall survival (OS) in patients that have undergone stem cell transplants to treat haematopoietic malignancies. A clear increase in RFS and OS can be observed in both hetero- and homozygotes for the RAET1L*02 allele over the homozygotes for RAET1L*01. (Taken from Antoun *et al*, 2012)

In addition, the mechanism for this improved survival effect of the RAET1L*02 gene is very poorly understood. It may be due to enhanced cell surface expression with the *02 allele product, either through enhanced transcription, preferential transport to the cell surface, or resistance to degradation or shedding. Alternatively the RAET1L*02 gene product could exhibit improved binding with the NKG2D receptor, eliciting a stronger lymphocyte response. Polymorphisms and mutations in other NKG2D ligands have shown variation in binding affinity for NKG2D (Steinle *et al*, 2001; Radaev *et al*, 2002). Analysis of the molecular interaction between NKG2D and the ULBP6*01 and *02 variants, as well as determining the functional role and capabilities of these variant ligands and the cells that express them, is crucial in determining an explanation for the improved survival effect of RAET1L*02. Elucidating the molecular basis for these observations may hopefully lead to improved prognostics, transplantation protocols and potentially anti-cancer therapy.

PROJECT AIMS

Primary Aim:

To determine the molecular mechanism underlying the improved survival of HSCT patients that display at least one copy of the RAET1L*02 allele.

This will be carried out via two secondary aims:

1) Investigating the binding of ULBP6 with NKG2D using Surface plasmon resonance (SPR).

- Express, purify and biotinylate SDMs of ULBP6*02 in *Drosophila* expression system.
- Use SPR to determine binding affinities of ULBP6*01, *02 and the two SDMs (ULBP6*02 L86R and ULBP6*02 T127I) for NKG2D.
- Use SPR to investigate the kinetics of the NKG2D-ULBP6 interaction.

2) Determining the structure of the NKG2D-ULBP6 complex using X-ray crystallography.

- Express and purify *E. coli*-derived NKG2D
- Express and purify *E. coli*-derived ULBP6*02
- Produce diffraction-grade crystals of the NKG2D-ULBP6*02 complex
- Determine three dimensional structure of the NKG2D-ULBP6*02 complex by X-ray crystallography


MATERIALS AND METHODS

2.1 ULBP6-NKG2D binding affinity experiments.

2.1.1 Site directed mutagenesis (SDM) and analysis.

For expression of ULBP6*02 proteins for use in Surface Plasmon Resonance studies, the pMT/BiP/V5-His plasmid vector (Invitrogen) was transfected into eukaryotic S2 *Drosophila* cells. The RAET1L gene had previously been cloned into the vector (Figure 2.1), but two SDMs of pMT/BiP/V5-His containing the ULBP6*02 C14S were carried out to create mutations corresponding to each of the residues altered between the two alleles of ULBP6 being investigated (*01 and *02). 200 ng DNA template, 200 μ M dNTPs, 125 ng forward primer and 2.5 units Pfu Ultra Hotstart enzyme (Stratagene) was added to 1x Pfu buffer, and made up to 50 μ L with PCR grade water. The PCR reaction was carried out using a thermocycler set to the following program:

98°C	98°C	55°C	68°C	72°C	4°C
3mins	45secs	45secs	8mins	10mins	∞
X16 cycles					



SDMs were digested with 10 units of DpnI (New England Biolabs) for 1 hour to degrade parental DNA before transformation. Correct DNA amplification was checked using 1% agarose gel electrophoresis run in TBE buffer (89 mM Tris base, 89 mM Boric acid and 2 mM EDTA) at 80 V. Ethidium bromide was used to visualise DNA.

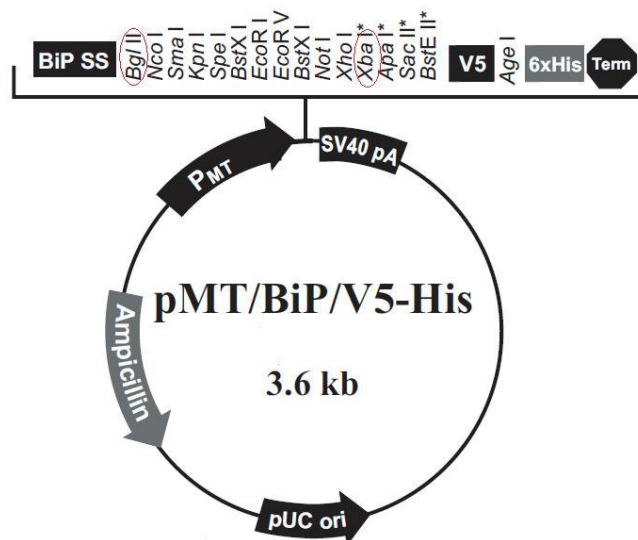


Figure 2.1: Vector map of pMT/ BiP/ V5-His. Cloning sites for the RAET1L genes are circled in red.

2.1.2 Primer Details.

Primers were used previously to mutate ULBP6*01 to ULBP6*02. The details of the primers used to generate the two intermediary mutants (ULBP6*02 L86R and ULBP6*02 T127I SDMs) are shown below.

Primer no.1

CTT (L) > CGT (R)

5' CAGAGCAACTGCTTGACATTCAGCTGG

PEF72

Forward: 5' CTTACAGAGCAACTGCGTGACATTCAGCTGGAG 3'

Reverse:	5'	CTCCAGCTGAATGTCACGCAGTTGCTCTGTAAG	3'
GC	content:	51.52%	Location: 8-40
Melting	temp:	79.4°C	Mismatched bases: 1

Primer no.2

ACC (T) > ATC (I)

5' GTATCGATGGACAGACCTCCTACTCTTTG

PEF73

Forward:	5'	GTATCGATGGACAGATCTTCCTACTCTTTGAC	3'
Reverse:	5'	GTCAAAGAGTAGGAAGATCTGTCCATCGATAC	3'
GC	content:	43.75%.	Location: 9-40
Melting	temp:	75.4°C.	Mismatched bases: 1

2.1.3 Transfection and culture of S2 *Drosophila* cells.

3 ml of S2 *Drosophila* cells at 1×10^6 cells/ ml were plated into a 6 well plate and incubated at 27°C in complete growth medium (Schneider's *Drosophila* medium plus L-glutamine and 10% foetal calf serum) until they had grown to $2 - 4 \times 10^6$ cells/ml. The Invitrogen calcium phosphate transfection kit (2M CaCl_2 , 2x Hepes buffered saline, dH_2O) was used to co-transfect 9.5 µg plasmid DNA with 0.5 µg pCoHygro plasmid (Invitrogen - Figure 2.2) into the *Drosophila* cells, which were then incubated at 27°C for 24 hours before being washed and re-plated in fresh medium for another 48 hour incubation. The cells were then centrifuged

and re-suspended in complete growth medium supplemented with 300 µg/ml hygromycin B to select for successful transformation, and grown in the same well for 3 weeks, replacing the medium, with antibiotic, every 4 – 5 days. The cell cultures were upscaled to T-75 flasks, 125 ml and then 500 ml Erlenmeyer flasks swirled at 80 rpm with 0.05% Plurionic F-68 surfactant to prevent clumping.

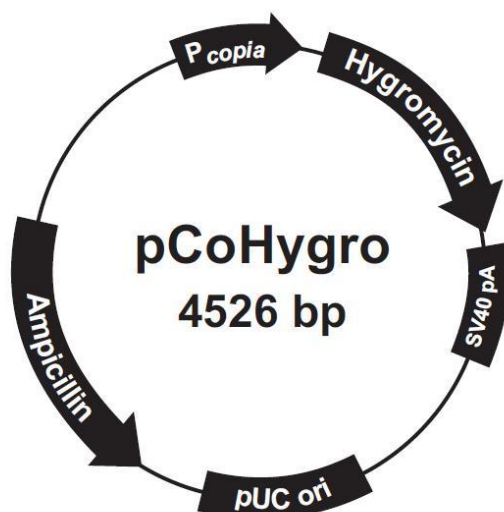


Figure 2.2: Vector map of the pCoHygro antibiotic resistance construct.

2.1.4 Induction of protein expression and collection of supernatant.

Once the cells had reached $3 - 5 \times 10^6$ cells/ml in the 500 ml flasks, protein expression was induced by addition of 500 µM CuSO₄ and the cells were incubated for 5 days at 27°C at 80 rpm. The cell cultures were then pelleted by centrifugation at 100 g for 10 minutes and the supernatant containing the target proteins decanted, centrifuged again at 2,500 rpm for 10 minutes and then stored at 4°C with 0.02% NaN₃. An aliquot of the supernatant was taken to test for target protein expression by Western blot analysis.

2.1.5 Purification of target proteins.

Target proteins were purified from the culture supernatant first by dialysis in 1:10 PBS using a 10kDa-restricted dialysis tube overnight at 4°C to remove soluble amino acids, particularly histidine, which interfere with nickel binding in the following step. Dialysed supernatant was then passed through 1 ml of Ni-NTA agarose beads (Qiagen) packed in an Econo-column (BioRad) that had been equilibrated with 1x PBS/ 10 mM imidazole, at ~1 ml/min overnight at 4°C. Non-specific proteins were washed from the column with ~100 ml 1x PBS/ 10 mM imidazole, before His-tagged proteins were eluted using 10 ml 1x PBS/ 250 mM imidazole. 1 ml fractions were collected and OD₂₈₀ measured to determine protein concentration, and analysed by Western blot.

2.1.6 Biotinylation of target proteins.

To facilitate immobilisation via streptavidin binding for BIAcore experiments, the purified *Drosophila* expressed ULBP6*02 mutants were biotinylated. A PD10 desalting column (GE Healthcare) was equilibrated with biotinylation buffer (100 mM Tris pH 7.5, 20 mM NaCl, 5 mM MgCl₂) before ~3 ml protein sample was loaded and then eluted with an equal volume of biotinylation buffer. Following this buffer exchange, biotinylation was carried out using 0.56 mM Biotin (Sigma), 1 mM ATP (Sigma) 1x protease inhibitors (Roche) and BirA enzyme. The mixture was incubated at room temperature for 1 hour and then at 4°C overnight. Buffer exchange was performed as before, this time equilibrating column and eluting the protein with PBS. 100 µl aliquots were stored at -20°C and analysed for protein using a streptavidin-HRP Western blot.

2.1.7 Protein analysis (Western blot).

Protein samples were separated by SDS-PAGE as described above, then transferred to a PVDF membrane (Hybond LFP, GE Healthcare) in transfer buffer (10% methanol, 190 mM glycine, 25 mM Tris) at 400 mA for 1 hour. The membrane was then blocked to prevent non-specific interactions using either 5% milk in 1x Tris-buffered saline (20 mM Tris pH 7.5, 150 mM NaCl) + 0.1% Tween (TBS-T), or 3% bovine serum albumin (BSA) in 1x TBS-T (streptavidin blot). The membrane was washed three times with TBS-T before incubation with mouse anti-C terminal His primary antibody (Invitrogen) at 1:10,000 in TBS-T at room temperature for 1 hour. For the streptavidin-HRP blot, streptavidin-HRP (Invitrogen) was added at 1:20,000 after the block, incubated for 1 hour and then washed three times with TBS-T prior to the chemiluminescence step, below. Unbound primary antibody was washed off with 3 TBS-T washes before transfer of the membrane into 5% milk in TBS-T with 1:20,000 secondary antibody (HRP-conjugated anti-mouse goat antibody (Sigma)). This was incubated for one hour at room temperature before being washed 3 times with TBS-T and then bound antibody fluorescence was detected using EZ-ECL Chemiluminescence Detection Kit for HRP (Biological Industries). Light sensitive film (Amersham Hyperfilm MP, GE Healthcare) was placed on the membrane in a dark room before being developed.

2.1.8 Surface Plasmon Resonance

Surface Plasmon Resonance experiments were carried out using a BIAcore 3000 instrument (BIAcore, GE Healthcare). Experiments were performed at 25⁰C using HBS-EP buffer (10 mM HEPES pH 7.4, 150 mM NaCl, 3.4 mM EDTA, 0.005% P20 surfactant). Following docking of a blank CM5 sensor chip and priming with water, the instrument was normalised with 500 µl BIA normalising solution flowed at 10 µl/min. The chip was then activated with a 1:1 mix of 50 µl 0.2 M N-ethyl-N5 (3-diethylaminopropyl)-carbodiimide (EDC) and 50 µl 0.5 M N-hydroxysuccinimide (NHS), flowed at 10 µl/min. 60 µl 0.5 mg/ml streptavidin was then flowed over the sensor chip, before 70 µl 1 M ethanolamine pH 8.5 was flowed to block any unbound binding sites on the chip. Unbound streptavidin was removed with 500 µl pH 2.5 glycine-HCl. Biotinylated proteins (ULBP6*01, ULBP6*02, ULBP6*02 T127I SDM, ULBP6*02 L86R SDM and a control protein - EPCR) were immobilised in HBS-EP buffer at a flow rate of 5 µl/min. Biotinylated proteins were flowed until a gain of ~1,000 response units was registered using the BIAevaluation software. Prior to flowing over the sensor chips, purified NKG2D was filtered to remove aggregates by size exclusion chromatography using a Superdex HR200 column (GE Healthcare), using FPLC as described above. A 10-fold serial dilution of NKG2D was performed from a starting concentration of 0.85 µl/ml and then the analytes were flowed over each flow cell at a rate of 5 µl/min, with a typical injection time of 325 s and a wait time between injections of 7,300 s.

2.2 X-Ray Crystallography

Previous attempts to isolate and purify ULBP6*02 led to problems with cross-dimerisation of ULBP6 molecules from a cysteine residue at position 14, that resulted in incorrect re-folding and lack of crystals. To ameliorate this, the C14 residue was mutated to a serine (K. Ali, unpublished). The resulting PCR product was cloned into the pCR-blunt vector and sequenced to confirm correct sequence and restriction sites. The insert was then digested out of the pCR-blunt vector and sub-cloned into the pET23a expression vector (Novagen). ULBP6*02 C14S has been demonstrated to exhibit preferential crystal formation over the non-mutated version. For the purposes of this report, ULBP6*02 will be used to denote the ULBP6*02 C14S mutant, unless specifically stated.

2.2.1 Bacteria transformation.

50 µl aliquots of competent *E. coli* cells (BL21 pLys DE3 (Bioline) for NKG2D or Rosetta BL21 derivatives (Novagen) for ULBP6) were thawed on ice before a 30 minute incubation with 10 µl of relevant plasmid DNA (pET23a expression vector with NKG2D/RAET1L gene cloned into it). The cells were then heat shocked for 90 seconds at 42°C in a water bath and then chilled on ice. 200 µl of super optimised broth with catabolite repression (SOC medium) was then added to the cells and the mixture was incubated for 1 hour at 37°C and 200 rpm to allow transformation of the cells and incorporation of the antibiotic resistance gene. 100 µl of the culture was plated onto Luria Broth (LB)-ampicillin agar plates and incubated overnight at 37°C to allow colony formation.

2.2.2 Protein expression.

A single colony from the LB-amp plates was picked and inoculated into 20 ml LB with 100 µg/mL ampicillin. This culture was incubated at 37°C for typically 2-3 hours until the medium was cloudy, before being added to 4 L LB with 100 µg/mL ampicillin, split equally between two 5 L conical flasks. The flasks were incubated at 37°C and 200 rpm until the optical density (OD) at 600 nm reached between 0.4 and 0.6, and at this point a 100 µL aliquot was taken for pre-induction analysis by SDS-PAGE. Protein expression was induced by adding 500 µM isopropyl β-D-1-thiogalactopyranoside (IPTG), and the cultures were then incubated for 4 hours at 37°C at 200 rpm. A second aliquot was taken at this stage for post-induction analysis.

2.2.3 Inclusion body preparation.

Bacterial cultures were pelleted at 4°C and 5,000 rpm in a Beckman Coulter Avanti J-26 XP centrifuge. The pellets were resuspended in ~30 ml ice cold phosphate buffered saline (PBS) (2.7 mM KCl, 137 mM NaCl, 8.1 mM Na₂HPO₄, 1.76 mM KH₂PO₄, pH 7.4) and then sonicated in five 45 s bursts using a Misonix 3000 sonicator. The cell lysate was then pelleted by centrifugation for 15 minutes at 4°C and 13,500 rpm in a Sorvall RC 5C plus centrifuge. The pellets were then resuspended and homogenised 3 times in 30 ml of Triton wash buffer (500 mM Tris-HCl pH 8, 0.5% Triton X-100, 200 mM NaCl, 10 mM EDTA, 0.5% Na Azide) with 2mM DTT, to remove hydrophobic cellular debris and contaminants. The homogenised lysate was centrifuged for 10 minutes at 4°C and 13,500 rpm between each wash, before a resuspension wash (500 mM Tris-HCl pH 8, 200 mM NaCl, 10 mM EDTA, 0.1% Na Azide with

2mM DTT), homogenisation and centrifugation was performed to remove the detergent. The inclusion body pellet was then solubilised in denaturant buffer (8M urea, 25mM MES pH6.5, 10mM EDTA, 0.5mM DTT for NKG2D) or (6M Guanidine-HCl, 50mM MES pH6.5, 12.5mM EDTA pH8.0, 1mM DTT for ULBP6*02) and incubated for 3 hours at 4°C on a rotary rocker. Insoluble material was removed by centrifugation for 30 minutes at 4°C and 13,500 rpm, and the supernatant stored in 1 ml aliquots at -80°C for refolding. Supernatant protein concentration was determined using a Bradford dye-binding assay (BioRad).

2.2.4 Inclusion body re-folding.

Denatured inclusion bodies were refolded using the Garboczi oxidative dilution method (Garboczi *et al*, 1992). For NKG2D, ~15 mg protein was refolded at 4°C in 500 ml refolding buffer (0.24M L-arginine, 2mM EDTA pH 8.0, 100mM Tris pH 8.0, 2.5mM reduced glutathione, 0.245 mM oxidised glutathione and 100 µM PMSF protease inhibitor), via three pulses of 5 mg protein over the course of 2 days. For ULBP6*02, ~25 mg protein was refolded at 4°C in 1 L refolding buffer, via 5 pulses of 5 mg protein over 3 days. For each pulse, one third of the 5 mg protein was diluted into 20 ml refolding buffer and added drop-wise to the beaker to reduce protein aggregation, repeated twice. The final protein solution was reduced to 10 ml using an ultrafiltration device (Amicon) fitted with a 10 kDa membrane under 50 psi N₂ at 4°C. The concentrated sample was then filtered using a 0.45 µm acrodisc to remove unfolded aggregates.

2.2.5 Size exclusion chromatography.

Protein purification was carried out by size exclusion chromatography (SEC), performed using a Superdex S200 column (GE Healthcare) and AKTA Fast Protein Liquid Chromatography (FPLC) (GE Healthcare). The column was pre-equilibrated and chromatography carried out with 20 mM Tris pH 8 and 50 mM NaCl buffer, at room temperature and a 3 ml/min flow rate. Eluate was collected in 5 ml fractions, and those corresponding to peaks of interest were pooled, reduced to 500 µl using an 10kDa ultrafiltration unit (Millipore) and analysed for purity using SDS-PAGE.

2.2.6 Anion-exchange chromatography.

Further protein purification was carried out where necessary by anion-exchange chromatography, performed using a ResourceQ column (GE Healthcare) and AKTA FPLC. 500 µl samples from SEC were diluted into 6 ml low-salt buffer (20 mM Tris pH 8 and 5 mM NaCl) and loaded onto the column with the same buffer in Line A and a high salt buffer (20 mM Tris pH 8 and 1 M NaCl) in Line B to generate the NaCl gradient. Eluate was collected in 750 µl fractions and those corresponding to peaks of interest pooled, reduced to 500 µl as previously and stored at -20°C.

2.2.7 Protein analysis (SDS PAGE).

Analysis of protein purity was carried out using sodium dodecyl sulphate polyacrylamide gel electrophoresis (SDS-PAGE). Typically 10 µg protein was added to 2 µl running buffer (125 mM Tris pH 8, 8M urea, 10% glycerol, 6% SDS, bromophenol blue) and loaded onto a 15% acrylamide gel consisting of a resolving gel (765mM Tris pH 8.8, 0.2% SDS, 15% acrylamide (Protogel), 0.1% ammonium persulphate and 5 µL of tetramethylethylenediamine (TEMED) (Sigma)) and a stacking gel (150mM Tris pH 6.8, 0.12% SDS, 0.1% ammonium persulphate and 5 µL of TEMED). For reduced sample analysis, the running buffer contained 200 mM DTT and the sample was denatured by incubating at 96°C for 10 minutes prior to loading. Protein gels were run at 100 mV through the stacking gel and 180 mV through the resolving gel and stained using coomassie blue (0.5 g Brilliant blue, 250 ml methanol, 50 ml acetic acid) for 1 hour before de-staining overnight in destain buffer (30% methanol, 10% acetic acid). Gels were imaged using Genesnap software.

2.2.8 Protein crystallisation.

Crystallisation of NKG2D-UIBP6 complex was carried out with concentrations of protein complex from 10.6 – 12.4 mg/ml. To determine optimum conditions for crystallisation, small scale screening was conducted using the hanging drop vapour diffusion method, using three screen conditions (Pact condition 26, 27 & 38 (Qiagen)) previously identified as being conducive to complex crystallisation (K. Ali, unpublished). Hanging drops were formed of between 200 and 800 nl total volume (50% complex, 50% screen condition) on a 96-well plate seal (TTP LabTech) suspended over a 96-well plate (Iwaki) containing 100 µl relevant

screen condition. Pipetting was performed using the Mosquito nanolitre crystallisation robot (TTP Labtech). Large scale crystallisation was carried out using 1 μ l complex and between 1 and 4 μ l screen, mixed on a cover slip and suspended above 1 ml screen condition in 24-well Linbro plates (Molecular Dimensions). Plates were incubated at 23°C for 3-10 days to allow crystal formation. Crystal formation was assessed using a light microscope (LEICA).

2.2.9 X-ray diffraction data collection.

Selected crystals were picked using cryoloops and flash-cooled in liquid nitrogen. The screen condition contained 25% polyethylene glycol (PEG) which served as a cryo-protectant. Crystals were stored in a cryogenic dewar (Molecular Dimensions) prior to X-ray diffraction experiments. X-ray diffraction patterns were obtained using a Micromax 007HF rotating anode X-ray generator (Rigaku) and a Saturn charged coupled device. Data collection and manipulation was carried out using CrystalClear (Rigaku) software, and intensity data integrated, scaled and merged using the XDS suite software (Kabsch, 2010). Structure determination has been carried out using molecular replacement with MOLREP (Winn *et al*, 2011).

RESULTS

3.1 Investigating the molecular mechanism for enhanced survival in patients with RAET1L*02 allele.

3.1.1 Analysis of binding data for ULBP6*01 and ULBP6*02 with NKG2D.

In order to determine the molecular mechanism behind the surprising improvement in overall survival (OS) and relapse-free survival (RFS) demonstrated in HSCT patients exhibiting the ULBP6*02 allele (Antoun *et al*, 2012), previous work had investigated the binding affinity between NKG2D and the two allelic forms of ULBP6, ULBP6*01 and ULBP6*02. The affinity of the NKG2D-ULBP6 interaction was determined by Surface Plasmon Resonance experiments, with the dissociation constant (K_d) determined both by non-linear curve fitting and Scatchard analysis (Figure 3.1). Maximum specific binding (ULBP6 response minus EPCR control protein response) for ULBP6*01 and ULBP6*02 was ~1,100 RU and ~1,350 RU, respectively. K_d was determined to be ~12 – 15 nM for ULBP6*02/NKG2D and ~123 – 140 nM for ULBP6*01/ NKG2D, which represents an approximately 10 fold increase in affinity of the receptor for the ligand in the case of *02 allelic form compared with the *01 form. Based on this data, a reasonable hypothesis would be that the lower affinity ULBP6*01 allele in HSCT patients is associated with worsened OS and RFS due to reduced tumour killing by NKG2D-expressing cytotoxic lymphocytes, when compared with patients expressing the higher affinity ULBP6*02 allele.

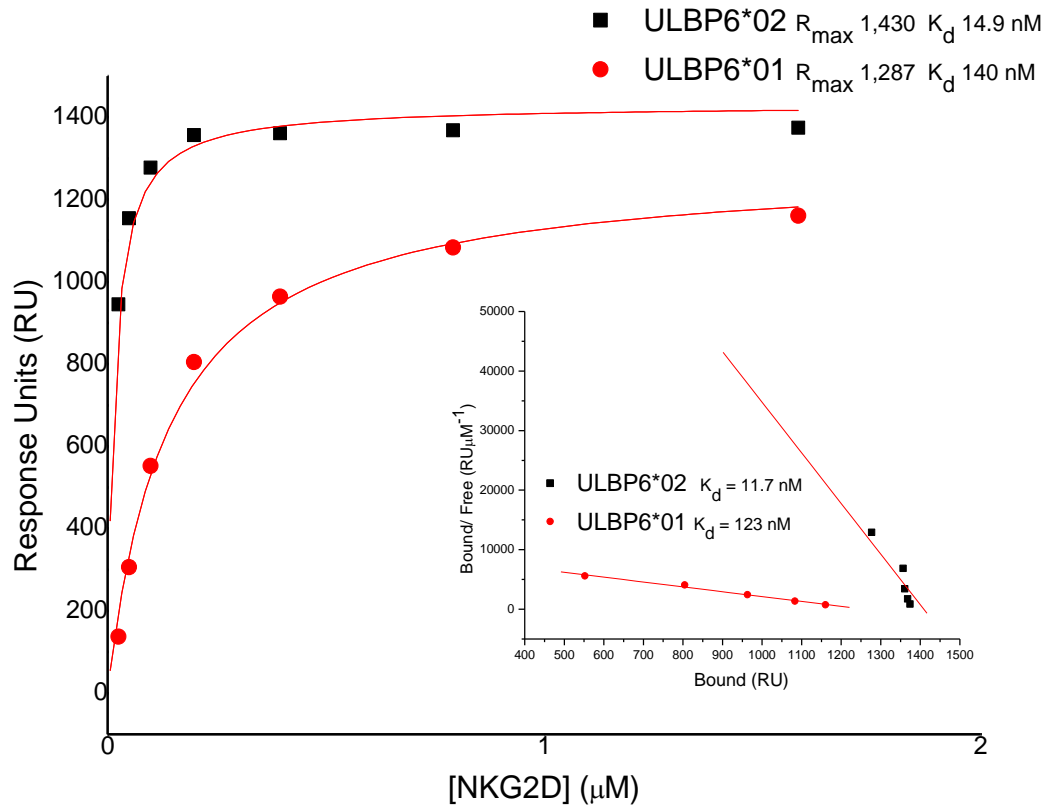


Fig. 3.1: The affinity of the NKG2D-ULBP6*01 and *02 interaction, determined by SPR.

(main) Non-linear curve fitting of the Langmuir binding isotherm to the data yielded R_{max} and K_d for ULBP6*01, ULBP6*02. In all cases the saturation point (R_{max}) was nearly reached at the highest concentration of flowed NKG2D. (inset) Scatchard analysis of the data yielded K_d (slope = $-1/K_d$) by linear regression. Predicted K_d are indicated on the plot. The NKG2D-ULBP6*01 interaction was determined to have an approximately 10 fold lower affinity than the NKG2D-ULBP6*02 interaction (123 nM and 11.7 nM respectively).

3.1.2 Identification of ULBP6*02 SDMs

Since there are only two single nucleotide polymorphisms (SNP) in the coding region between the two RAET1L genes, a key aim was to determine which, if any, were critical in affecting the affinity of NKG2D for these ligands. The two amino acid polymorphisms that are observed between ULBP6*01 and *02 are located at positions 86 and 127. The lower-affinity allele, ULBP6*01, which is associated with reduced overall survival in HSCT patients, possesses an arginine residue at position 86 (R86) and an isoleucine residue at position 127 (I127). In contrast, the higher affinity ULBP6*02 has leucine and threonine residues at these respective positions. Molecular modelling studies revealed the prospective position of these residues in the NKG2D-ULBP complex (Figure 3.2). From these analyses, position 86 was found to be located in the ULBP6-NKG2D interface, while position 127 is located distal to the binding site. A logical hypothesis would be that the observed differences in binding affinity for NKG2D between ULBP6*01 and ULBP6*02 may be due to the polymorphism at residue position 86. It is also possible that the change in amino acid position 127 alters the conformation of the ULBP6 protein, and indirectly affects binding affinity. To determine the importance of each residue to NKG2D-ULBP6 binding, two mutated forms of ULBP6*02 were generated by site directed mutagenesis, one with ULBP6*02 position 127 threonine mutated to the *01 isoleucine (T127I) and the other with ULBP6*02 position 86 leucine substituted to the *01 arginine (L86R). These SDMs were carried out in a *Drosophila* expression vector for transfection into an S2 *Drosophila* cell line.

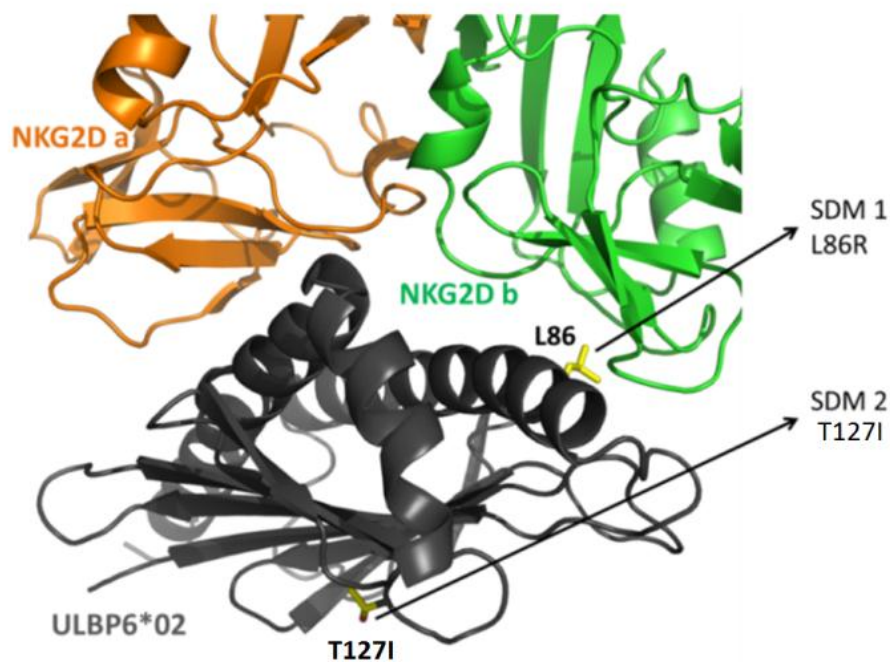


Figure. 3.2 Molecular model of the ULBP6*02-NKG2D complex generated by PyMol. ULBP6*02 is shown in black with the two amino acid changes between the *02 allele and the *01 allele highlighted with arrows. In ULBP6*01 L86 is changed to an arginine residue, while T127 is substituted for an isoleucine. ULBP6*02 cDNA was used as template to generate two SDMs, ULBP6*02 L86R and ULBP6*02 T127I, for transfection into S2 *Drosophila* cells.

3.1.3 Expression and purification of ULBP6*02 SDMs.

Previous attempts had been made to investigate the properties of the two intermediary mutant forms of ULBP6*02 (L86R and T127) by cloning the mutant genes into a prokaryotic expression vector and transforming *E. coli* cells for SDM expression in inclusion bodies which were then refolded *in vitro*, purified and flowed over immobilised NKG2D in SPR experiments. The K_d of the ULBP6*02-NKG2D interaction was measured at 23 nM, which compares with the same protein interaction using *Drosophila*-expressed ULBP6*02 at 3 nM. This variation may be due to the different expression system used, where it is possible that improved folding of the ULBP6*02 proteins would occur in *Drosophila* through use of the

cellular machinery of the host cells, rather than relying on *in vitro* refolding of *E. coli*-expressed protein. K_d for *E. coli* expressed ULBP6*02 T127I was ~33 nM and ULBP6*02 L86R was ~37 nM, which is not statistically different, and surprising given the modelling data presented in Figure 3.2. Bearing in mind the likely improved folding in *Drosophila*, it was decided to repeat the ULBP6*02 mutation studies using the *Drosophila* expression system.

Eukaryotic S2 *Drosophila* cells were transfected with the ULBP6*02 SDM - pMT/BiP/V5-His plasmid construct. Successful cloning and amplification of the construct was ascertained by DNA gel electrophoresis (Figure 3.3a) with a clear band migrating at around 4,000 bp. His-tagged protein expression was determined post induction by Western blot analysis of cell supernatant, which yielded strong bands at ~28 kDa (Figure 3.3b). Analysis of the ULBP6 amino acid sequence suggested 2 possible sites for N-linked glycosylation, which may account for the band migrating to a slightly higher molecular weight than that predicted by primary protein structure alone (~22 kDa). Protein purification was carried out using Ni-NTA agarose packed columns. SDS-PAGE analysis of the resulting eluate confirmed the presence of relatively pure, strong bands migrating at around 28 kDa, indicating successful purification (Figure 3.3c). Protein yields following Ni-NTA chromatography were 6.3 mg from 1 L supernatant for ULBP6*02 L86R and 4.2 mg from 1 L supernatant for ULBP6*02 T127I. Finally, purified ULBP6*02 SDMs were biotinylated to allow for immobilisation via streptavidin coupling on BIAcore chips. Effective biotinylation was confirmed by Western blot analysis using streptavidin-conjugated horseradish peroxidase (HRP) to allow visualisation of biotinylated proteins by chemiluminescence (Figure 3.3d). Bands for each SDM were observed at the predicted molecular weight of ULBP6*02, indicating successful biotinylation in advance of SPR experiments. Final concentrations of biotinylated protein for ULBP6*02 L86R and ULBP6*02 T127I were 2 and 1 mg/ml, respectively.

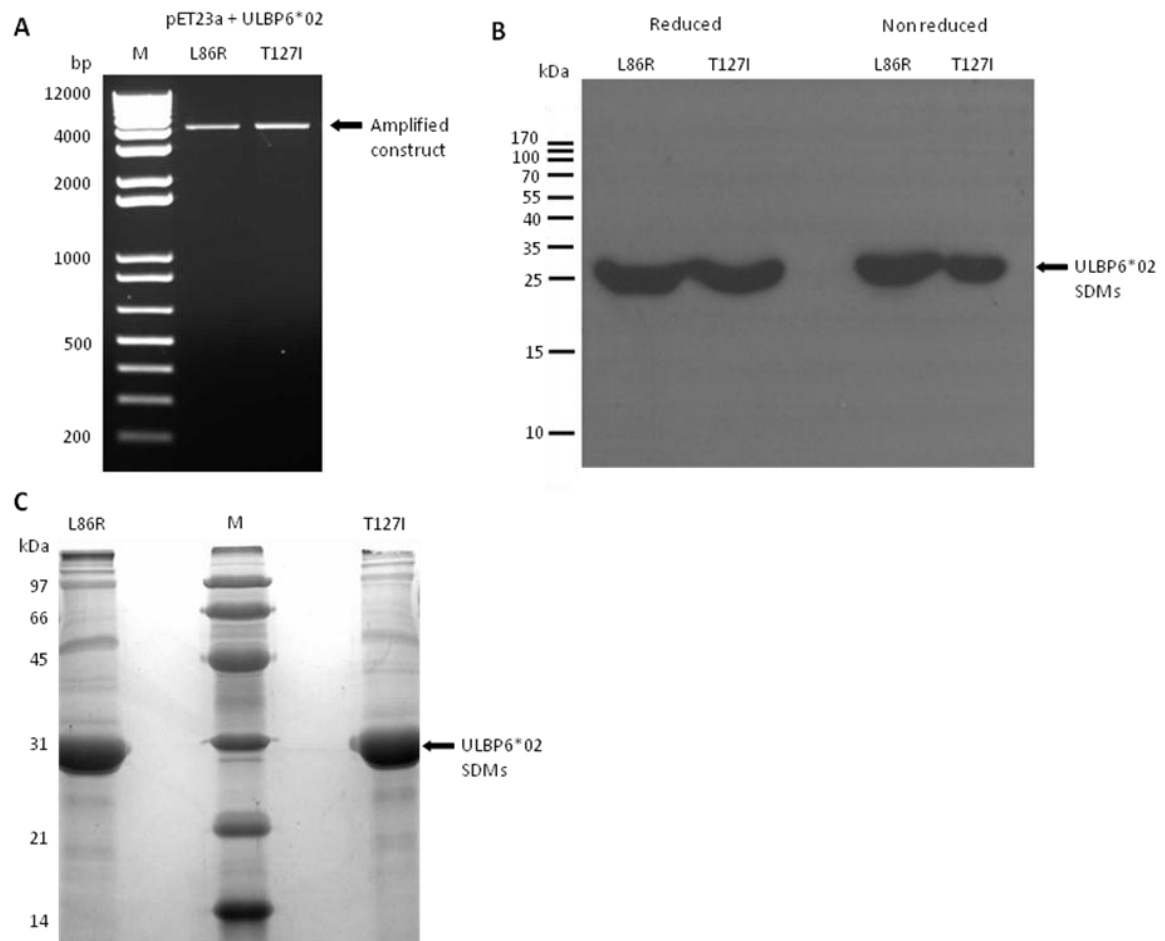


Figure 3.3: Expression, purification and biotinylation of *Drosophila* derived-ULBP6*02 L86R and ULBP6*02 T127I mutants. (a) DNA gel agarose electrophoresis of PCR-amplified transfection construct containing primers for ULBP6*02 L86R and T127I SDM proteins. Clear bands are present at ~4,000 bp indicating successful cloning of the SDM primers into the pMT/BiP/V5-His plasmid vector. (b) Western blot analysis of ULBP6*02 SDM protein expression in *Drosophila* S2 cells (induced with copper sulphate) using an anti-His tag mouse antibody and an anti-mouse goat HRP-linked secondary antibody. Both mutant proteins show high levels of expression. (c) SDS-PAGE analysis of ULBP6*02 L86R and T127I SDM proteins following purification by Ni-NTA chromatography. Strong bands are present for each SDM at ~30 kDa, indicating effective purification.

3.1.4 Binding affinity studies of ULBP6 isoforms and mutants with NKG2D

Surface Plasmon Resonance (SPR) is a method of detecting increases in refractive index close to a sensor surface, and is commonly used to measure protein-protein interactions. One protein, the ligand, is immobilised to a sensor surface, while the other, the analyte, is injected over the surface. As the analyte binds to the immobilised ligand, protein is concentrated and the refractive index increases. As increases in the refractive index have been found to be directly proportional to the amount of material concentrated at the surface, the signal detected, which is measured in Resonance Units (RU), gives an accurate indication of the extent of binding.

SPR is highly sensitive to the presence of aggregated protein, which leads to unrepresentatively slow dissociation due to multimeric binding. Before use in SPR experiments, recombinantly expressed renatured and S200 size-exclusion filtered NKG2D was purified further by size-exclusion chromatography on a high resolution HR200 column to remove any aggregates. A single well-defined peak at the expected elution volume, defined by molecular weight standards, demonstrated the sample was suitable for use in SPR (Figure 3.4).

To test specific binding of NKG2D to the immobilised ligands, NKG2D was simultaneously flowed over each ULBP6 isoform and mutant as well as a control protein, endothelial protein C receptor (EPCR), in separate flow cells. EPCR was selected as a negative control protein as it exhibits a similar overall structure to ULBP family members. Larger responses were observed when NKG2D was flowed over the ULBP6 variants as compared with the control, indicating specific binding (Figure 3.5). Significantly increased specific binding can be

observed with ULBP6*02 and ULBP6*02 T127I relative to ULBP6*01 and ULBP6*02 L86R.

Strikingly, the response of ULBP6*01 and ULBP6*02 L86R is almost identical.

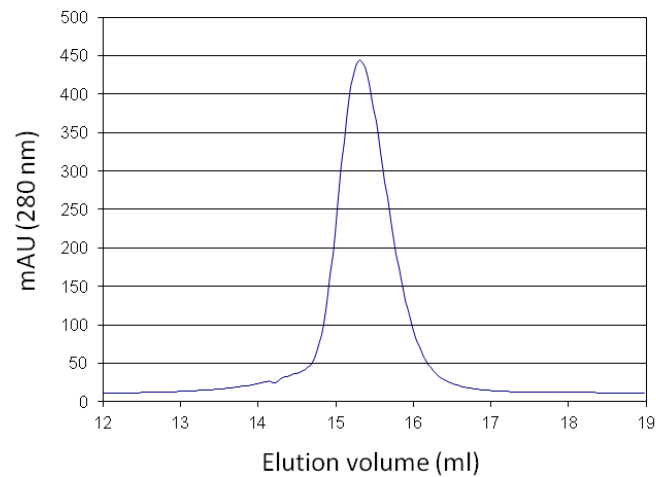


Fig 3.4 Purification of NKG2D by size exclusion. Recombinantly expressed, refolded and purified NKG2D was filtered by size-exclusion chromatography on a high resolution HR200 fast protein liquid chromatography column to remove any aggregates before SPR experiments. A well defined single peak of ~450 mAU is present at an elution volume of ~15.2 mL.

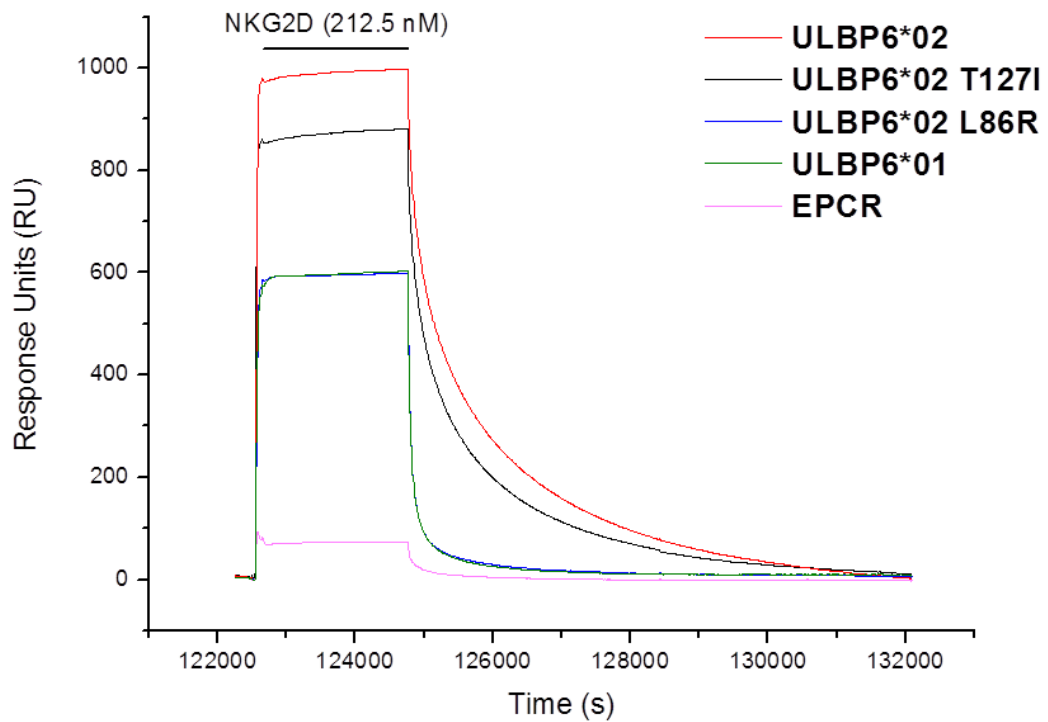


Figure 3.5: Analysis of NKG2D-ULBP6 interactions using Surface Plasmon Resonance. SPR profile of renatured *E. coli*-expressed NKG2D injected over flow cells immobilised with *Drosophila*-derived ULBP6*01, ULBP6*02, ULBP6*02 T127I, ULBP6*02 L86R or control EPCR. The NKG2D was flowed at 5 μ l/min, and the temperature was 25°C. All ULBP6 isoforms demonstrated greater binding response to NKG2D than the control EPCR, indicating specific binding. A distinct difference in specific unit binding can be observed between ULBP6*02 and ULBP6*01, with the ULBP6*02 T127I showing less binding than the wild type form, and the ULBP6*02 L86R almost exactly matching that of ULBP6*01.

The affinity of an interaction can be measured directly by equilibrium binding analysis, which involves varying the concentration of the analyte, and observing the change in binding response. In this case, the affinity of the NKG2D-ULBP6 interaction was determined by flowing varying concentrations of NKG2D over flow cells with immobilised ULBP6 isoform or an immobilised control protein, EPCR. Specific binding was calculated in each case by subtracting the control response detected from the immobilised ULBP6 response. These specific responses were then plotted against free NKG2D concentration. Since the dissociation constant (K_d) is equivalent to free ligand (NKG2D) concentration at half maximal binding, by determining the R_{max} (equivalent to the saturation point) from the plot by non-linear curve fitting, it was possible to calculate the K_d (Figure 3.6). The data shows that for all ULBP6 isoforms, R_{max} was almost reached, which suggests the injection time and flow speed of the analyte was sufficient to avoid significant mass transport-associated artefacts, i.e. the NKG2D-ULBP6 interaction was approaching equilibrium by the end of the injection period. Predicted K_d for ULBP6*02 and ULBP6*02 T127I were both around 16 nM, which indicates a high affinity interaction that is not affected by changing the position 127 threonine to ULBP6*01 isoleucine. Predicted K_d for ULBP6*02 L86R and ULBP6*01 were 117 nM and 138 nM respectively, in the region of 10 fold higher than ULBP6*02, indicating a lower affinity interaction that is likely due, in part at least, to the alteration.

The K_d for the NKG2D-ULBP6 interaction can also be determined by Scatchard analysis of the SPR data (ie. specific binding vs specific binding/free ligand concentration), and using linear regression where the slope of the linear plot = $-1/K_d$ (Figure 3.7). Analysis of this plot yields K_d similar to those predicted in Figure 3.6, with K_d for ULBP6*02 and ULBP6*02 T127I around 11 nM for both and K_d for ULBP6*02 L86R and ULBP6*01 at 114 and 144 nM respectively.

This is consistent with the hypothesis that it is the amino acid residue at position 86 of ULBP6 that is crucial in defining the affinity of NKG2D for ULBP6.

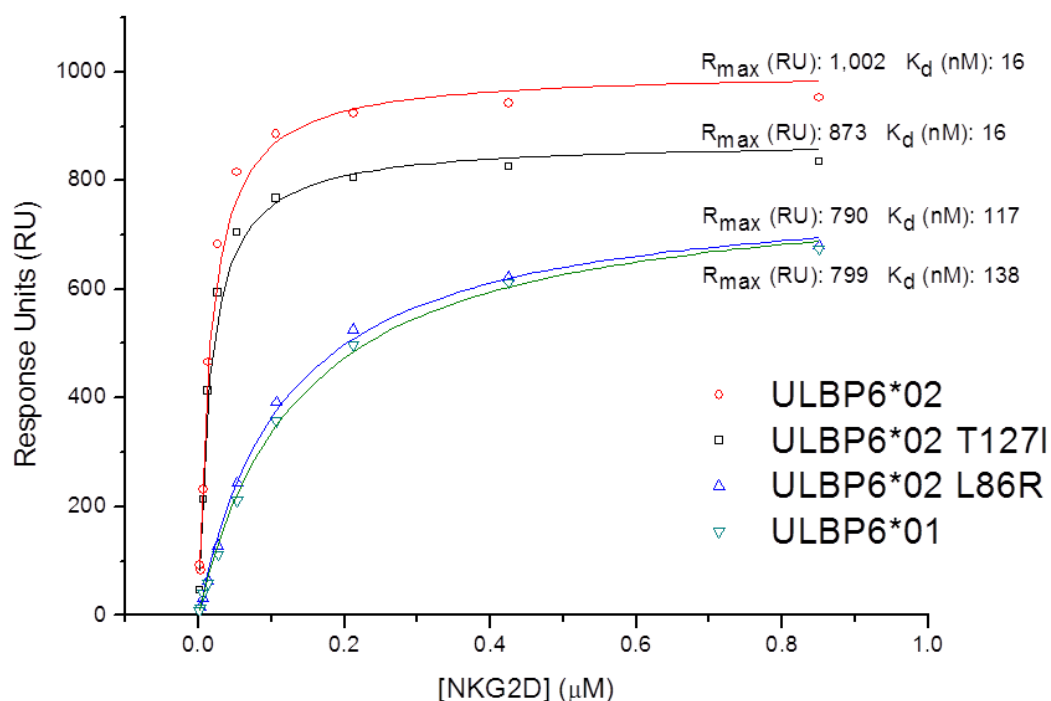


Figure 3.6: Equilibrium affinity measurement of the NKG2D-ULBP6 interaction affinity - Non-linear curve fitting of SPR binding data. Non-linear curve fitting of the Langmuir binding isotherm to the data yielded R_{max} and K_d for ULBP6*01, ULBP6*02, ULBP6*02 T127I and ULBP6*02 L86R. In all cases the saturation point (R_{max}) was nearly reached at the highest concentration of flowed NKG2D. Predicted K_d values are indicated on the plot. Similar K_d values were calculated for ULBP6*02 and ULBP6*02 T127I (16 nM), while those of ULBP6*01 and the ULBP6*02 L86R were almost an order of magnitude larger (138 nM and 117 nM respectively). The plot represents one data set from 4 experiments.

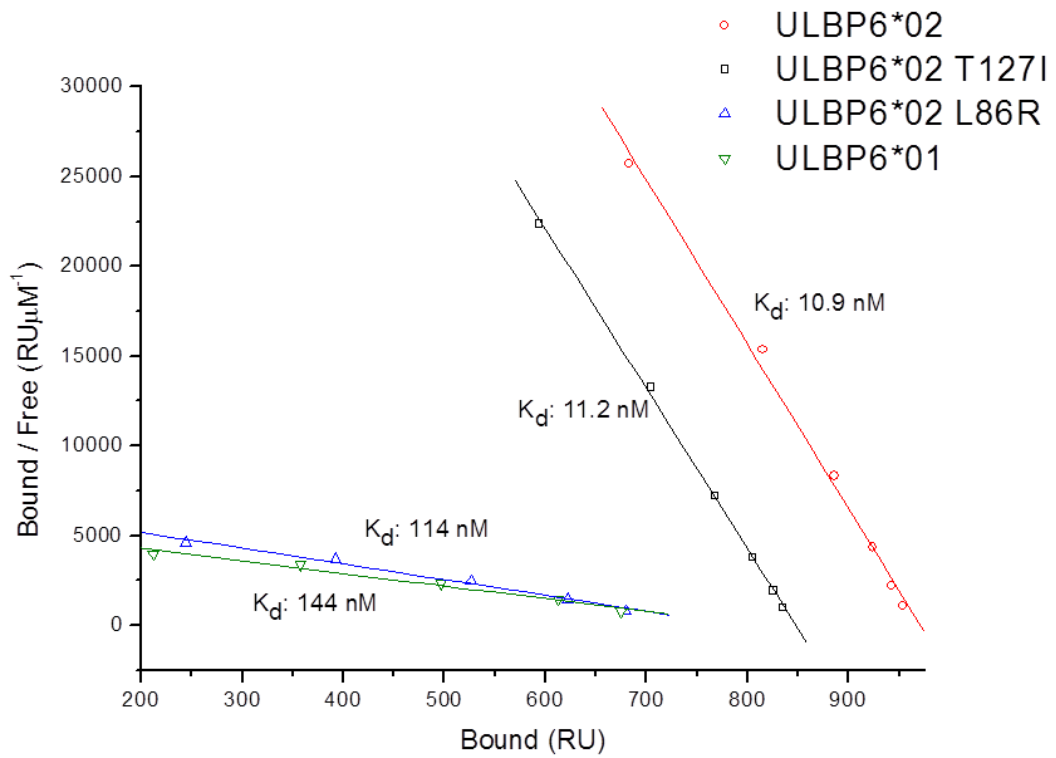


Figure 3.7: Scatchard analysis of the NKG2D-ULBP6 interaction. Scatchard analysis of the data yielded K_d (slope = $-1/K_d$) by linear regression. Predicted K_d are indicated on the plot. Removal of some of the skewing outliers leads to a more robust measurement of K_d than by non-linear curve fitting, with K_d for ULBP6*02 and ULBP6*02 T127I coming down to 10.9 nM and 11.2 nM respectively. The K_d for ULBP6*01 and ULBP6*02 L86R remain similar to those predicted by non-linear curve fitting (144 nM and 114 nM, respectively). The plot represents one data set from 4 experiments.

3.1.5 Kinetic analysis of NKG2D-ULBP6 interaction

Information about the kinetics of protein-protein interactions can be derived from directly monitoring the rate of decay of response during the dissociation phase, which is independent of protein concentration, to yield K_{off} . The rate of association is dependent on the association constant (K_{on}) and also the protein concentration, but can be derived from accurate measurement of the K_d and K_{off} . For both ULBP6*01 and *02, equilibrium was reached within around 300 seconds of NKG2D injection, but ULBP6*02 showed a far slower dissociation rate than ULBP6*01. First order exponentials fitted to the dissociation phase of the binding curves yielded K_{off} of $1.04 \times 10^{-2} \text{ s}^{-1}$ for ULBP6*01 and $7.64 \times 10^{-4} \text{ s}^{-1}$ for ULBP6*02 (Figure 3.8). This implies a half time of dissociation (the time taken for [ULBP6-NKG2D] to fall to half its starting value) of just over 1 minute (66 s) for ULBP6*01 and around 15 minutes for ULBP6*02, which is very long. Using K_{off} and K_d values enables calculation of the association constant, K_{on} , such that $K_{on} = K_{off} / K_d$. Therefore, the K_{on} for ULBP6*02 and ULBP6*01 consisted of $\approx 69,500 \text{ M}^{-1}.\text{s}^{-1}$ and $72,000 \text{ M}^{-1}.\text{s}^{-1}$, respectively. These rates are consistent with other protein-protein interactions (Davis *et al*, 1998), and indicates that the high affinities are not due to an unusually high K_{on} .

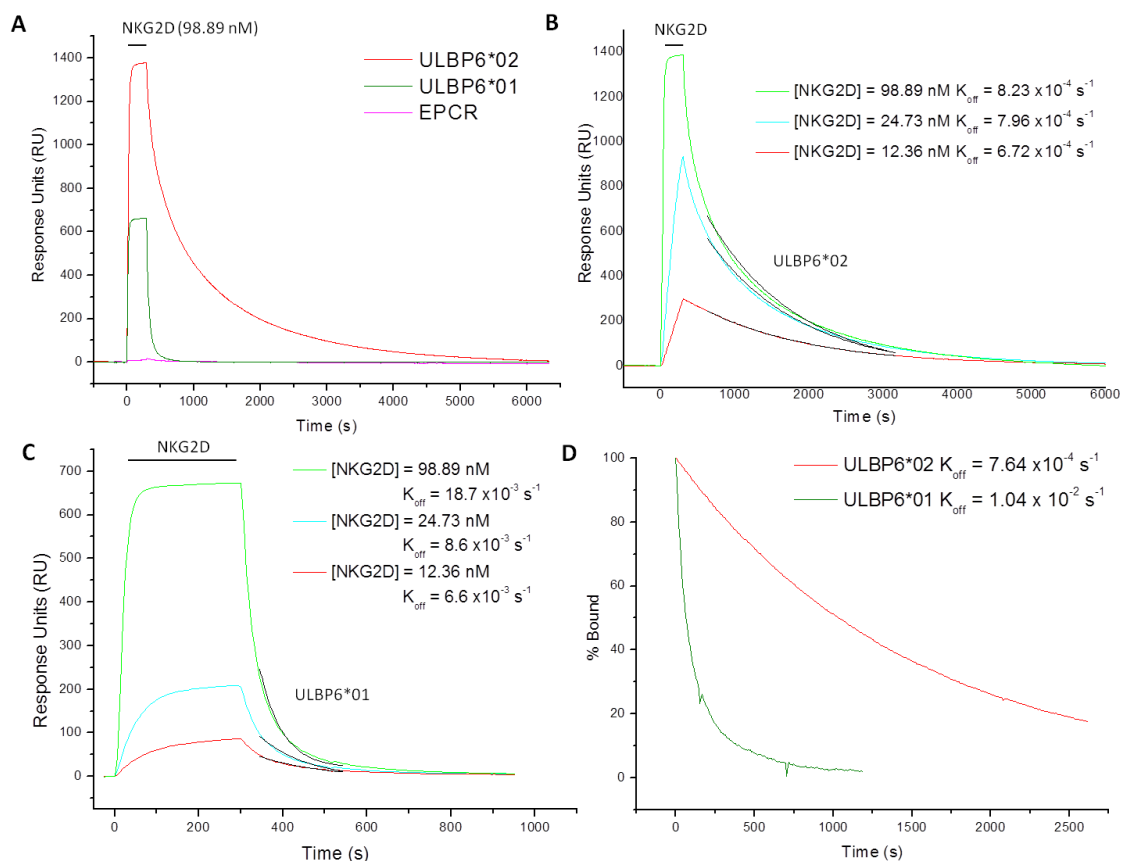


Fig 3.8 Kinetics analysis of NKG2D-ULBP6 interaction. (a) Renatured and purified NKG2D was flowed at 98.89 nM and 50 $\mu\text{l}/\text{min}$ at 25°C over flow cells containing streptavidin-immobilised ULBP6*01 (~650 RU), ULBP6*02 (~1400 RU) and control EPCR (~20 RU). Complete dissociation occurred after ~800 s (ULBP6*01) or ~6,000 s (ULBP6*02). (b and c) Varying concentrations of NKG2D were flowed over immobilised ULBP6*02 (b) and ULBP6*01 (c). The response from the control protein cell was subtracted from the ULBP6 response prior to plotting. The black lines represent first-order exponentials fitted to the data, with predicted dissociation rate constants (K_{off}) marked on the plots. The average K_{off} for ULBP6*02 is $7.64 \times 10^{-4} \text{ s}^{-1}$ and for ULBP6*01 is $1.04 \times 10^{-2} \text{ s}^{-1}$. (d) Normalised binding responses from NKG2D flowed over immobilised ULBP6*01 and *02. K_{off} for each allele is displayed on the plot.

3.2 Solving the NKG2D-ULBP*02 complex structure using X-ray Crystallography.

3.2.1 X-ray diffraction studies of NKG2D-ULBP6*02.

In order to prove the biological basis of the results found in section 3.1, and gain more information about how the NKG2D receptor recognises and binds to ULBP6*02, it was necessary to determine the structure of the NKG2D-ULBP6*02 complex. X-ray crystallography is capable of determining the three dimensional structures of proteins to a higher resolution than any other widely used techniques. The success of X-ray crystallography depends on forming crystals of sufficient size and density that they diffract incident x-ray radiation to form a diffraction pattern that can be used to calculate the protein structure. Amongst other factors, production of such crystals is often most dependent on protein purity.

A crystal of NKG2D-ULBP6*02 complex of approximately 100 x 100 microns in size had previously been grown using the methods presented in section 2, and was deemed suitable for diffraction experiments. The crystal had been soaked in mother liquor and flash cooled in liquid nitrogen. X-ray diffraction experiments were carried out at the University of Birmingham macromolecular diffraction facility. The NKG2D-ULBP6*02 complex crystal diffracted X-rays to a 3.2 Å resolution (Figure 3.9), in the C2 space group with unit cell parameters of $a = 82.4 \text{ Å}$, $b = 81.9 \text{ Å}$, $c = 74 \text{ Å}$ and $\alpha = 90^\circ$, $\beta = 105.8^\circ$, $\gamma = 90^\circ$. A total of 720 images were collected with an exposure of 10 s per frame, each covering an oscillation angle of 0.5° . The crystal to detector distance was set to 100 mm. Data collection was calculated by CrystalClear software and resulting intensity data were scaled and merged using XDS Suite programs. Relevant processing statistics are presented in Table 3.1.

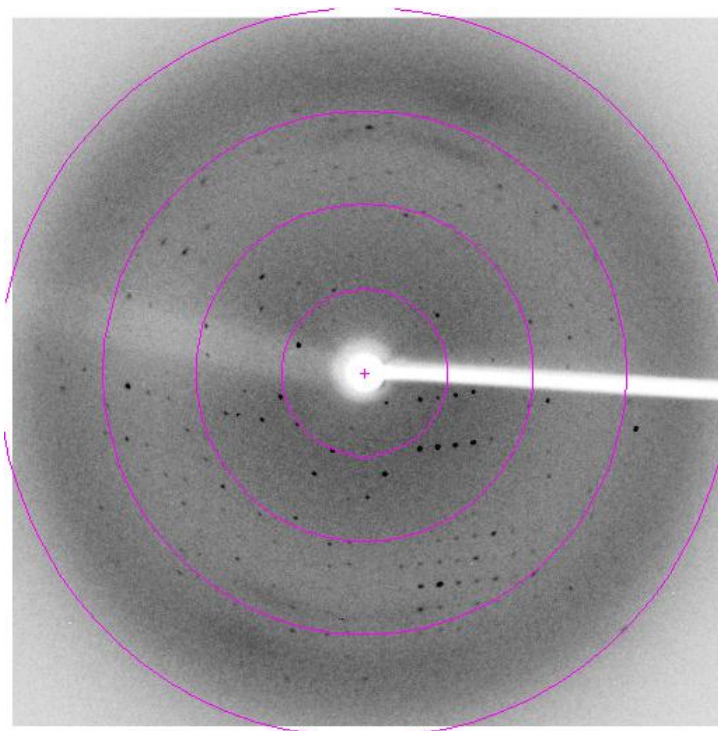


Figure 3.9: X-ray diffraction pattern generated from crystallised NKG2D-ULBP6*02 complex.

Resolution Limits	20 – 3.2 Å (3.3 – 3.2 Å)
Unit Cell Dimensions	a = 82.4 Å, b = 81.9 Å, c = 74 Å; α = 90°, β = 105.8°, γ = 90°
Space Group	C2
Total Observations	40,398 (2,133)
Unique Observations	7,336 (494)
Multiplicity	5.51 (4.32)
Completeness (%)	92.3 (70.5)
R _{merge} (%)	12.9 (49.4)
I/σI	13.1 (2.9)

Table 3.1: Data processing statistics for NKG2D-ULBP6*02 complex. X-ray diffraction data were processed using XDS Suite programs. Numbers in parentheses correspond to the highest resolution shell (3.3-3.2 Å).

Assuming the NKG2D-ULBP6*02 crystals have one molecule per asymmetric unit, the solvent content was determined as 52% (Kantardjieff & Rupp, 2003). To determine the NKG2D-ULBP6*02 structure, molecular replacement was used to calculate initial phase information. The only ULBP family molecule to have had X-ray diffraction data published in complex with NKG2D to date is ULBP3 (Radaev *et al*, 2001). Hence, the NKG2D-ULBP3 complex was used as the phasing model in the subsequent molecular replacement calculations. Despite identifying rotational and translational function solutions for the NKG2D dimer, no significant solutions were found for the ULBP6 molecule using the NKG2D-ULBP3 complex as the phasing model. This lack of success may be due to ULBP3 having structurally different regions to ULBP6. Indeed, sequencing studies have shown a 58% sequence homology between ULBP3 and ULBP6, which may have affected the superimposition process during molecular replacement. Although it is possible to use alternative methods such as multi-wavelength anomalous dispersion (MAD) or multiple isomorphous replacement (MIR) to solve the phase problem, it was deemed unfeasible due to the time constraints associated with this project. Alternatively, the failure of molecular replacement to provide phase information could be attributed to poor quality of the initial NKG2D-ULBP6*02 diffraction data. Hence, it was decided that a possible route for successful NKG2D-ULBP6*02 structure determination consisted of growing larger NKG2D-ULBP6*02 complex crystals in order to collect higher resolution data. Importantly, this would require the production of high levels of purified NKG2D and ULBP6*02 protein for crystallisation complex trials.

3.2.2 Expression and purification of NKG2D

Human NKG2D had previously been cloned into a pET23a vector. This expression vector was transformed into competent BL21 *E. coli* bacteria, which were then grown up in 4 L cultures. Analysis for expression of the NKG2D by SDS-PAGE showed an over-expressed band at approximately 15 kDa, which corresponds to the molecular weight of NKG2D of 15.82 kDa, as predicted from the primary sequence (Figure 3.10a). NKG2D inclusion bodies were then purified from culture lysate and solubilised in an 8M urea buffer (O'Callaghan *et al*, 1998). A typical yield of ~300 mg NKG2D inclusion body material was obtained from each 4 L culture. SDS-PAGE analysis of the inclusion body material suggested NKG2D was present in sufficiently high purity and quantity for refolding (Figure 3.10a). Following refolding by the Garboczi dilution method, re-natured NKG2D was purified by size exclusion chromatography (SEC) using an S200 column. A single major peak of around 300 mAU (per 50 mg of refolded inclusion bodies) was observed eluting at around 230 mL, which is consistent with dimeric NKG2D (~30 kDa), as determined by comparison with molecular weight standards (Figure 3.10b). Indeed, previous structural studies have shown that NKG2D crystallises as a dimer (Wolan *et al*, 2001). Corresponding fractions were pooled and analysed by SDS-PAGE for purity. A strong single band migrating at ~15 kDa confirmed monomeric NKG2D, and the sample was deemed suitable for crystallisation complex trials, despite the likely presence of dimeric NKG2D, represented by the band migrating at ~30 kDa in non-reducing conditions (Figure 3.10c).

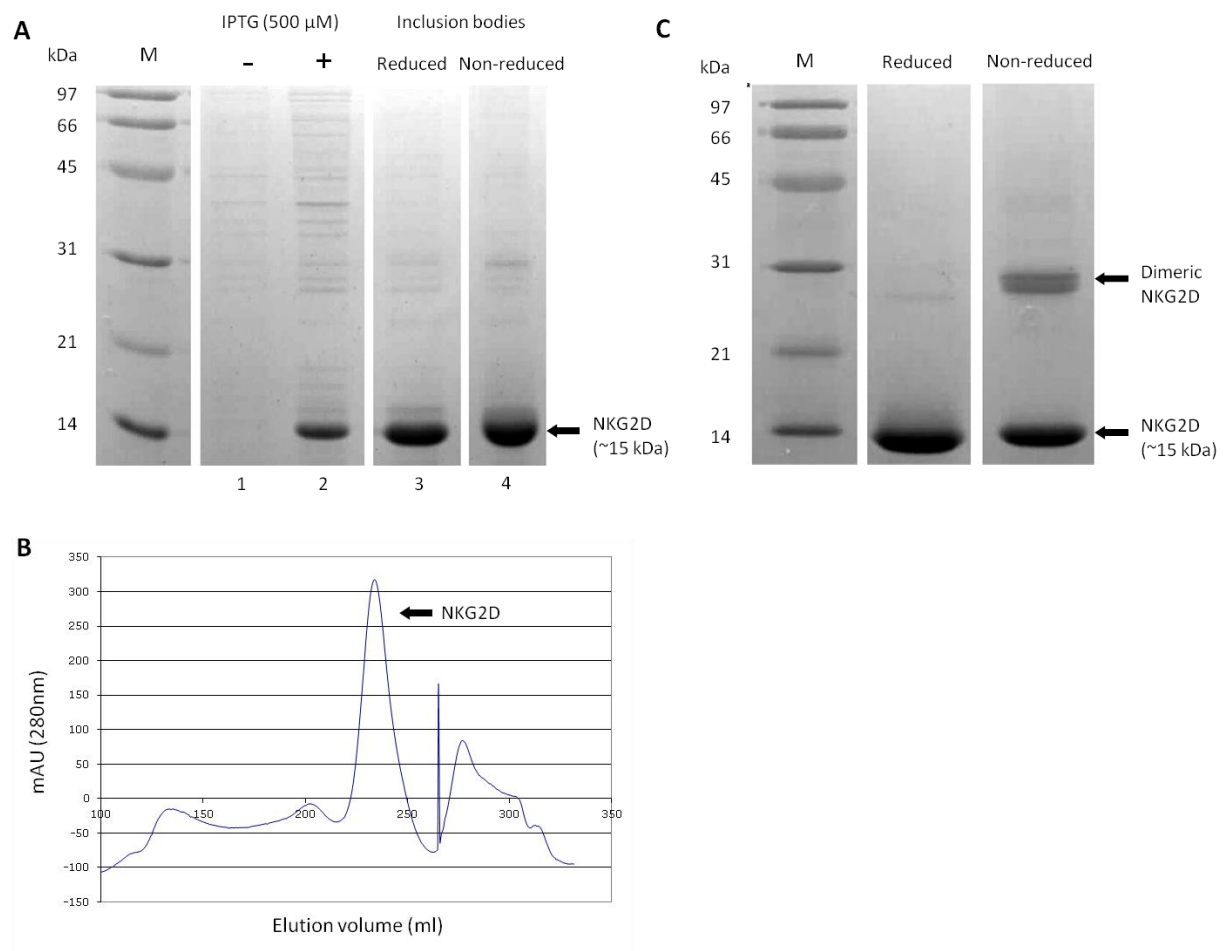


Figure 3.10: Expression and purification of E. coli derived NKG2D. (a) SDS-PAGE analysis of NKG2D-pET23 vector transformed BL-21 E. coli protein expression pre (- lane 1) and post (+ lane 2) IPTG induction. A strong band post IPTG induction at ~15 kDa corresponds with the predicted molecular weight of NKG2D. SDS-PAGE analysis of purified NKG2D inclusions following solubilisation in 8M urea under reducing (Lane 3) and non-reducing (Lane 4) conditions (b) Typical elution profile for NKG2D following purification by SEC (S200 column). A major peak at ~230 ml (310 mAU) is observed. (c) SDS-PAGE analysis of SEC peak fractions. The presence of a single band migrating at ~15 kDa confirms NKG2D and the level of purity is deemed suitable for complex crystallisation trials. The band at ~30 kDa under non-reducing conditions most likely represents the NKG2D homodimer.

3.2.3 Expression and purification of ULBP6

Human ULBP6*02 C14S SDM had previously been cloned into a pET23a expression vector. The C14S SDM was found necessary to prevent cross-dimerisation of ULBP6*02 by disulphide bridges forming between the C14 residues during refolding, which inhibited successful crystallisation in previous trials. Hereafter, ULBP6*02 C14S SDM will be referred to as ULBP6*02. The ULBP6*02-pET23a expression vector was transformed into Rosetta *E. coli* cells, which were grown up in 4 L cultures. Analysis for expression of ULBP6*02 by SDS-PAGE showed an over-expressed band at approximately 22 kDa, corresponding with the predicted molecular weight of ULBP6 of 20.48 kDa (Figure 3.11a). ULBP6*02 inclusion bodies were then purified from culture lysate and solubilised in 6M Guanidine-HCl before refolding. Transformations typically yielded ~300 mg inclusion bodies. Analysis of the inclusion body material showed the same bands migrating to ~22 kDa, indicating presence of ULBP6*02. Following refolding, ULBP6*02 was purified by SEC, typically yielding a major peak of around 100 mAU per 50 mg refold, eluting at around 235 mL. This is consistent with the predicted molecular weight of ULBP6*02, as confirmed by the molecular weight standards run on the same column (Figure 3.11b). Fractions corresponding with the major peak were pooled and analysed by SDS-PAGE (Figure 3.11c). Two distinct and strong bands are observed migrating at ~22 and 30 kDa, respectively. The 22 kDa most likely corresponds with ULBP6*02. A slight shift in the band migration to higher weight can be observed for ULBP6*02 under reducing conditions, which implies the protein is migrating at a slower rate because it is less compact without the disulphide bonds intact. This shift is evidence of ULBP6*02 protein refolding having taken place. There second band that migrates to around 30 kDa most likely represents an unidentified contaminant protein that has carried over from the inclusion body preparation. A further purification step would be necessary to isolate ULBP6*02 from the contaminant protein before proceeding with crystallisation complex trials.

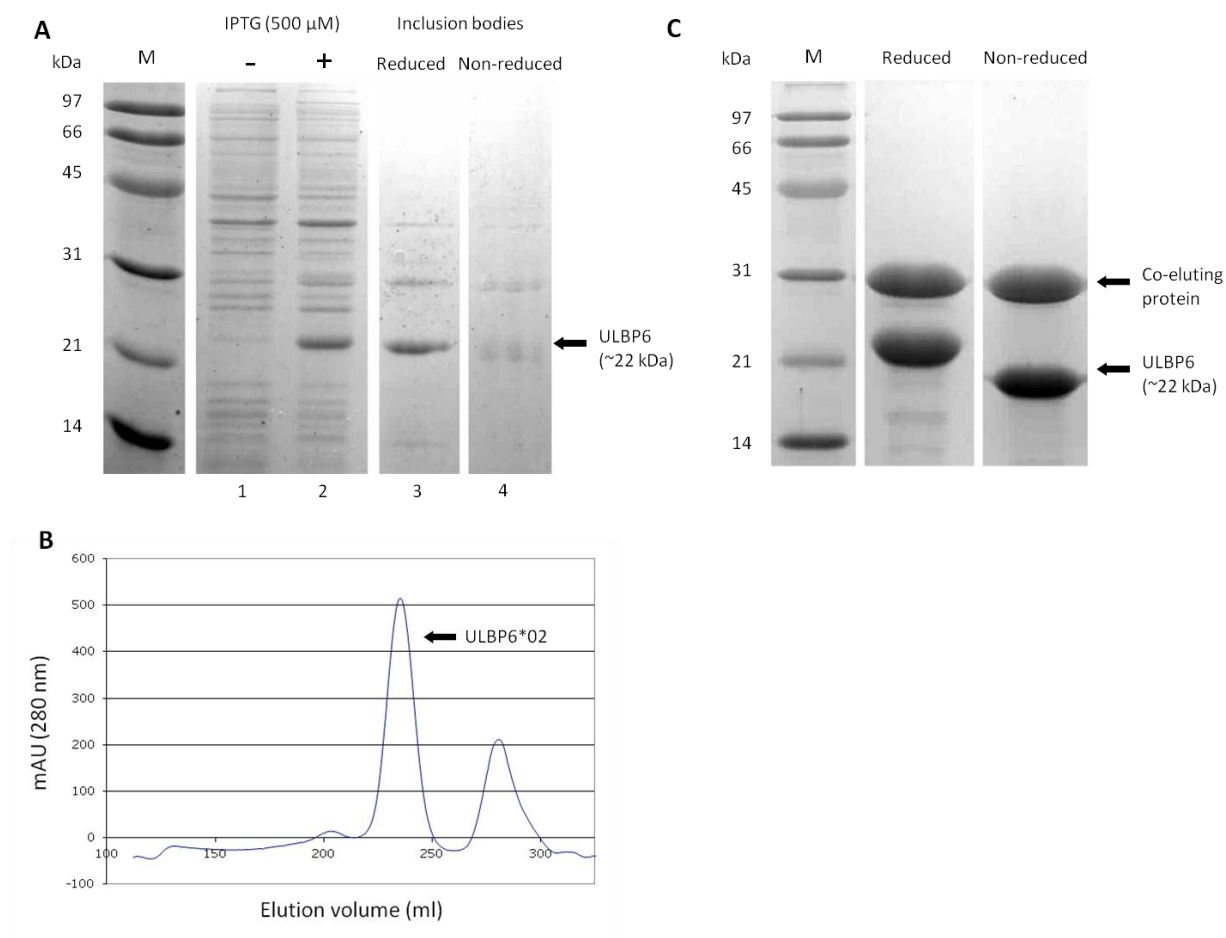


Figure 3.11: Expression and purification of *E. coli* derived ULBP6*02. (a) SDS-PAGE analysis of ULBP6-pET23 vector transformed Rosetta *E. coli* protein expression pre (- Lane 1) and post (+ Lane 2) IPTG induction. An over-expressed band post IPTG induction at ~22 kDa corresponds with the predicted molecular weight of ULBP6*02. SDS-PAGE analysis of purified ULBP6*02 inclusions following solubilisation in 6M G-HCl under reducing (Lane 3) and non-reducing (Lane 4) conditions (b) Typical elution profile for ULBP6*02 following purification by SEC (S200 column). A major peak at 235 ml (510 mAu) is observed. (c) SDS-PAGE analysis of SEC peak fractions. Two distinct bands are observed at ~22 kDa (corresponds to ULBP6*02) and ~30 kDa (represents a co-eluting contaminant).

To separate ULBP6*02 from the co-eluting contaminant protein, the fractions corresponding to the SEC major peak at ~235 mL were pooled, concentrated and purified by anion exchange chromatography (AEC), using a ResourceQ column. The resulting elution profile displayed two distinct peaks, one of around 65 mAU eluting at a NaCl gradient of around 8% and the other of around 100 mAU eluting at around 14% NaCl (Figure 3.12a). SDS-PAGE analysis of the two peaks showed Peak 1 contained a single band migrating at ~30 kDa, while Peak 2 contained a single band migrating at ~22 kDa, consistent with ULBP6*02 (Figure 3.12b). The shift towards higher molecular weight under reducing conditions seen before is evident here also. These results showed complete separation of the two proteins, and that ULBP6*02 was purified sufficiently to proceed with complex crystallisation trials.

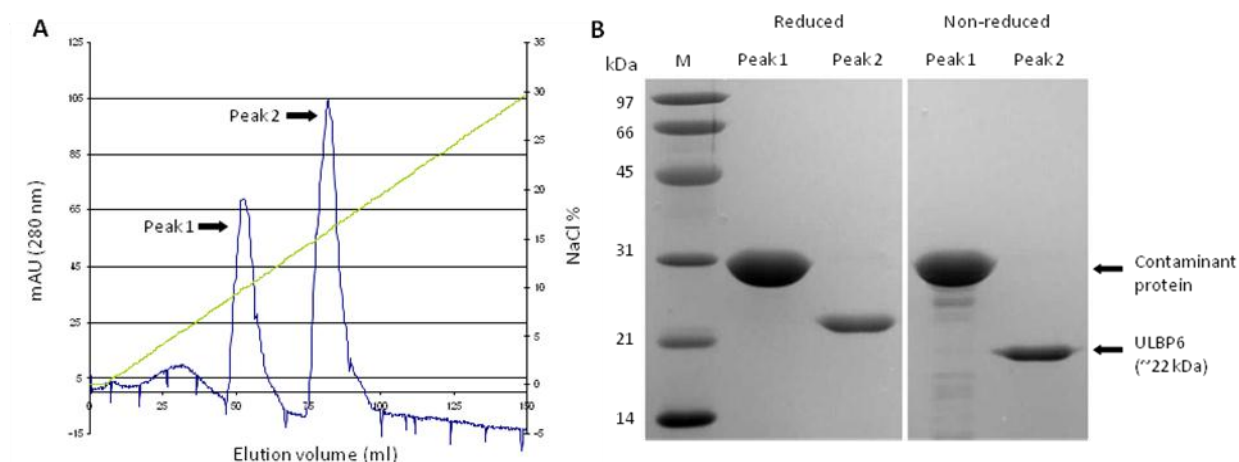


Figure 3.12: Additional purification of *E. coli* derived ULBP6*02 with AEC. (a) Typical elution profile for ULBP6*02 and contaminant protein using AEC (ResourceQ column). Two distinct peaks are observed; Peak 1 and Peak 2 elute at a NaCl gradient of 8 and 14%, respectively. (b) SDS-PAGE analysis of AEC Peaks 1 and 2. Peak 2 shows a band at ~22 kDa which corresponds to ULBP6*02, whereas Peak 1 contains a contaminant band (~30 kDa). This demonstrates that AEC has been effective at separating the contaminant and ULBP6*02 proteins. Peak 2 fractions were pooled and used for crystallisation trials.

3.2.4 NKG2D-ULBP6*02 crystallisation trials

Since the aim of these trials was to grow larger crystals than previously obtained (100 x 100 microns), up-scaling of the hanging drop equilibrating mixture was likely to be the best method of growing larger crystals. However, achieving successful large scale crystallisation proved to be difficult even though the crystals were reproducibly generated in small scale trials with the Mosquito crystallisation robot. Initially, reproduction of previously achieved crystallisation was sought, to confirm a solid base for large scale experiments. Previous small scale trials had found NKG2D-ULBP6*02 complex to crystallise at 12.4 mg/ml in three conditions from the Pact screen. To replicate this crystallisation, repeat small scale trials were performed using 100 nl complex protein at 12.4 mg/mL, equilibrated against 100 nl Pact screen 26 (0.1 M sodium propionate, sodium cacodylate, and BIS-TRIS propane buffer (PCB), pH 5.0 and 25% polyethylene glycol (PEG) 1500), 27 (as 26 but at pH 6.0) and 38 (0.1 M DL-malic acid, MES, Tris base (MMT), pH 5.0 and 25% PEG 1500). Crystallisation hits were observed in all 3 PACT conditions, with crystal sizes ranging between 5 and 25 microns in length, confirming that these conditions were a suitable start point for generating larger crystals (Figure 3.13a). The majority of the trials tended to produce showers of crystals, indicating an over abundance of nucleation sites. Furthermore, each of these drops exhibited uncharacteristically high levels of precipitation. One possibility for reducing the number of nucleation sites was to decrease the protein complex concentration. Therefore, subsequent small scale optimisation of the NKG2D-ULBP6 complex consisted of lowering the complex concentration from 12.4 mg/ml to 10.6 mg/ml. Alongside this strategy the size of the hanging drop sizes were increased (between 200 and 400 nl). Using this approach regular crystals of up to 160 microns were observed forming after 3 -5 days, with the complex at 10.6 mg/mL equilibrated against Pact screen 26 (Figure 3.13b). Finally, large scale crystallisation trials were performed using the same protein concentration and screen

condition, using 1 μ l NKG2D-ULBP6 complex. After failure to generate any crystals with 1:1 complex:screen mixtures, the experiments were repeated with complex equilibrated in between 1.5 and 3 μ l screen. Large crystals of up to 250 microns in length and 20 microns in depth formed after 3 – 5 days (Figure 3.13c). Several crystals from the optimised small-scale and large scale trials were selected and flash cooled in liquid nitrogen, ready for X-ray diffraction experiments.

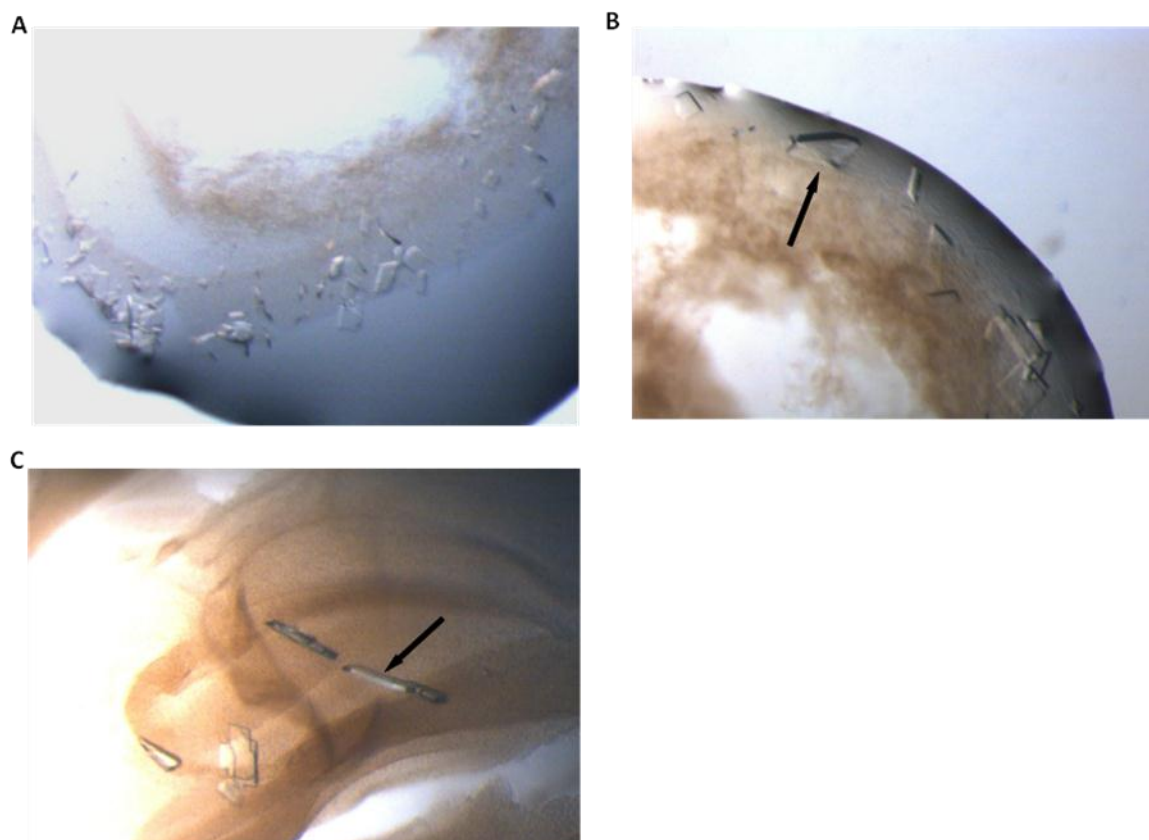


Figure 3.13: Crystallisation of the NKG2D-ULBP6*02 complex. (a) Crystals of NKG2D-ULBP6*02 complex were grown using the Mosquito robot. NKG2D-ULBP6 complex at 12.4 mg/ml (100 nl) was equilibrated against 0.1 M sodium propionate, sodium cacodylate, and BIS-TRIS propane buffer (PCB), pH 6.0 and 25% PEG 1500 (100nl), forming showers of small jagged crystals. (b) Small-scale optimisation of the NKG2D-ULBP6*02 crystals. NKG2D-ULBP6*02 complex at 10.6 mg/ml was equilibrated (400 nl) 0.1 M PCB buffer, pH 5.0 and 25% PEG 1500 (400 nl), forming regular crystals of up to 160 x 20 microns. (c) Large-scale optimisation of the NKG2D-ULBP6*02 crystals. NKG2D-ULBP6*02 complex at 10.6 mg/ml (1 μ l) was equilibrated against 0.1 M PCB buffer, pH 5.0 and 25% PEG 1500 (3 μ l), forming large crystals with depth. Crystals marked with an arrow were flash-cooled in liquid nitrogen for X-ray diffraction experiments.

DISCUSSION

Recent studies conducted on haematopoietic stem cell transplant (HSCT) patient cohorts have discovered a correlation between patient NKG2D-ligand ULBP6 alleles and overall survival following treatment (Antoun *et al*, 2012). Those patients possessing at least one copy of the second most common RAET1L gene (RAET1L*02), which encodes ULBP6*02, had a 14% better overall survival at 8 years post-transplant than those without. In addition, these patients had a 19% improved relapse-free survival (RFS) rate, and for RAET1L*02 homozygotes, this increased to 33%. There are several important aspects of this research to consider. Firstly, the change in survival correlates with patient (recipient) genotype and not donor genotype. Secondly, the data generated seems to indicate that the improved survival is likely due to increase in the so-called Graft versus Leukaemia effect (GvL), rather than decrease in the poor-outcome associated Graft versus Host disease (GvHD). Thirdly, the difference in improved survival rate in patients with ULBP6*02 is remarkably large considering the small differences in sequence between ULBP6*01 (the most common allele) and ULBP6*02, just two amino acids in the coding region. This large improvement suggests that ULBP6 in general is important as a focus of anti-tumour immune responses.

Successful HSCTs tend to work via two mechanisms. The first, and primary, mechanism is the repopulation of ablated recipient bone marrow, allowing the formation of a new, healthy lymphocyte population that can function in the recipient to restore a working non-malignant immune system (Thomas *et al*, 1975). The second mechanism is the targeting of residual tumour populations that have resisted the chemo- and radiotherapy treatment prior to transplant. This targeting is mediated by cytotoxic lymphocytes in the donor infusion that are capable of recognising stressed cells in the recipient, and eliminating them (Weiden *et al*, 1979). If ULBP6 is expressed on the surface of stressed cells in the host, then

the recognition and binding of these ligands with the NKG2D activating receptors on the donor cytotoxic cells could mediate GvL (Vivier *et al*, 2012). The fact that it is the recipient genotype for ULBP6 that correlates with improved survival in HSCTs is supportive of this hypothesis.

As well as attacking recipient tumour cells, donor lymphocytes can also instigate an auto-immune like response against recipient non-tumourigenic tissue (GvHD), which is often fatal. If the NKG2D-ULBP6*02 improvement in overall survival (OS) was due to reduced GvHD, one could expect there to be a correlation between expression of RAET1L*02 and reduced non-relapse related mortality, which was not the case. This suggests that improved GvL is the primary method by which ULBP6*02 expression in host cells contributes towards overall survival. Strong GvL effects are very hard to predict and vary from patient to patient (Kolb *et al*, 1995), so it is possible that genetic effects such as the possession of a RAET1L*02 gene could contribute to this variability.

Sequence comparison of the RAET1L*01 and RAET1L*02 gene revealed there to be only 2 coding amino acid changes from the *01 form to the *02 form, with structural modelling studies suggesting that one of these amino acid changes occurs in the ULBP6-NKG2D binding interface. In order to determine the molecular mechanism that underlies the Antoun *et al* results, this study undertook to measure the binding affinity of NKG2D for both allelic forms as well as for mutants of the ULBP6*02 protein that were generated with each amino acid altered individually to the ULBP6*01 sequence.

Following successful cloning, transfection and biotinylation of the two ULBP6*02 mutants L86R and T127I, SPR binding experiments were carried out to determine what the affinity of the NKG2D-ligand interaction was for both ULBP6*01 and *02, as well as the mutant intermediates. Binding affinities (K_d) of NKG2D with ULBP6*01 and ULBP6*02 were 144 nM and 11 nM respectively, which represents a 13-fold increase in affinity of the *02 form. This

data supports the hypothesis that increased affinity of NKG2D for ULBP6*02 over the *01 form is responsible for increased induced cytotoxicity, either by induction of a stronger or a more prolonged cytotoxic response, which in turn increases the GvL effect in RAET1L*02⁺ HSCT patients, leading to enhanced RFS. K_d of the L86R and T127I ULBP6*02 mutants with NKG2D were 114 nM and 11 nM respectively, which strongly suggests that it is the amino acid at position 86 that influences the NKG2D-ULBP6 interaction. This is consistent with the structural modelling data which suggest that amino acid position 86 is in the binding site, while 127 is distal to the NKG2D-ULBP6 binding interface. In ULBP6*02, amino acid 86 is a hydrophobic leucine residue that protrudes into an area of the NKG2D-ULBP6 binding interface that is predominantly hydrophobic. Hence, one would expect favourable hydrophobic interactions and corresponding high affinity for the NKG2D-ULBP6*02 interaction. However, introduction of a long, positively charged arginine side chain into this interface, as in the case of ULBP6*01, would be unfavourable for binding and therefore likely to be associated with a reduced affinity. Despite this, ULBP6*01 is the most common allele in Euro-Caucasoid populations (Antoun *et al*, 2010), which suggests there may be detrimental implications for those in possession of the higher affinity *02 form. One hypothesis would be that possession of the *02 form leads to higher incidence of auto-immune complications – NKG2D has often been cited as a mediator of auto-immunity (Caillat-Zucman, 2006). Alternately, ULBP6*01 may have a reduced affinity for the viral protein UL-16, which is produced by hCMV to avoid immunodetection of infected cells by binding to and sequestering stress ligands such as ULBP6.

It is clear that these affinities are both high with respect to those of NKG2D and its other ligands, where the highest previously recorded was for NKG2D-ULBP1 (Antoun, unpublished) at 228 nM, and the lowest for NKG2D-ULBP2 at 47,400 nM. With this in mind, could a change in affinity from “high” in the case of ULBP6*01 to “very high” in the case of *02, really be responsible for such a remarkable improvement in HSCT patient outcome? There

are several alternative hypotheses for the effect of ULBP6*02 expression, beyond improved killing due to higher affinity NKG2D-ULBP6*02 interactions. As well as there being two coding region polymorphisms between *01 and *02, there are 3 non-coding polymorphisms, and previous studies on other NKG2D ligands (NKG2DL) have shown that polymorphisms in the promoter regions do have an impact on gene expression (Rodriguez-Rodero *et al*, 2007). It is possible that ULBP6*02 has a higher rate of transcription due to a promoter region polymorphism, generating a higher cell surface expression and concomitant increased targeting by NKG2D-expressing lymphocytes. It is also plausible that a regulatory microRNA has a greater effect on the transcription of ULBP6*01 than it does on *02. hCMV-miR-UL112 has been shown to selectively downregulate MICB but not MICA, despite almost identical binding sites (Stern-Ginossar *et al*, 2007). The same group later identified many microRNAs that affect MICA/B transcription and that they are upregulated in cancer cells (Stern-Ginossar *et al*, 2008).

Alternately, ULBP6*02 may be more resistant to proteolytic cleavage from the cell surface by matrix metalloproteinases or endoplasmic reticulum protein 5, perhaps due to the T127I mutation which is putatively located on the membrane-facing side of the ULBP6 extracellular domain. Since cancer cells have been demonstrated to increase the shedding of extracellular domains of other NKG2D ligands (Kaiser *et al*, 2007), it is possible that ULBP6 is affected and that enhanced retention in the membrane of the *02 form would help maintain the cytotoxic response against the ULBP6-expressing cell, increasing killing. An important step in determining the relative importance of any of these mechanisms will be to examine the relative transcription and surface expression of the two alleles and identifying whether there is any difference, and if so, at which stage of the transcription, translation and surface expression sequence.

Whether any of these mechanisms have a role in the HSCT scenario needs further scrutiny, but the increased affinity of NKG2D for ULBP6*02 is certainly one possibly significant reason for improved outcome. In addition to the binding affinity, SPR experiments gave insight into the kinetics of the NKG2D-ULBP6 interaction. The dissociation constant (K_{off}) was $1.04 \times 10^{-2} \text{ s}^{-1}$ for ULBP6*01 and $7.64 \times 10^{-4} \text{ s}^{-1}$ for ULBP6*02, which suggests a slow dissociation in both cases but particularly in the case of ULBP6*02, with a NKG2D-ULBP6*02 complex half-life of around 15 minutes. When compared with T-cell receptor/ MHC interactions this is extremely long (Simpson *et al*, 2011; van der Merwe & Davis, 2003), and the biological implications are not entirely clear. On the one hand, this long receptor-ligand half-life may stimulate more potent cytotoxicity, but some models of receptor-ligand interaction have suggested that it is the number of separate receptor stimulations by ligand binding that act cumulatively to prompt the cell into cytolytic activity, rather than the absolute strength of the receptor-ligand interaction (Rabinowitz *et al*, 1996). This is likely the case with TCR-peptide MHC interactions, where it has been shown that activation is dependent not on affinity but on dissociation rate of ligand from the receptor (Lyons *et al*, 1996). If NKG2D-NKG2DL functioned in a similar fashion, this would suggest that ULBP6*02 may actually decrease the cytotoxicity of NKG2D-expressing lymphocytes through slow dissociation, reducing the number of interactions between ligand and receptor, as has been described for the interaction between TCR and peptide-MHC (Kalergis *et al*, 2001). Clearly this is counter-intuitive to the results presented by Antoun *et al*, but may provoke the need for an alternative hypothesis to explain the results found.

Tumour cells have been demonstrated to reduce NKG2D expression in circulating lymphocytes through chronic stimulation of their NKG2D receptors (Oppenheim *et al*, 2005). In some cases this occurs through over-expression of NKG2DL (McGilvray *et al*, 2010) which are shed either proteolytically or in exosomes and then bind in soluble form to NKG2D, and in other cases by prolonged binding to membrane anchored NKG2DL. It is possible that the

slowly dissociating ULBP6*02 ligand has a reduced capacity to downregulate NKG2D due to long and therefore relatively few interactions with NKG2D, as compared with ULBP6*01. This would effectively reduce the ability of ULBP6*02-expressing tumour cells to evade immune detection and elimination.

Another question raised by these data is that if possession of the RAET1L*02 gene has such a marked effect on survival, why is haematological malignancy still arising in the first place? The likely answer comes from this immunoediting hypothesis, where, in a diseased state, malignant cells reduce lymphocytic NKG2D expression and eventually evade immune detection. On transplant, donor lymphocytic cells with a full complement of NKG2D receptors are able to detect the malignant cells and destroy them. This lends weight to this idea that it is reduced immune evasion by malignant cells expressing ULBP6*02 that leads to enhanced patient survival, compared with those expressing ULBP6*01, since any residual leukaemic cells that evade the donor lymphocytes will likely do so again through the same immunoediting processes.

Although the data suggest that it is a GvL effect that is most likely responsible for the ULBP6 polymorphism effect on HSCT patient outcome, it is possible that there are also important indirect mechanisms involved. For example, if ULBP6 was expressed on the surface of recipient antigen presenting cells, which is quite possible considering the patient will have undergone chemo- and/or radiotherapy (Rosental *et al*, 2012), then enhanced killing of these cells by NKG2D-expressing donor lymphocytes could contribute to a reduced GvHD effect, and thereby likely improve patient overall survival.

There is no doubt that proving the structure of the NKG2D-ULBP6 complex would be beneficial in determining the molecular mechanism behind the improved ULBP6*02⁺ patient outcome. At present, differences in binding affinities of NKG2D for ULBP6*01 and *02 can only be explained by structural modelling and molecular predictions. There could be

conformational changes in NKG2D upon ligand binding which cannot be accounted for solely by modelling, particularly since the NKG2D binding site has been demonstrated to be flexible and accommodate a wide variety of ligands (Radaev *et al*, 2001). Only solving the crystal structure of the NKG2D-ULBP6*02 complex will allow these questions to be answered and the molecular mechanism to be confirmed. Following attempts to determine the structure of the complex from a crystal grown previously, which diffracted to 3.2 Å, additional crystals were grown following recombinant expression, refolding and purification of NKG2D and ULBP6*02. Despite exhaustive screening and optimisation strategies the best diffraction obtained from these crystals was 3.7 Å. Hence, there is a need to repeat large-scale crystallisation trials in order to produce better quality crystals and get a better diffraction dataset. Nevertheless, reproducibility on a large-scale is not always guaranteed when growing protein crystals, especially in complex, and this work has achieved this, so it is reasonable to predict that eventually diffraction-grade crystals will be grown on a large enough scale to generate high resolution data and solve the complex structure.

To fully elucidate the role of NKG2D and ULBP6 in the post-HSCT setting, it is vital that functional assays are performed to investigate which cytotoxic cells are responsible for the NKG2D-ULBP6 mediated killing, and in what proportion. As well as describing the relative potency of effector cells, such experiments may also be able to ascertain whether there is a functional difference in cytotoxic cells towards cells transfected with either ULBP6*01 or ULBP6*02, which would certainly help refine the mechanistic hypothesis. This work would have clinical implications for the HSCT setting, as it has become clear that pre-transplant conditioning regimes, as well as subsequent therapies such as T-cell infusions, are vitally important in affecting HSCT outcome. Defining the role of lymphocytic subsets in NKG2D-ULBP6 mediated anti-tumour effects may inform decisions made in treatment of haematological malignancies, which will build on the already apparent prognostic and stratification implications of ULBP6 genotype in HSCT patients.

REFERENCES

- Antoun A., Vekaria D., Salama R. A., Pratt G., Jobson S., Cook M., Briggs D. & Moss P. 2012. The genotype of RAET1L (ULBP6), a ligand for human NKG2D (KLK1), markedly influences the clinical outcome of allogeneic stem cell transplantation. *Br J Haematol.* 159 (5)589-598
- Antoun, A., Jobson, S., Cook, M., O'Callaghan, C.A., Moss, P., & Briggs, D.C. 2010. Single nucleotide polymorphism analysis of the NKG2D ligand cluster on the long arm of chromosome 6: Extensive polymorphisms and evidence of diversity between human populations. *Hum.Immunol.*, 71, (6) 610-620
- Becknell B., Caligiuri M. A. 2005. Interleukin-2, interleukin-15, and their roles in human natural killer cells. *Adv Immunol.* 86: 209-239
- Bennett N. J., Ashiru O., Morgan F. J., Pang Y., Okecha G., Eagle R. A., Trowsdale J., Sissons J. G., Wills M. R. 2010. Intracellular sequestration of the NKG2D ligand ULBP3 by human cytomegalovirus. *J Immunol.* 185 (2)1093-1102
- Blazar, B.R., Murphy, W.J., & Abedi, M. 2012. Advances in graft-versus-host disease biology and therapy. *Nat.Rev.Immunol.*, 12, (6) 443-458
- Bleakley M., Riddell S. R. 2004. Molecules and mechanisms of the graft-versus-leukaemia effect.
- Borrego F., Kabat J., Kim D. K., Lieto L., Maasho K., Peña J., Solana R., Coligan J. E. 2002. Structure and function of major histocompatibility complex (MHC) class I specific receptors expressed on human natural killer (NK) cells. *Mol Immunol.* 38 (9) 637-660
- Caillat-Zucman S. 2006. How NKG2D ligands trigger autoimmunity? *Hum Immunol.* 67 (3) 204-207
- Cao W., Xi X., Hao Z., Li W., Kong Y., *et al.* 2007. RAET1E2, a soluble isoform of the UL16-binding protein RAET1E produced by tumor cells, inhibits NKG2D-mediated NK cytotoxicity. *J. Biol. Chem.* 282 18922–28
- Cerwenka, A., Bakker, A.B., McClanahan, T., Wagner, J., Wu, J., Phillips, J.H., & Lanier, L.L. 2000. Retinoic acid early inducible genes define a ligand family for the activating NKG2D receptor in mice. *Immunity.*, 12, (6) 721-727
- Cerwenka, A., Lanier L. L. 2001. Natural killer cells, viruses and cancer. *Nat Rev Immunol.* 1 (1) 41-49

Champsaur M., Lanier L. L. 2010. Effect of NKG2D ligand expression on host immune responses. *Immunol Rev.* 235 (1) 267-285

Chang, C., Dietrich, J., Harpur, A.G., Lindquist, J.A., Haude, A., Loke, Y.W., King, A., Colonna, M., Trowsdale, J., & Wilson, M.J. 1999. Cutting edge: KAP10, a novel transmembrane adapter protein genetically linked to DAP12 but with unique signaling properties. *J.Immunol.*, 163, (9) 4651-4654

Choi B. K., Kim Y. H., Kang W. J., Lee S. K., Kim K. H., Shin S. M., Yokoyama W. M., Kim T. Y., Kwon B. S. 2007. Mechanisms involved in synergistic anticancer immunity of anti-4-1BB and anti-CD4 therapy. *Cancer Res.* 67 (18) 8891-8899

Cosman, D., Mullberg, J., Sutherland, C.L., Chin, W., Armitage, R., Fanslow, W., Kubin, M., & Chalupny, N.J. 2001. ULBPs, novel MHC class I-related molecules, bind to CMV glycoprotein UL16 and stimulate NK cytotoxicity through the NKG2D receptor. *Immunity.*, 14, (2) 123-133

Culpepper D. J., Maddox M. K., Caldwell A. B., McFarland B. J. 2011. Systematic mutation and thermodynamic analysis of central tyrosine pairs in polyspecific NKG2D receptor interactions. *Mol Immunol.* 48 (4) 516-523

Davis M. M., Boniface J. J., Reich Z., Lyons D., Hampl J., Arden B., Chien Y. 1998. Ligand recognition by alpha beta T cell receptors. *Annu Rev Immunol.* 16 523-544

Diefenbach A., Jamieson A. M., Liu S. D., Shastri N., Raulet D. H. 2000. Ligands for the murine NKG2D receptor: expression by tumor cells and activation of NK cells and macrophages. *Nat Immunol.* 1 (2) 119-126.

Diefenbach A., Raulet D. H. 2002. The innate immune response to tumors and its role in the induction of T-cell immunity. *Immunol Rev.* 188 9-21

Dunn C., Chalupny N. J., Sutherland C. L., Dosch S., Sivakumar P. V., Johnson D. C., Cosman D. 2003. Human cytomegalovirus glycoprotein UL16 causes intracellular sequestration of NKG2D ligands, protecting against natural killer cell cytotoxicity. *J Exp Med.* 197 (11) 1427-1439

Eagle, R. A., Jafferji I., Barrow A. D. 2009a. Beyond Stressed Self: Evidence for NKG2D Ligand Expression on Healthy Cells. *Curr Immunol Rev.* 5 (1) 22-34

Eagle, R. A., Trowsdale J. 2007. Promiscuity and the single receptor: NKG2D. *Nat Rev Immunol.* 7 (9) 737-744

Eagle, R.A., Traherne, J.A., Hair, J.R., Jafferji, I., & Trowsdale, J. 2009b. ULBP6/RAET1L is an additional human NKG2D ligand. *Eur.J.Immunol.*, 39, (11) 3207-3216

Espinoza J. L., Takami A., Yoshioka K., Nakata K., Sato T., Kasahara Y., Nakao S. 2012. Human microRNA-1245 down-regulates the NKG2D receptor in natural killer cells and impairs NKG2D-mediated functions. *Haematologica*. 97 (9) 1295-1303

Fernández-Messina L., Reyburn H. T., Valés-Gómez M. 2012. Human NKG2D-ligands: cell biology strategies to ensure immune recognition. *Front Immunol*. 3 299

Garboczi, D.N., Hung, D.T., & Wiley, D.C. 1992. HLA-A2-peptide complexes: refolding and crystallization of molecules expressed in *Escherichia coli* and complexed with single antigenic peptides. *Proc.Natl.Acad.Sci.U.S.A*, 89, (8) 3429-3433

Garrity, D., Call, M.E., Feng, J., & Wucherpfennig, K.W. 2005. The activating NKG2D receptor assembles in the membrane with two signaling dimers into a hexameric structure. *Proc.Natl.Acad.Sci.U.S.A*, 102, (21) 7641-7646

Gatti RA, Good RA. 1971. Occurrence of malignancy in immunodeficiency diseases. A literature review. *Cancer*. 28 (1) 89-98

Gilfillan S., Ho E. L., Cella M., Yokoyama W. M., Colonna M. 2002. NKG2D recruits two distinct adapters to trigger NK cell activation and costimulation. *Nat Immunol*. 3 (12) 1150-1155

Goker, H., Haznedaroglu, I.C., & Chao, N.J. 2001. Acute graft-vs-host disease: pathobiology and management. *Exp.Hematol.*, 29, (3) 259-277

Groh V., Wu J., Yee C., Spies T. 2002. Tumour-derived soluble MIC ligands impair expression of NKG2D and T-cell activation. *Nature*. 419 (6908) 734-738

Groh, V., Bahram, S., Bauer, S., Herman, A., Beauchamp, M., & Spies, T. 1996. Cell stress-regulated human major histocompatibility complex class I gene expressed in gastrointestinal epithelium. *Proc.Natl.Acad.Sci.U.S.A*, 93, (22) 12445-12450

Groh, V., Rhinehart, R., Randolph-Habecker, J., Topp, M.S., Riddell, S.R., & Spies, T. 2001. Costimulation of CD8 α T cells by NKG2D via engagement by MIC induced on virus-infected cells. *Nat.Immunol.*, 2, (3) 255-260

Guerra, N., Tan, Y.X., Joncker, N.T., Choy, A., Gallardo, F., Xiong, N., Knoblaugh, S., Cado, D., Greenberg, N.M., & Raulet, D.H. 2008. NKG2D-deficient mice are defective in tumor surveillance in models of spontaneous malignancy. *Immunity*., 28, (4) 571-580

Houchins, J.P., Yabe, T., McSherry, C., & Bach, F.H. 1991. DNA sequence analysis of NKG2, a family of related cDNA clones encoding type II integral membrane proteins on human natural killer cells. *J.Exp.Med.*, 173, (4) 1017-1020

Hubbard T. J., Aken B. L., *et al.* 2007. Ensembl 2007. *Nucleic Acids Res*. 35(Database issue):D610-7

Jamieson, A.M., Diefenbach, A., McMahon, C.W., Xiong, N., Carlyle, J.R., & Raulet, D.H. 2002. The role of the NKG2D immunoreceptor in immune cell activation and natural killing. *Immunity*, 17, (1) 19-29

Jinushi M., Vanneman M., Munshi N. C., Tai Y. T., Prabhala R. H., *et al.* 2008. MHC class I chain-related protein A antibodies and shedding are associated with the progression of multiple myeloma. *Proc. Natl. Acad. Sci. USA* 105 1285–90

Jung H., Hsiung B., Pestal K., Procyk E., Raulet D. H. 2012. RAE-1 ligands for the NKG2D receptor are regulated by E2F transcription factors, which control cell cycle entry. *J Exp Med*. 209 (13) 2409-2422

Kabsch W. XDS. 2010. *Acta Crystallogr D Biol Crystallogr*. 66 (Pt 2) 125-132

Kaiser B. K., Yim D., Chow I. T., Gonzalez S., Dai Z., Mann H. H., Strong R. K., Groh V., Spies T. 2007. Disulphide-isomerase-enabled shedding of tumour-associated NKG2D ligands. *Nature*. 447 (7143) 482-486

Kalergis A. M., Boucheron N., Doucey M. A., Palmieri E., Goyarts E. C., Vegh Z., Luescher I. F., Nathenson S. G. 2001. Efficient T cell activation requires an optimal dwell-time of interaction between the TCR and the pMHC complex. *Nat Immunol*. 2 (3) 229-234

Kantardjieff K. A., Rupp B. 2003. Matthews coefficient probabilities: Improved estimates for unit cell contents of proteins, DNA, and protein-nucleic acid complex crystals. *Protein Sci*. 12 (9) 1865-1871.

Kasahara M, Yoshida S. 2012. Immunogenetics of the NKG2D ligand gene family. *Immunogenetics*. 64 (12) 855-867

Kolb H. J. 2008. Graft-versus-leukemia effects of transplantation and donor lymphocytes. *Blood*. 112 (12) 4371-4383

Kolb H. J., Schattenberg A., Goldman J. M., Hertenstein B., Jacobsen N., Arcese W., Ljungman P., Ferrant A., Verdonck L., Niederwieser D., van Rhee F., Mittermueller J., de Witte T., Holler E., Ansari H; European Group for Blood and Marrow Transplantation Working Party Chronic Leukemia. 1995. Graft-versus-leukemia effect of donor lymphocyte transfusions in marrow grafted patients. *Blood*. 86 (5) 2041-2050

Lee J. C., Lee K. M., Kim D. W., Heo D. S. 2004. Elevated TGF- β 1 secretion and down-modulation of NKG2D underlies impaired NK cytotoxicity in cancer patients. *J. Immunol*. 172 7335–40

Li, P., Morris, D.L., Willcox, B.E., Steinle, A., Spies, T., & Strong, R.K. 2001. Complex structure of the activating immunoreceptor NKG2D and its MHC class I-like ligand MICA. *Nat.Immunol.*, 2, (5) 443-451

Liu X. V., Ho S. S., Tan J. J., Kamran N., Gasser S. 2012. Ras activation induces expression of Raet1 family NK receptor ligands. *J Immunol.* 189 (4) 1826-1834

Lyons, D. S., Lieberman, S. A., Hampl, J., Boniface, J. J., Chien, Y., Berg, L. J., and Davis, M. M. 1996. A TCR binds to antagonist ligands with lower affinities and faster dissociation rates than to agonists. *Immunity* 5, 53-61.

McGilvray R. W., Eagle R. A., Rolland P., Jafferji I., Trowsdale J., Durrant L. G. 2010. ULBP2 and RAET1E NKG2D ligands are independent predictors of poor prognosis in ovarian cancer patients. *Int J Cancer.* 127 (6) 1412-1420

McGilvray R. W., Eagle R. A., Watson N. F., Al-Attar A., Ball G., Jafferji I., Trowsdale J., Durrant L. G. 2009. NKG2D ligand expression in human colorectal cancer reveals associations with prognosis and evidence for immunoediting. *Clin Cancer Res.* 15 (22) 6993-7002

McSweeney, P.A., Niederwieser, D., Shizuru, J.A., Sandmaier, B.M., Molina, A.J., Maloney, D.G., Chauncey, T.R., Gooley, T.A., Hegenbart, U., Nash, R.A., Radich, J., Wagner, J.L., Minor, S., Appelbaum, F.R., Bensinger, W.I., Bryant, E., Flowers, M.E., Georges, G.E., Grumet, F.C., Kiem, H.P., Torok-Storb, B., Yu, C., Blume, K.G., & Storb, R.F. 2001. Hematopoietic cell transplantation in older patients with hematologic malignancies: replacing high-dose cytotoxic therapy with graft-versus-tumor effects. *Blood*, 97, (11) 3390-3400

Meehan K. R., Talebian L., Tosteson T. D., Hill J. M., Szczepiorkowski Z., Sentman C. L., Ernstoff M. S. 2013 Adoptive cellular therapy using cells enriched for NKG2D+CD3+CD8+T cells after autologous transplantation for myeloma. *Biol Blood Marrow Transplant.* 19 (1) 129-137

van der Merwe, P. A., Davis, S. J. 2003. Molecular interactions mediating T cell antigen recognition. *Annu Rev Immunol.* 21 659-684

Molinero L. L., Fuertes M. B., Girart M. V., Fainboim L., Rabinovich G. A., Costas M. A., Zwirner N. W. 2004. NF-kappa B regulates expression of the MHC class I-related chain A gene in activated T lymphocytes. *J Immunol.* 173 (9) 5583-5590

Moretta L., Locatelli F., Pende D., Marcenaro E., Mingari M. C., Moretta A. 2011. Killer Ig-like receptor-mediated control of natural killer cell alloreactivity in haploidentical hematopoietic stem cell transplantation. *Blood.* 117(3) 764-771

Muller, S., Zocher, G., Steinle, A., & Stehle, T. 2010. Structure of the HCMV UL16-MICB complex elucidates select binding of a viral immunoevasin to diverse NKG2D ligands. *PLoS.Pathog.*, 6, (1) e1000723

Nausch N., Cerwenka A. 2008. NKG2D ligands in tumor immunity. *Oncogene.* 27 (45) 5944-5958

Nice T. J., Coscoy L. , Raulet D. H. 2009 Posttranslational regulation of the NKG2D ligand Mult1 in response to cell stress. *J Exp Med.* 206 (2) 287-298

O'Callaghan C. A., Tormo J., Willcox B. E., Blundell C. D., Jakobsen B. K., Stuart D. I., McMichael A. J., Bell J. I., Jones E. Y. 1998. Production, crystallization, and preliminary X-ray analysis of the human MHC class Ib molecule HLA-E. *Protein Sci.* 1998 7 (5) 1264-1266

Oppenheim D. E., Roberts S. J., Clarke S. L., Filler R., Lewis J. M., Tigelaar R. E., Girardi M., Hayday A. C. 2005 Sustained localized expression of ligand for the activating NKG2D receptor impairs natural cytotoxicity in vivo and reduces tumor immunosurveillance. *Nat Immunol.* 6 (9) 928-937

Park Y. P., Choi S. C., Kiesler P., Gil-Krzewska A., Borrego F., Weck J., Krzewski K., Coligan J. E. 2011. Complex regulation of human NKG2D-DAP10 cell surface expression: opposing roles of the γ c cytokines and TGF- β 1. *Blood.* 118 (11) 3019-3027

Rabinowitz J. D., Beeson C., Lyons D. S., Davis M. M., McConnell H. M. 1996. Kinetic discrimination in T-cell activation. *Proc Natl Acad Sci USA* 93 (4) 1401-1405

Radaev S., Kattah M., Zou Z., Colonna M., Sun P. D. 2002. Making sense of the diverse ligand recognition by NKG2D. *J Immunol.* 169 (11) 6279-6285

Radaev S., Rostro B., Brooks A. G., Colonna M., Sun P. D. 2001. Conformational plasticity revealed by the cocrystal structure of NKG2D and its class I MHC-like ligand ULBP3. *Immunity.* 15 (6) 1039-1049

Radosavljevic M., Cuillerier B., Wilson M. J., Clément O., Wicker S., Gilfillan S., Beck S., Trowsdale J., Bahram S. 2002. A cluster of ten novel MHC class I related genes on human chromosome 6q24.2-q25.3. *Genomics* 79 (1) 114-123

Raulet, D. H. 2003. Roles of the NKG2D immunoreceptor and its ligands. *Nat.Rev.Immunol.*, 3, (10) 781-790 *Nat Rev Cancer.* 4 (5) 371-380

Raulet, D. H., Gasser S., Gowen B. G., Deng W., Jung H. 2013. Regulation of Ligands for the NKG2D Activating Receptor. *Annu Rev Immunol.* [Epub ahead of print]

Raulet, D. H., Guerra N. 2009. Oncogenic stress sensed by the immune system: role of natural killer cell receptors. *Nat Rev Immunol.* 9 (8) 568-580

Rincon-Orozco B., Kunzmann V., Wrobel P., Kabelitz D., Steinle A., Herrmann T. 2005. Activation of V gamma 9V delta 2 T cells by NKG2D. *J Immunol.* 175 (4) 2144-2151

Rodríguez-Rodero S., González S., Rodrigo L., Fernández-Morera J. L., Martínez-Borra J., López-Vázquez A., López-Larrea C. 2007. Transcriptional regulation of MICA and MICB: a

novel polymorphism in MICB promoter alters transcriptional regulation by Sp1. *Eur J Immunol.* 37 (7) 1938-1953

Rosental B., Appel M. Y., Yossef R., Hadad U., Brusilovsky M., Porgador A. 2012. The effect of chemotherapy/radiotherapy on cancerous pattern recognition by NK cells. *Curr Med Chem* 19 (12) 1780-1791

Routes JM, Ryan S, Morris K, Takaki R, Cerwenka A, Lanier LL. 2005. Adenovirus serotype 5 E1A sensitizes tumor cells to NKG2D-dependent NK cell lysis and tumor rejection. *J Exp Med.* 202 (11) 1477-1482

Ruggeri, L., Capanni, M., Urbani, E., Perruccio, K., Shlomchik, W.D., Tosti, A., Posati, S., Rogaia, D., Frassoni, F., Aversa, F., Martelli, M.F., & Velardi, A. 2002. Effectiveness of donor natural killer cell alloreactivity in mismatched hematopoietic transplants. *Science*, 295, (5562) 2097-2100

Simpson A. A., Mohammed F., Salim M., Tranter A., Rickinson A. B., Stauss H. J., Moss P. A., Steven N. M., Willcox B. E. 2011. Structural and energetic evidence for highly peptide-specific tumor antigen targeting via allo-MHC restriction. *Proc Natl Acad Sci U S A.* 108 (52) 21176-21181

Steinle A., Li P., Morris D. L., Groh V., Lanier L. L., Strong R. K., Spies T. 2001. Interactions of human NKG2D with its ligands MICA, MICB, and homologs of the mouse RAE-1 protein family. *Immunogenetics.* 53 (4) 279-287

Stern-Ginossar N., Elefant N., Zimmermann A., Wolf D. G., Saleh N., Biton M., Horwitz E., Prokocimer Z., Prichard M., Hahn G., Goldman-Wohl D., Greenfield C., Yagel S., Hengel H., Altuvia Y., Margalit H., Mandelboim O. 2007. Host immune system gene targeting by a viral miRNA. *Science.* 317 (5836) 376-381

Stern-Ginossar N., Gur C., Biton M., Horwitz E., Elboim M., Stanitsky N., Mandelboim M., Mandelboim O. 2008. Human microRNAs regulate stress-induced immune responses mediated by the receptor NKG2D. *Nat Immunol.* 9 (9) 1065-1073

Song H, Kim J, Cosman D, Choi I. 2006. Soluble ULBP suppresses natural killer cell activity via downregulating NKG2D expression. *Cell. Immunol.* 239:22–30

Textor S., Fiegler N., Arnold A., Porgador A., Hofmann T. G., Cerwenka A. 2011. Human NK cells are alerted to induction of p53 in cancer cells by upregulation of the NKG2D ligands ULBP1 and ULBP2. *Cancer Res.* 71(18):5998-6009

Thomas, E.D., Lochte, H.L., Jr., Cannon, J.H., Sahler, O.D., & Ferrebee, J.W. 1959. Supralethal whole body irradiation and isologous marrow transplantation in man. *J.Clin.Invest*, 38, 1709-1716

Upshaw J. L., Arneson L. N., Schoon R. A., Dick C. J., Billadeau D. D., Leibson P. J. 2006. NKG2D-mediated signaling requires a DAP10-bound Grb2-Vav1 intermediate and phosphatidylinositol-3-kinase in human natural killer cells. *Nat Immunol.* 7 (5) 524-532

Upshaw J. L., Leibson P. J. 2006. NKG2D-mediated activation of cytotoxic lymphocytes: unique signaling pathways and distinct functional outcomes. *Semin Immunol.* 18 (3) 167-175

Vagin, A., Teplyakov A. 1997. MOLREP: an automated program for molecular replacement. *J. Appl. Cryst.* (30), 1022-1025.

Van Belle T. L., von Herrath M. G. 2009. The role of the activating receptor NKG2D in autoimmunity. *Mol Immunol.* 47 (1) 8-11

Venkataraman G. M., Suci D., Groh V., Boss J. M., Spies T. 2007. Promoter region architecture and transcriptional regulation of the genes for the MHC class I-related chain A and B ligands of NKG2D. *J Immunol.* 178 (2) 961-9

Vivier, E., Ugolini, S., Blaise, D., Chabannon, C., & Brossay, L. 2012. Targeting natural killer cells and natural killer T cells in cancer. *Nat.Rev.Immunol.*, 12, (4) 239-252

Waldhauer I., Goehlsdorf D., Gieseke F., Weinschenk T., Wittenbrink M., *et al.* 2008. Tumor-associated MICA is shed by ADAM proteases. *Cancer Res.* 68 6368–76

Watson, A.A., Christou, C.M., & O'Callaghan, C.A. 2011. Expression, purification and crystallization of the human UL16-binding protein ULBP1. *Protein Expr.Purif.*, 79, (1) 44-48

Wittenbrink, M., Spreu, J., & Steinle, A. 2009. Differential NKG2D binding to highly related human NKG2D ligands ULBP2 and RAET1G is determined by a single amino acid in the alpha2 domain. *Eur.J.Immunol.*, 39, (6) 1642-1651

Wolan D. W., Teyton L., Rudolph M. G., Villmow B., Bauer S., Busch D. H., Wilson I. A. 2001. Crystal structure of the murine NK cell-activating receptor NKG2D at 1.95 Å. *Nat Immunol.* 2 (3)248-254

Wu, J., Song, Y., Bakker, A.B., Bauer, S., Spies, T., Lanier, L.L., & Phillips, J.H. 1999. An activating immunoreceptor complex formed by NKG2D and DAP10. *Science*, 285, (5428) 730-732

Zafirova, B., Wensveen, F.M., Gulin, M., & Polic, B. 2011. Regulation of immune cell function and differentiation by the NKG2D receptor. *Cell Mol.Life Sci.*, 68, (21) 3519-3529

Zhang C., Zhang J., Niu J., Zhou Z., Zhang J., Tian Z. 2008a. Interleukin-12 improves cytotoxicity of natural killer cells via upregulated expression of NKG2D. *Hum Immunol.* 69 (8) 490-500

Zhang C., Niu J., Zhang J., Wang Y., Zhou Z., Zhang J., Tian Z. 2008b. Opposing effects of interferon-alpha and interferon-gamma on the expression of major histocompatibility complex class I chain-related A in tumors. *Cancer Sci.* 99 (6) 1279-1286



**Investigating neuroblastoma mediated
immunosuppression**

STUART HUNTER

A thesis submitted to the University of Birmingham

for the degree of

Master of Research (Molecular and Cellular Biology)

Supervisors: Dr F. J. Mussai; Dr. C. De Santo, School of Cancer Sciences

Investigating neuroblastoma mediated immunosuppression

Neuroblastoma, the most common extracranial solid tumour in children, has a long term survival rate of 45% but a very poor outcome in high-risk categorised patients, despite aggressive current therapies. In order to develop more effective immunotherapies, it is critical that we understand the immune microenvironment fostered by neuroblastoma tumours. In this study, we investigated potential mechanisms employed by neuroblastoma in suppression of the host's immune response. Using neuroblastoma-derived cell lines, we established that neuroblastoma is capable of suppressing allogeneic T cell proliferation *in vitro*, and that this suppression is not dependent on cell: cell contact. Active Arginase II is present in suppressive cell lines, and inhibition of this enzyme restored T cell proliferation, suggesting for the first time enhanced arginine metabolism as a mechanism of immunosuppression in neuroblastoma. We then established that neuroblastoma-derived cell lines are capable of activating monocytes to CD68⁺ macrophages, and that these macrophages also suppressed T cell proliferation. Finally, using biopsied tumour material from neuroblastoma patients, we established arginase-dependent suppression of T cell proliferation and macrophage activation by neuroblastoma *ex vivo*, confirming the physiological relevance of the cell line data. These results support the hypothesis that neuroblastoma creates an immunosuppressive microenvironment that may enhance disease progression.

CONTENTS

INTRODUCTION	1
The cellular basis of immune homeostasis.....	45
Induction of T cell anergy	18
Regulatory T cells	18
Macrophage polarisation	18
Cancer Immunoediting	45
Tumour mediated immunosuppression	45
Tumour associated macrophages	18
Treg induction	18
Myeloid derived suppressor cells	18
Nutrient depletion	18
Neuroblastoma	45
The immunology of neuroblastoma	18
 PROJECT AIMS	 17
 MATERIALS AND METHODS.....	 18
Cell lines	18
Patient Samples.....	19
Isolation of T cells/ monocytes	20
T cell proliferation assays ..	21
Monocyte polarisation assay.....	22
Flow cytometry	22
Reverse transcription polymerase chain reaction (RT-PCR).....	23
Western blotting	24
Arginase activity assay	25
Enzyme linked immunosorbent assay (ELISA).....	25

RESULTS	31
Neuroblastoma-derived cell line mediated suppression of T cell activity.....	31
Neuroblastoma cell lines suppress T cell proliferation <i>in vitro</i>	31
Neuroblastoma-derived cell line suppression of T cell proliferation is dependent on the action of arginase enzymes.....	33
Suppressive neuroblastoma-derived cell lines express active Arginase II	34
Neuroblastoma-derived cell line mediated macrophage activation	45
Neuroblastoma tumour tissue is immunosuppressive and induces macrophage activation <i>ex vivo</i>.....	45
DISCUSSION.....	55
REFERENCES	62

INTRODUCTION

1.1 The cellular basis of immune homeostasis

During the course of a normal infection or other challenge to the immune system, the body launches a series of defences, beginning with an innate response mediated by macrophages and natural killer (NK) cells and, if necessary, following up with a dendritic cell (DC) and T cell-mediated adaptive response that confers immunological memory. In an adaptive immune response, T cells are activated by recognition of their cognate antigen being presented by major histocompatibility complex (MHC) molecules. Following activation, they then go on to rapidly proliferate and either directly destroy infected or damaged cells bearing their cognate antigen, or release a variety of pro- or anti-inflammatory cytokines that help to co-ordinate and regulate the immune response.

The majority of effector T cells are programmed to die once antigen stimulation is removed, and consequently the immune response is reduced once the pathogen that instigated the response has been destroyed. However, there are several additional mechanisms that exist to reduce or limit an immune response. In most cases these are likely linked to the avoidance of autoimmune effects brought about by unwanted reaction to self-antigen, but several pathological conditions, including cancer, can hijack these mechanisms for their own purposes.

1.1.1 Induction of T cell anergy

In healthy individuals, several homeostatic mechanisms exist to maintain a physiologically suitable number of circulating naive T-cells in the periphery. Although T-cells with a high avidity for self-antigens are removed from the T-cell population in the thymic selection process (Kappler *et al*, 1987), successful maturation of thymocytes requires suitable interaction with self-antigen presenting MHC molecules, as well as stimulation of the interleukin-7 (IL-7) receptor by IL-7 (Takada *et al*, 2009). However, some self-reactive naive T-cells will escape the thymic selection process and reach the periphery (Liu *et al*, 1995). One mechanism to overcome this problem is induction of T-cell anergy, that is, a non-responsive state, usually occurring when the TCR has been stimulated by cogent antigen recognition in the absence of a co-stimulatory factor such as CD28 (Schwartz, 2003). Cells so stimulated display impaired TCR signalling, and are blocked at the G1/ S checkpoint of the cell cycle, leading to a hyporesponsive quiescence. T cell anergy can also be induced by environmental cues processed by the serine-threonine protein kinase mammalian target of rapamycin (mTOR) (Chappert & Schwartz, 2010). T cells are highly metabolically active, and their activation has been shown to depend on the availability of a wide variety of nutrients in their microenvironment (Fox *et al*, 2005). These nutrients include amino acids such as tryptophan (Mellor *et al*, 2003), arginine (Munder *et al*, 2013), glutamine (Carr *et al*, 2010), cysteine and lysine (Cobbold *et al*, 2009), as well as glucose (Cham *et al*, 2008), oxygen and ATP. An absence of these causes the cell to switch from an anabolic active state to a catabolic anergic state, a process regulated in a large part by mTOR (Powell & Delgoffe, 2010). This enforced quiescence is thought to help reduce the energy burden required to maintain the large and diverse T cell population. Anergy can also be induced through the secretion of suppressive cytokines such as IL-4, IL-10 and IL-13 by IL-4 induced T_H2 CD4⁺ helper lymphocytes, which also serve to stimulate the B cell mediated humoral response.

1.1.2 Regulatory T cells

Although regulatory T cells (Tregs) have defied cast-iron classification since their discovery during the 1980s, T cells expressing CD4, CD25 and the transcription factor forkhead box P3 (Foxp3) are generally considered to have immunoregulatory function (Fontenot *et al*, 2003). They consist of around 5% of the total CD4⁺ T cell population (Wing & Sakaguchi, 2010). Natural Tregs (nTregs) are selected for and mature in the thymus, as normal effector T cells are. nTregs serve to suppress T cell autoreactivity as well as excessive and unwanted immune responses to non-self-antigens, although the molecular mechanism by which they do this is still the subject of debate (Sakaguchi *et al*, 2008). Naïve T cells also acquire Foxp3 expression in the periphery, often following stimulation by the immunosuppressive cytokine TGF- β (Chen *et al*, 2003) or interleukin-2 (IL-2) (Laurence *et al*, 2007). These are induced Tregs (iTreg), and are hypothesised to act as a braking mechanism to prevent excessive effector T cell mediated response in the periphery. Tregs function by several known mechanisms: out-competing naive T cells for interactions with antigen presenting cells (APCs) (Takahashi *et al*, 1998), modulating APC function through secretion of immunosuppressive cytokines (von Boehmer, 2005) and expression of cytotoxic T lymphocyte-associated molecule-4 (CTLA-4) (Read *et al*, 2000), and in some cases direct lysis or inactivation of effector T cells. As well as CTLA-4, important cell surface receptors expressed by Tregs include programmed cell death protein 1 (PD-1) and glucocorticoid-induced TNFR family related gene (GITR), both of which have been attributed with immunosuppression (Wang *et al*, 2009; Shimizu *et al*, 2002). In this fashion, Tregs provide an additional mechanism to T cell anergy induction in the control of immune responses, although evidence suggests cross-talk between the two pathways to maintain a sufficient level of immunosuppression in the periphery (Chappert *et al*, 2010).

1.1.3 Macrophage polarisation

Macrophages are functionally diverse myeloid derived cells with a vital role in the innate immune response. Perhaps the most widely recognised role of macrophages is in inflammation, where in response to microbial detection via Toll-like receptors and subsequent transcription factor nuclear factor- κ B (NF- κ B) activation, macrophages secrete proinflammatory chemokines and cytokines such as tumour necrosis factor α (TNF- α), interleukin-1 (IL-1), IL-12 and CC chemokine ligand 2 (CCL-2). These cytokines serve to promote inflammation and induce an adaptive response by attracting T cells to the site of infection. However, macrophages are capable of responding to a wide variety of extracellular signals in a number of functionally different manners, with two of the most important induced phenotypes mirroring those of the T_H1/ T_H2 lymphocyte polarisation following pathogenic challenge (Mosser & Edwards, 2008). “Classically activated” macrophages (M1) follow the T_H1 pattern of cytokine secretion (proinflammatory, as described above) and play a similar inflammatory role to the T_H1 cells of the adaptive immune response. M1 polarisation is driven by microbially derived stimulants such as lipopolysaccharide (LPS) or interferon- γ (IFN- γ). “Alternatively activated” macrophages (M2) broadly follow the T_H2 pattern of cytokine release and are involved in immunoregulation and tissue remodelling, plus a number of other functions (Gordon, 2003). M2 polarisation is driven by cytokines such as IL-4 or IL-13 via the signal transducer and activator of transcription 6 (STAT-6) intracellular signalling cascade, or interleukin-10 (IL-10) via the STAT-3 signalling cascade (Biswas *et al*, 2012). In a normal healthy immune system, M2 polarised macrophages are usually associated with the resolution phase of the immune response, and as such express immunosuppressive cytokines such as interleukin-10 (IL-10) and transforming growth factor β (TGF β Gong *et al*, 2012). In addition, they display increased levels of phagocytosis-associated surface receptors, such as the mannose receptor

CD-206, and scavenging receptor CD-163, increasing their capacity for post-infection clear up of dead cells. Further to varied cytokine release, differentially polarised macrophages also exhibit differential metabolisms of various molecules, such as glucose, lipids, iron and various amino acids, including arginine, cysteine and tryptophan (Biswas & Mantovani, 2012).

1.2 Cancer Immunoediting

The role of the immune system in detecting and eliminating nascent tumours (immune surveillance) has been a subject of debate for over 100 years. After initial hypotheses were proposed and then refuted, it wasn't until the 1990s that improved mouse models allowed researchers to address the question on a sound scientific basis. Their findings, and those of the considerable body of work that followed, suggest that the immune system does indeed play a role in the suppression of tumours.

As well as eliminating potentially tumourigenic viruses and suppressing a pro-tumourigenic inflammatory environment through pathogen elimination, cells of the immune system have been shown to react directly against neoplastic cells through recognition of upregulated stress-related surface molecules or cancer-specific antigens. In this way, the immune system is capable of killing many tumours before they become clinically recognizable. This is the "Elimination" phase of the cancer immunoediting concept proposed by Schreiber and colleagues, and if completed, the host will remain cancer free (Schreiber *et al*, 2011). The most immunogenic tumour cells will be eliminated rapidly, but on occasion some cells will evade immune detection. In this case, rapid outgrowth of the tumour may be prevented

through the action of the adaptive immune response, where a constantly evolving T cell population remain capable of keeping the nascent tumour in check – the “Equilibrium” phase. During this time, the immune system will place a lot of selective pressure on the tumour, and due to this the tumour may lose immunogenicity, mainly through loss of antigen, become insensitive to immune effector mechanisms, or create an environment whereby the immune response is dampened and rendered ineffectual. This is the “Escape” phase of cancer immunoediting, and since this phase leads to pathogenesis and detectable disease, much of the research in tumour immunology over the last 20 years has focused on elements of this phase in an effort to develop novel cancer therapies.

1.3 Tumour mediated immunosuppression

As described by the cancer immunoediting concept, eradication of many tumours is carried out by cells of both the adaptive and innate immune responses; cytotoxic T lymphocytes (CTLs) and natural killer (NK) cells respectively. Studies have shown the benefit of a high tumour infiltrate of CD8⁺ lymphocytes to positive patient outcome in a number of solid tumours, including breast cancer (Mahmoud *et al*, 2011), melanoma (Oble *et al*, 2009) and colorectal cancer (Galon *et al*, 2006). However, many attempts to stimulate this apparent anti-tumour activity, by methods such as vaccination or adoptive T cell transfer, have produced limited successful results, and this is thought to be due to the immunosuppressive environment created by the tumour itself. Several mechanisms have been identified by which tumour cells can suppress the immune response and promote tumour outgrowth (Rabinovich *et al*, 2007). Some of these pathways act on lymphoid lineage cells, either by disabling effector T cell function through secretion and/or expression of immunosuppressive or apoptosis inducing factors, or recruitment of regulatory cells to the tumour

microenvironment. Others act on the myeloid lineage cells, for example by arresting development of dendritic cells and monocytes, thereby forming populations of myeloid derived suppressor cells (MDSCs), or through recruitment and polarisation of macrophages to the immunosuppressive M2 phenotype. This section will look at each of these mechanisms in more detail.

1.3.1 Tumour associated macrophages

Inflammation has been termed the seventh hallmark of cancer (after Hanahan & Weinberg, 2000), as inflammatory conditions are linked with a pro-tumourigenic and metastatic microenvironment (Lin & Karin, 2007). In some cases, inflammation is directly attributed to the onset of cancer, for example, chronic hepatitis C infection is attributed with the development of hepatocellular carcinoma (HCC Levrero, 2006) and *Helicobacter pylori* infection has been linked with the onset of gastric cancer (Luigiano *et al*, 2012). A major component of any inflammatory response is the infiltration of macrophages, and indeed macrophages have been demonstrated, via immunohistochemical staining, to consist of a large proportion of the tumour mass in some solid tumours (Kelly *et al*, 1988). Increased tumour associated macrophage (TAM) burden has been linked with poor patient prognosis in several cancers, including Hodgkin's disease (Steidl *et al*, 2010) pancreatic (Kuruhara *et al*, 2011) and breast cancer (Tang, 2013). Tumour influence on macrophages and their fate is a major component of the immunomodulatory action of many tumours. Large areas of necrotic and hypoxic cells are common in many solid tumours, a condition that naturally instigates inflammation and the recruitment of macrophages (Doedens *et al*, 2010). In addition, increased recruitment of circulating monocytes to the tumour microenvironment is

mediated by chemokines such as CCL2 (Bailey *et al*, 2007), macrophage colony-stimulation factor (M-CSF Pyonteck *et al*, 2012) and CXCL12, secreted by neoplastic cells and the tumour associated stromal compartment. In this way, tumours both passively and actively recruit monocytes to their locality. Once present in the tumour microenvironment, the monocytes often differentiate favouring the M2 phenotype, as directed by tumour-secreted cytokines such as IL-10, TGF β , IL-4 and IL-13 (Biswas & Mantovani, 2010). These TAMs then foster tumour progression through a number of mechanisms; inhibitory modulation of cytotoxic T cells, secretion of pro-angiogenic and remodelling signals which in turn support tumour expansion and metastasis, and secretion of pro-survival and proliferation factors (Ruffell *et al*, 2012). Although the mechanisms remain unclear, studies in mice suggest TAMs can promote T cell anergy through the metabolism of available arginine, through activation of the enzymes arginase or inducible nitric oxide synthase (iNOS Choi *et al*, 2009). In addition TAMs in human HCC have been demonstrated to upregulate PD-L1 (Kuang *et al*, 2009), which instigates inhibition of activated T cells via the PD-1 receptor, and prostaglandin E2 (PGE2). TAMs secrete vascular endothelial growth factor, an important mediator of angiogenesis, which in turn has a positive impact on tumourigenesis (Stockmann *et al*, 2008) by improving blood supply and increasing available nutrients to the hyperproliferating tumour cells. M-CSF, as well as inducing macrophage recruitment, also serves to enhance TAM epidermal growth factor (EGF), which regulates epithelial cell migration and enhances tumour cell mobility (Wyckoff *et al*, 2004). TAMs also promote tissue remodelling through the secretion of matrix metalloproteinases and cathepsins, which allow tumour cell migration and metastasis (Kessenbrock *et al*, 2010).

1.3.2 Treg induction

Since Tregs compete with naïve T cells and inhibit the activity of effector T cells, their potential for disrupting the eradication of tumour cells by CTLs is clear. The role in suppressive T cells in the promotion of tumour development was proven by North and colleagues in the 1980s (North & Bursacker, 1984). Use of blocking antibody inoculation of mice has identified the CD4⁺ CD25⁺ Foxp3⁺ Tregs as prime instigators of this T cell mediated immunosuppression in cancer, where researchers found long term tumour immunity was conferred in mice after CD25⁺ cell knockout (Onizuka *et al*, 1999). Increased numbers of infiltrating Treg cells has been recorded in many human cancers including pancreatic and breast (Liyanage *et al*, 2002), and some studies have suggested that a high proportion of Treg in the tumour infiltrating lymphocyte population correlates with poor outcome (Perrone *et al*, 2008). Indeed, Curiel and co-workers showed that Tregs did indeed suppress tumour-specific CTL activity in ovarian cancer (Curiel *et al*, 2004). Observed Treg suppression in tumours is possibly a result of the fact that some nTregs will exist for the cancer-testis antigens, a collection of antigens expressed only by transformed cells and male germ cells, but most of the Tregs associated with tumours seem to be iTregs, likely induced by immunosuppressive cytokine release by the tumour cells, tumour-associated stromal cells or TAMs (Anthony *et al*, 2005).

1.3.3 Myeloid derived suppressor cells

Myeloid derived suppressor cells (MDSC) are a highly heterogeneous population of immature myeloid cells, precursors of dendritic cells, macrophages and granulocytes. In

healthy individuals, these immature myeloid cells will rapidly differentiate, but in the typically inflammatory tumour microenvironment, these cells are prevented from doing this, and they subsequently exert a highly immunosuppressive influence on the anti-tumour T cell population (Gabrilovich *et al*, 2012). In an active state, these cells are characterised by their production of arginase 1, iNOS, and/ or reactive oxygen species (ROS), and suppression of T cell activity, but they have no defined set of surface markers, making their identification challenging. Nevertheless, a large increase in apparent MDSC numbers has been demonstrated in studies of cancer patient blood samples (Görgün *et al*, 2013).

Several molecular instigators of MDSC formation have been attributed to various cancers, including cell surface expression and/or secretion of M-CSF, IL-6, PGE2, cyclooxygenase 2 (COX-2) and VEGF (Lechner *et al*, 2010). These factors mostly act through the Janus kinase (JAK) proteins and STAT3 transcription factor signalling cascade to increase the survival and proliferation of the immature myeloid cells, thereby preventing differentiation and promoting MDSC expansion (Gabrilovich & Nagaraj, 2009). In addition to the pro-survival signalling, activation of the suppressive MDSC phenotype seems to require the presence of factors secreted by activated T cells or tumour-associated stromal cells, factors such as IFN- γ , IL-4 and TLR ligands.

Active MDSC suppress T cell activity through the action of arginase I and iNOS, both of which deplete L-arginine availability in the microenvironment, causing decreased expression of the CD3 ζ -chain of the T cell receptor (TCR) complex, resulting in a loss of antigen signalling capability and T cell anergy (Raber *et al*, 2012). MDSC have also been demonstrated to secrete ROS and peroxynitrite, both powerful suppressors of T cell activity through

modification of the TCR and other vital proteins (Nagaraj *et al*, 2007). Mouse model work has demonstrated that MDSC have a role in the formation of iTregs, adding another potential layer of suppressive activity to this population of cells (Huang *et al*, 2006).

1.3.4 Nutrient depletion

In addition to the MDSC-derived nutrient depleting enzymes, many tumours have been demonstrated to upregulate catabolic enzymes themselves (Singer *et al*, 2011). Indolamine-2,3-dioxygenase (IDO) degrades tryptophan into kynurenine which subsequently downregulates T cell expression of the TCR CD3 ζ -chain through a lack of available tryptophan (Fallarino *et al*, 2006). IDO expression and activity has been documented in prostate, cervical and pancreatic cancers, and elevated serum levels of tryptophan catabolites have been linked with poor prognosis in colorectal cancer patients (Brandacher *et al*, 2006). Arginine depletion by tumour-derived arginase II has been detected in acute myeloid leukaemia (Mussai *et al*, 2013), as well as in several tumour derived cell lines (Tate *et al*, 2008). Neoplastic cells generally exhibit altered metabolism, relying on glycolysis for energy production (Warburg, 1961). The resulting depletion of glucose and high levels of lactate in the microenvironment has been shown via *in vitro* studies to suppress CTL activity (Fischer *et al*, 2007).

1.4 Neuroblastoma

Neuroblastoma is a neuroendocrine tumour of the sympathetic nervous system, developing from neural crest areas including adrenal glands and nerves of the neck, chest and abdomen. It is the most common extracranial solid tumour in children, accounting for approximately

9% of all childhood cancers, and has a long-term survival rate of 45%, although the rate for those diagnosed with “high-risk” metastatic Stage IV disease is much worse, with only one third of patients so diagnosed expected to survive (Schmidt *et al*, 2005). Infants under 12 months of age diagnosed with neuroblastoma are the most successfully treated; spontaneous disease regression has been noted in some cases (Carvalho, 1973). Neuroblastoma in older children often does not present until metastasis has occurred, and the predominant methods of treatment for these high risk patients is aggressive chemotherapy and stem-cell transplantation, with generally poor outcome and relapse remains common (Matthay *et al*, 1999). These variations in disease pathologies seem to be characterised by distinct genetic and biological characteristics. Advance stage neuroblastoma tumours tend to be associated with amplification of the *N-myc* gene and with loss or rearrangement of part of the short arm of chromosome 1 (Brodeur *et al*, 1984). p73, which has structural and functional homologies to the p53 tumour suppressor gene, has been mapped to this region. *N-myc* is an oncogene encoding a transcription factor that promotes hyperproliferation.

1.4.1 The immunology of neuroblastoma

As with many cancers, recent efforts into the treatment of neuroblastoma have looked, amongst other avenues, at immunotherapy as a potential addition to traditional chemo- and radiotherapies and/ or surgery. Despite neuroblastoma cells often exhibiting the cancer testis-antigen melanoma antigen-1 (MAGEA1 Corrias *et al*, 1996) and apparently tumour-specific antigen disialoganglioside 2 (GD2 Wu *et al*, 1986), no natural immune response to these peptides has been reported. Although engineering reactive T cells specific to these

antigens or other neuroblastoma related peptides such as the anti-apoptotic protein survivin (Coughlin *et al*, 2006; Fest *et al*, 2009) remains a viable source of potential immunotherapies, any successful immunotherapy will require knowledge of any immunosuppressive mechanisms used by the tumour to evade elimination. Consequently, a body of work dedicated to understanding the interaction of neuroblastoma and the immune system is gradually being built up by numerous groups.

Lymphocyte-mediated inhibition of cultured neuroblastoma cell line propagation was first demonstrated in 1968 (Hellström *et al*, 1968), although there is only limited data to document the infiltration of CTLs in neuroblastoma. CD3⁺ lymphocytes (CTLs and NK cells) have been observed by immunohistochemistry in neuroblastoma tumour sections (Apps *et al*, 2013), but several factors have been demonstrated to be released by neuroblastoma that have a negative regulatory effect on T cells. These factors include solubilised MHC-Class 1 polypeptide-related sequence A (MICA), which when membrane bound acts as a stress ligand that is recognised by the NKG2D receptor of NK cells and CTLs but in soluble form down-regulates the same receptors on the surface of the effector cells (Raffaghello *et al*, 2004). In addition, neuroblastoma cells have been demonstrated to secrete galectin-1 (Gal-1), which induces apoptosis in T cells and DCs (Soldati *et al*, 2011), and macrophage migratory inhibitory factor, which has been demonstrated to inhibit T lymphocyte activation both *in vitro* (Yan *et al*, 2006) and *in vivo* (Zhou *et al*, 2008). One study also demonstrated that neuroblastoma expressed membrane bound TNF- α was capable of inducing CXCL20 chemokine ligand 20 (CCL20) expression in TAMs, which attracted invariant NKT cells to the hypoxic tumour microenvironment, where they are rendered anergic (Liu *et al*, 2012).

Tumour associated macrophages have been observed in neuroblastoma, and their presence has been correlated with worsened 5-year prognosis (Song *et al*, 2009), as well as more advanced stage of disease progression (Asgharzadeh *et al*, 2012). This study also confirmed a higher proportion of these TAMs were M2 polarised in Stage IV disease, as determined by surface expression of the scavenging receptor CD163. In addition to the immunosuppressive effects detailed earlier, Morandi and colleagues discovered the release of soluble HLA-G (sHLA-G) non-classical MHC class 1 molecules by neuroblastoma-associated macrophages correlated with relapse. sHLA-G inhibits CTL and NK response through CD8 ligation mediated apoptosis or upregulation of the Fas ligand, inducing Fas mediated cell death (Morandi *et al*, 2007). Interestingly, it appears there may be a difference in the immune infiltrate of paediatric cancers compared with inflammation-associated adult cancers, with apparent heavier macrophage burden and reduced lymphocyte and DC burden in paediatric solid tumours (Vakkila *et al*, 2006). The mechanism of macrophage activation and polarisation has not been defined, however.

Little evidence exists for an immunosuppressive role of Tregs in neuroblastoma, although the STAT-3 pathway has been observed to be up-regulated in neuroblastoma (Zeng *et al*, 2010), a pathway linked to induction of Tregs, reduction of CTL cytotoxicity and inhibition of DC differentiation, which may lead to MDSC formation (Yu *et al*, 2007). Myeloid cells with immunosuppressive activity have been found in the blood and tumour of neuroblastoma patients (Santilli *et al*, 2013) although Gowda and co-workers found MDSC to be reduced in high-risk versus low-risk neuroblastoma patients (Gowda *et al*, 2011). The exact role and effect of MDSC in neuroblastoma obviously remains unclear, and warrants further investigation.

Despite an increasing number of studies that attempt to document the interaction of neuroblastoma with the immune system, a great deal is still very poorly understood, regarding both the amplitude and the mechanism of any immunoregulatory effects of this tumour on both its microenvironment and host on a systemic level.

PROJECT AIMS

Primary Aim:

To determine the magnitude and mechanism of suppression of T cell proliferation mediated by neuroblastoma *in vitro*.

Secondary Aims:

- 1) To determine the magnitude and mechanism of suppression of T cell proliferation *in vitro* by co-culture of neuroblastoma-derived cell lines with allogeneic T cells.
- 2) To determine the effect of neuroblastoma-derived cell lines on allogeneic monocytes *in vitro*, and to establish the extent of immunosuppression mediated by co-cultured monocytes.
- 3) Reproduce any findings from secondary aims 1 and 2 in primary human neuroblastoma tumour samples.

MATERIALS AND METHODS

2.1 Cell lines

Five human neuroblastoma cell lines were obtained. IMR-32, isolated from a 1 year old male, exhibiting 1pdel chromosomal abnormality and N-myc amplification. LA-N-1, isolated from a 2 year old female, exhibiting 1pdel chromosomal abnormality and N-myc amplification. SK-N-AS, isolated from an 8 year old female, exhibiting 1pdel chromosomal abnormality but no N-myc amplification. Kelly, source unknown, which displays N-myc amplification. SK-N-MC isolated from a 14 year old female, a line originally thought to be neuroblastoma derived, but most likely Askin's tumour (Ewing family of tumours) in origin (Dunn *et al*, 1994). Cell lines were cultured in RPMI-1640 (Sigma), with 10% foetal calf serum (FCS), 2 mM L-glutamine, 1 mM sodium pyruvate, penicillin/ streptomycin (25 mg) and non-essential amino acids (1x), hereafter referred to as R10. Cell lines were split every 3-5 days, with fresh media added 24 hours before each experiment.

2.2 Patient Samples

Neuroblastoma tumour samples were kindly donated by Dr Carmel McConville, University of Birmingham. Neuroblastoma cells from patients were obtained by chopping freshly-excised neuroblastoma tumours into small pieces and digesting them with collagenase (Worthington Biochemical Corporation) for 30 minutes at 37°C. Following this step, digested material was filtered using a cell strainer and neuroblastoma cells were purified by incubation with anti-GD2-PE antibody for 20 minutes followed by incubation with anti-PE coated magnetic beads (Miltenyi Biotec).

2.3 Isolation of T cells/ monocytes.

Human peripheral blood mononuclear cells (PBMC) were isolated from the blood of healthy donors using a Ficoll gradient (Lymphoprep™, Fresenius Kabi Norge AS, density 1.077 ± 0.001 g/ml). Following blood separation by centrifugation at 2,000 rpm for 30 minutes, PBMC were collected from the “ring” using a Pasteur pipette and collected, washed in phosphate buffered saline (PBS) with 10% bovine serum albumin (BSA), then incubated at 4°C for 20 minutes with anti-CD14 coated magnetic beads (Miltenyi Biotec) to allow purification of CD14⁺ monocytes. This mixture was washed again in PBS + 10% BSA (MACS buffer), before being resuspended in 2 ml MACS buffer and injected onto a magnetic activated cell sorting (MACS) column (Miltenyi Biotec). CD14⁻ cells were eluted with 2 washes of 3 ml MACS buffer, and CD14⁺ cells were washed with 5 ml MACS buffer using a syringe. Both positively (monocytes) and negatively selected cells were washed in RPMI then resuspended in R10 culture medium + 50 μ M β -mercaptoethanol for use in further experiments. Purity of isolated monocytes was verified by flow cytometry staining for CD14⁺CD11b⁺ cells.

2.4 T cell proliferation assays.

96-well flat bottom plates were coated with 50 μ l anti-CD3 at 3 μ g/ml and incubated at 4°C overnight. Cell lines were harvested, irradiated (5,000 rad) to prevent further proliferation, resuspended in R10 + 50 μ M β -mercaptoethanol and plated in 50 μ l at the relevant concentrations. Alternately, supernatants harvested from 500,000 neuroblastoma cell line following 96 hour incubation were added at varying concentrations in a final volume of 100

μl in place of the cell lines. T cells obtained from donor PBMC were added at 200,000 cells in 50 μl per well, and finally 50 μl anti-CD28 was added to a final concentration of 2 μg/ml. In certain experiments, N^ω-hydroxy-L-arginine (0.5 mM, NOHA) and L-N^ω-monomethyl arginine (0.5 mM, L-NMMA) were added to MLR cultures to inhibit arginase and iNOS activity, respectively. Cells were then incubated at 37°C, 5% CO₂ for 96 hours before 1 μCi per well [³H]-thymidine (Perkin Elmer Life Sciences) was added and the cells incubated for a further 16 hours. Incorporation of [³H]-thymidine was measured using a Packard TopCount NXT microplate scintillation and luminescence counter. Data are presented as the percentage of PBMC-derived T cell proliferation driven by CD3 and CD28 stimulation in the presence of irradiated neuroblastoma cell lines compared with the same proliferation in the absence of cell lines (equivalent to 100%).

2.5 Monocyte polarisation assay

Neuroblastoma cell lines were harvested and plated in 24-well flat bottom plates, before CD14⁺ cells isolated from healthy donor blood as previously described were added, either directly or in a 1 μm pore size Transwell (Corning). Positive controls were generated using CD14⁺ cells alone stimulated with 40 ng/ mL granulocyte macrophage colony-stimulation factor (GM-CSF). 0.5 mM NOHA and L-NMMA were added in certain experiments to investigate the effect of arginase and iNOS inhibition. The cells were then incubated at 37°C for 72 hours, before being harvested and incubated for 20 minutes at 4°C with anti-CD11b coated magnetic beads to isolate myeloid-derived cells using a MACS column as described earlier. Monocyte polarisation was assessed by incubation with either anti-CD206-PE, anti-CD163-PE or anti-CD115-PE (eBioscience) detailed below. CD11b⁺ cells were then washed,

irradiated and resuspended in R10 + 50 μ M β -mercaptoethanol and plated into a 96-well flat bottom plate previously coated with anti-CD3 for assessment of effect on T cell proliferation, as described above.

2.6 Flow cytometry

Cells were stained for surface markers in a round bottom 96 well plate for 20 minutes at 4°C, washed and resuspended in 200 μ L FACS buffer (PBS + 10% FCS). For intracellular CD68 staining, following surface staining, cells were fixed and permeabilised using fixation/permeabilization solution containing 4% formaldehyde and 0.1% saponin (eBioscience), then washed, incubated with anti-CD68-FITC (eBioscience) for 20 minutes at 4°C and resuspended in FACS buffer. Samples were acquired using an Accuri C6 flow cytometer, Accuri CFlow Plus software.

2.7 Reverse transcription polymerase chain reaction (RT-PCR)

RT-PCR was used to detect gene expression of arginase I, arginase II and iNOS in neuroblastoma cell lines. RNA was extracted from pellets of 1×10^6 neuroblastoma or control line with RNeasy columns (Qiagen). Pellets were lysed in 350 μ L Buffer RLT and homogenised before adding 1:1 volume:volume 70% ethanol. The lysate was then transferred to an RNeasy spin column, centrifuged at 10,000 rpm for 15 s, before the column was washed with 700 μ L Buffer RW1 and twice with 500 μ L Buffer RPE to remove the ethanol. RNA was eluted with 30 μ L dH₂O, and then quantified with a Nanodrop

spectrophotometer. cDNA was synthesized SuperScript™ III Reverse Transcriptase (Invitrogen) following the manufacturer's instructions, then PCR performed using the primers detailed below and Platinum *Taq* DNA polymerase (Invitrogen). The PCR products were analysed by gel electrophoresis on a 2% agarose gel, and were visualised by staining with ethidium bromide.

Arginase I - Forward primer 5'CTCTAAGGGACAGCCTCGAGGA3'

Reverse primer 5'TGGGTCACTTCCATGATATCTA3'

Arginase II - Forward primer 5'ATGTCCCTAAGGGGCAGCCTCTCGCGT3'

Reverse primer 5'CACAGCTGTAGCCATCTGACACAGCTC3'

iNOS - Forward primer 5'CGGTGCTGTATTCCTTACGAGGCGAAGAAGG3'

Reverse primer 5'GGTGCTGCTTGTTAGGAGGTCAAGTAAAGGGC3'

GAPDH - Forward primer 5'CCAGCCGAGCCACATCGCTC3'

Reverse primer 5'ATGAGCCCCAGCCTTCTC3'

2.8 Western blotting

Lysates of neuroblastoma cell lines were prepared by incubation of 5×10^6 cells with lysis buffer (150 mM NaCl, 20 mM Tris-HCl pH 7.5, 2mM ethylenediaminetetraacetic acid (EDTA), 1% Triton X-100) with protease inhibitors (Roche). Lysates were centrifuged at 13,000 rpm for 30 minutes and supernatants collected, 15 μ L of which was then added to 2 μ L running buffer (125 mM Tris pH 8, 8M urea, 10% glycerol, 6% SDS, bromophenol blue, 200 mM DTT) and loaded onto a 12.5% acrylamide gel consisting of a resolving gel (765mM Tris pH 8.8, 0.2% SDS, 12.5% acrylamide (Protogel), 0.1% ammonium persulphate and 5 μ L of tetramethylethylenediamine (TEMED) (Sigma)) and a stacking gel (150mM Tris pH 6.8, 0.12% SDS, 0.1% ammonium persulphate and 5 μ L of TEMED). Protein gels were run at 100 mV through the stacking gel and 180 mV through the resolving gel and then transferred to a PVDF membrane (Hybond LFP, GE Healthcare) in transfer buffer (10% methanol, 190 mM glycine, 25 mM Tris) at 400 mA for 1 hour. The membrane was then blocked to prevent non-specific interactions using 5% milk in 1x Tris-buffered saline (20 mM Tris pH 7.5, 150 mM NaCl) + 0.1% Tween (TBS-T). The membrane was washed three times with TBS-T before incubation with goat anti-arginase 1 or 2 primary antibody (Santa Cruz) at 1:1000 in TBS-T overnight at 4°C. Unbound primary antibody was washed off with 4 TBS-T washes before transfer of the membrane into 5% milk in TBS-T with 1:20,000 secondary antibody (horseradish peroxidase-conjugated anti-goat rabbit antibody (Sigma)). This was incubated for one hour at room temperature before being washed 3 times with TBS-T and then bound antibody fluorescence was detected using EZ-ECL Chemiluminescence Detection Kit for HRP (Biological Industries). Light sensitive film (Amersham Hyperfilm MP, GE Healthcare) was placed on the membrane in a dark room before being developed.

2.9 Arginase activity assay

Arginase activity in neuroblastoma cell pellets and supernatants was determined from measuring production of urea following incubation with arginine. Lysis buffer (0.1% Triton X-100, 5 µg pepstatin, 5 µg antipain, 5 µg aprotinin) was added to 3×10^6 pelleted cell line cells or 50 µL cell line supernatant and the samples incubated at 37°C for 30 minutes, vortexed every 10 minutes. Lysates were collected by centrifugation at 13,000 rpm for 20 minutes. Arginase was activated 10 mM MnCl_2 was added with 25 mM Tris-HCl buffer and the mixture incubated at 56°C for 10 minutes. 0.5 M L-arginine was added as a substrate and incubated at 37°C for 60 minutes before the hydrolysis was stopped by addition of 800 µL acid solution mixture ($\text{H}_2\text{SO}_4/\text{H}_3\text{PO}_4/\text{H}_2\text{O}$ 1:3:7). Urea production was quantified by measuring absorbance at 540 nm using a BioRad 680 microplate compared to a standard curve, following addition of 9% α -isonitrosopropiophenone and heating at 100°C for 30 – 45 minutes.

2.8 Enzyme linked immunosorbent assay (ELISA)

For measurement of cytokine production, supernatants of neuroblastoma cell lines were collected 96 hours following plating. The amounts of IL-1 β , IL-4, IL-6, IL-10, IL-13, GM-CSF and TNF α were measured using capture and biotinylated antibodies purchased from e-Bioscience. The plates were washed with PBS and blocked with 1% of BSA for 1 hour at room temperature. Supernatant samples were plated for 2 hours at room temperature. Finally, a streptavidin-HRP-coupled goat anti-mouse IgG (e-Bioscience) was added for 1 hour. Colour reactions were developed with 3,3',5,5'-tetramethylbenzidine (TMB; Sigma-Aldrich), and the absorbance was measured at 490 nm.

RESULTS

3.1 Neuroblastoma-derived cell line mediated suppression of T cell activity.

3.1.1 Neuroblastoma cell lines suppress T cell proliferation *in vitro*.

In order to establish a basis for further experiments using fresh primary tissue, we set out to examine the effect of co-cultured neuroblastoma cell lines on T cell proliferation *in vitro*, and to determine the nature of any direct mechanisms of T cell suppression mediated by neuroblastoma. To investigate if neuroblastoma cell lines could directly inhibit T cell proliferation, a T cell proliferation assay was performed using the following neuroblastoma cells lines; SK-N-AS, IMR-32, LA-N-1, Kelly and SK-N-MC.

All cell lines were irradiated and co-cultured with allogeneic T cells for 96 h (Figure 3.1). When plated at a 1:1 ratio of neuroblastoma: T cells, four of the five lines tested exhibited strong suppression of T cell proliferation, limiting proliferation to under 30% of the control. One cell line, SK-N-AS, did not suppress T cell proliferation even at this high concentration of cell line cells. Three of the suppressive cell lines (LA-N-1, Kelly and SK-N-MC) appear to lose suppressive ability when plated at 1 to every 4 T cells, but IMR-32 suppresses T cell proliferation even at the lowest concentration of cell line cells, a 1:8 ratio. These results highlight the heterogeneous nature of cell lines and perhaps reflect the heterogeneous nature of the tumours from which the cell lines were derived, but nevertheless indicate that neuroblastoma-derived cells are capable of inhibiting T cell proliferation *in vitro*.

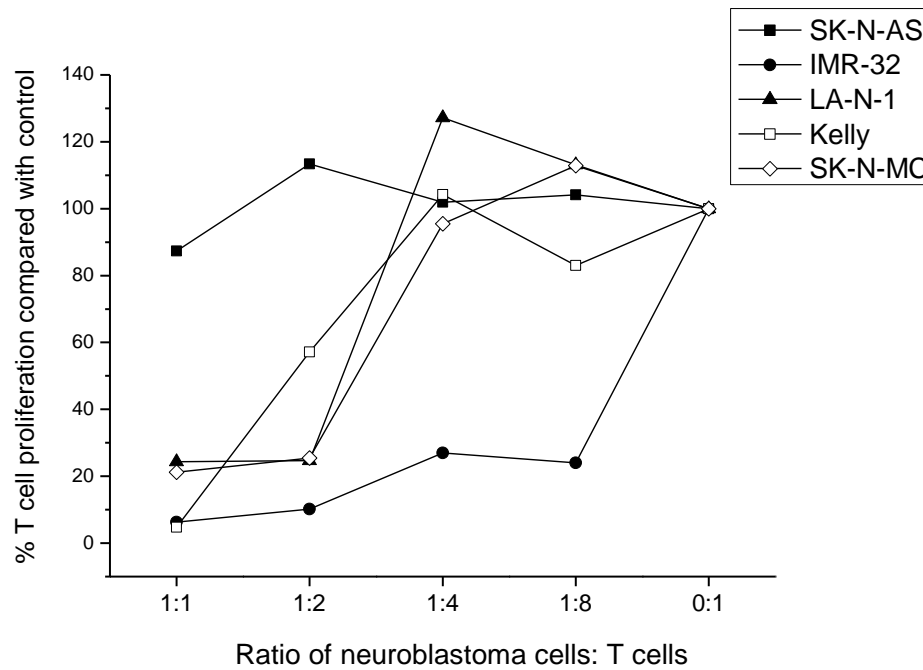


Figure 3.1: Neuroblastoma-derived cell lines inhibit allogeneic T cell proliferation in co-culture. Five neuroblastoma cell lines were cultured with allogeneic T cells from a healthy donor in an MLR. The ratio of neuroblastoma cells: T cells ranged from 1:1 to 1:8. T cell proliferation was measured by [3 H]-thymidine incorporation after 96 hours. Four of the cell lines (IMR-32, LA-N-1, Kelly and SK-N-MC) strongly suppressed T cell proliferation at a 1:1 ratio, with proliferation at less than 30% than that of the control of T cells cultured alone (100% proliferation). One cell line (IMR-32) displayed strong suppression of proliferation at all ratios, while one cell line (SK-N-AS) did not suppress T cell proliferation at any ratio. These data are representative of four independent experiments.

To further explore the potential mechanism of neuroblastoma mediated inhibition of T cell proliferation, we attempted to determine whether the suppressive effect was mediated through direct cell: cell contact with the T cells, or mediated indirectly through the release of soluble factors or removal of nutrients from the culture medium.

The previously conducted T cell proliferation assay was repeated using a transwell system to separate the T cells, plated in the lower compartment, and neuroblastoma cells, plated in the upper compartment. The same inhibition of T cell proliferation was observed using the transwell system as when the co-cultures were plated normally in cell: cell contact (Figure 3.2a). These data suggest that the suppressive activity of these cell lines is not dependent on cell: cell contact, but occurs through secretion of immunosuppressive mediator or through depletion of nutrients vital to the proliferation of T cells.

This hypothesis is supported by the results of an experiment where supernatants harvested from cell lines cultured in R10 were added at varying concentrations to allogeneic T cells from a healthy donor, which were stimulated by antibodies in a proliferation assay as before (Figure 3.2b). At a high concentration of cell line supernatant (87.5% of the total 200 μ l of culture volume), all four of the cell line supernatants tested suppressed T cell proliferation to less than 10% of the control T cell population. However, at a culture volume with 50% supernatant, the four suppressive cell lines still inhibited T cell proliferation to around 10% that of the control. As with the cell: cell assay, IMR-32 supernatant demonstrated the most potent suppression of T cell proliferation.

To exclude the possibility that neuroblastoma cells suppress T cell proliferation by inducing death of the T cells, we stained the T cells with propidium iodide (PI) after 96 h of co-culture with neuroblastoma cells. PI is a fluorescent molecule that binds nucleic acids and can therefore be used to differentiate apoptotic cells, since it cannot penetrate viable cell membranes.

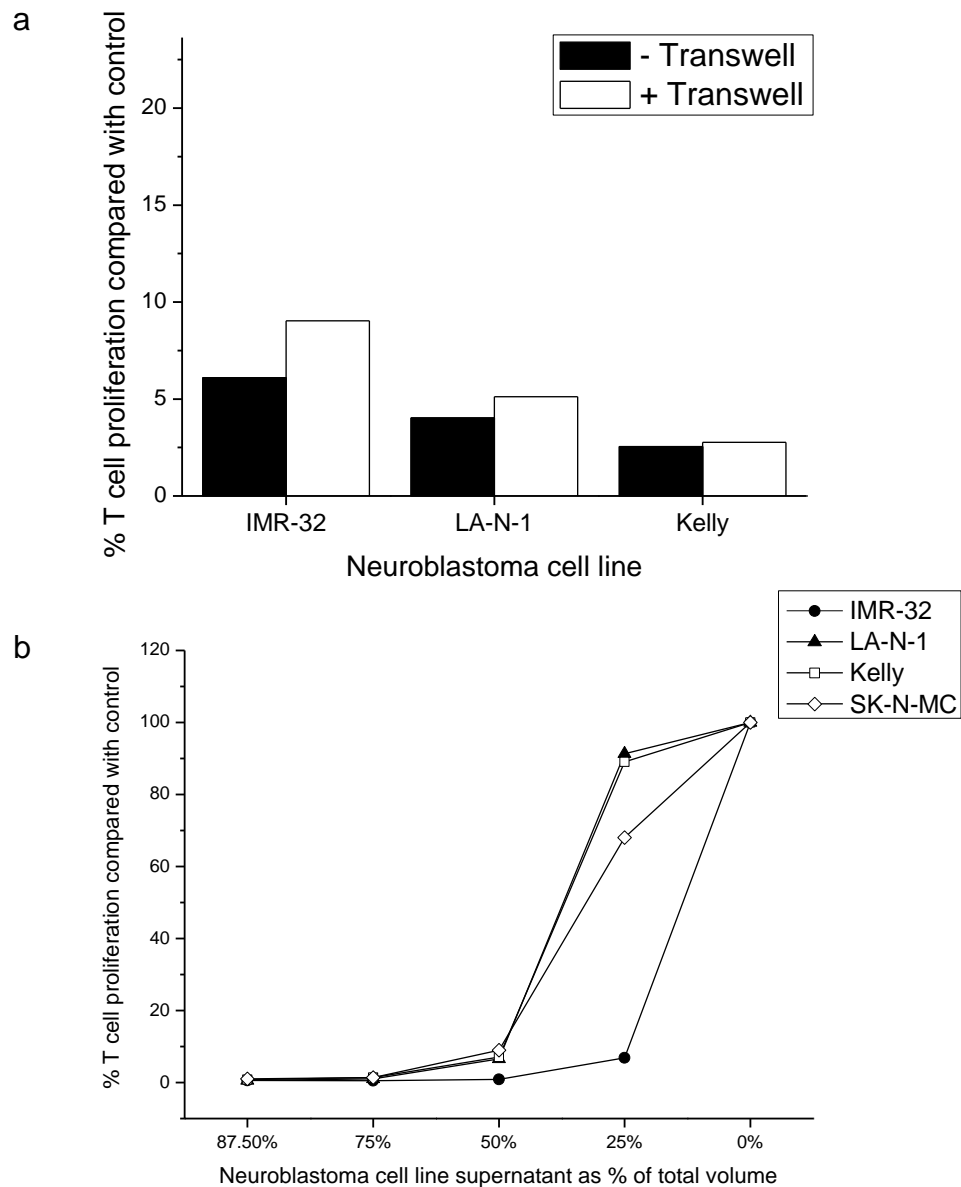


Figure 3.2: Neuroblastoma-derived cell lines inhibit T cell proliferation using a contact independent mechanism. (a) Three neuroblastoma cell lines were plated in the upper well of a transwell assay system at a ratio of 1:2 with allogeneic T cells from a healthy donor on the bottom well, in an MLR. T cell proliferation was measured by [^3H]-thymidine incorporation after 96 hours. T cell proliferation remained unchanged whether using a transwell or not in all three cases tested. **(b)** Supernatants from 96 hour cultures of four suppressive neuroblastoma cell lines were added to T cell culture medium, at ratios varying between 87.5% and 25% of total culture volume. T cell proliferation was measured by [^3H]-thymidine incorporation after 96 hours. Supernatants of all four cell lines strongly suppressed T cell proliferation at 50% total culture volume. Data are representative of three independent experiments.

Flow cytometry of the stained cells (Figure 3.3) demonstrates that between 94.6% and 72.1% of the T cells remain viable post culture, suggesting neuroblastoma is not inducing T cell apoptosis, a mechanism of immune suppression that has been demonstrated in other solid cancers, either through cell: cell interactions or through secretion of soluble ligands such as PD-L1 (Murali & Mehrotra, 2011).

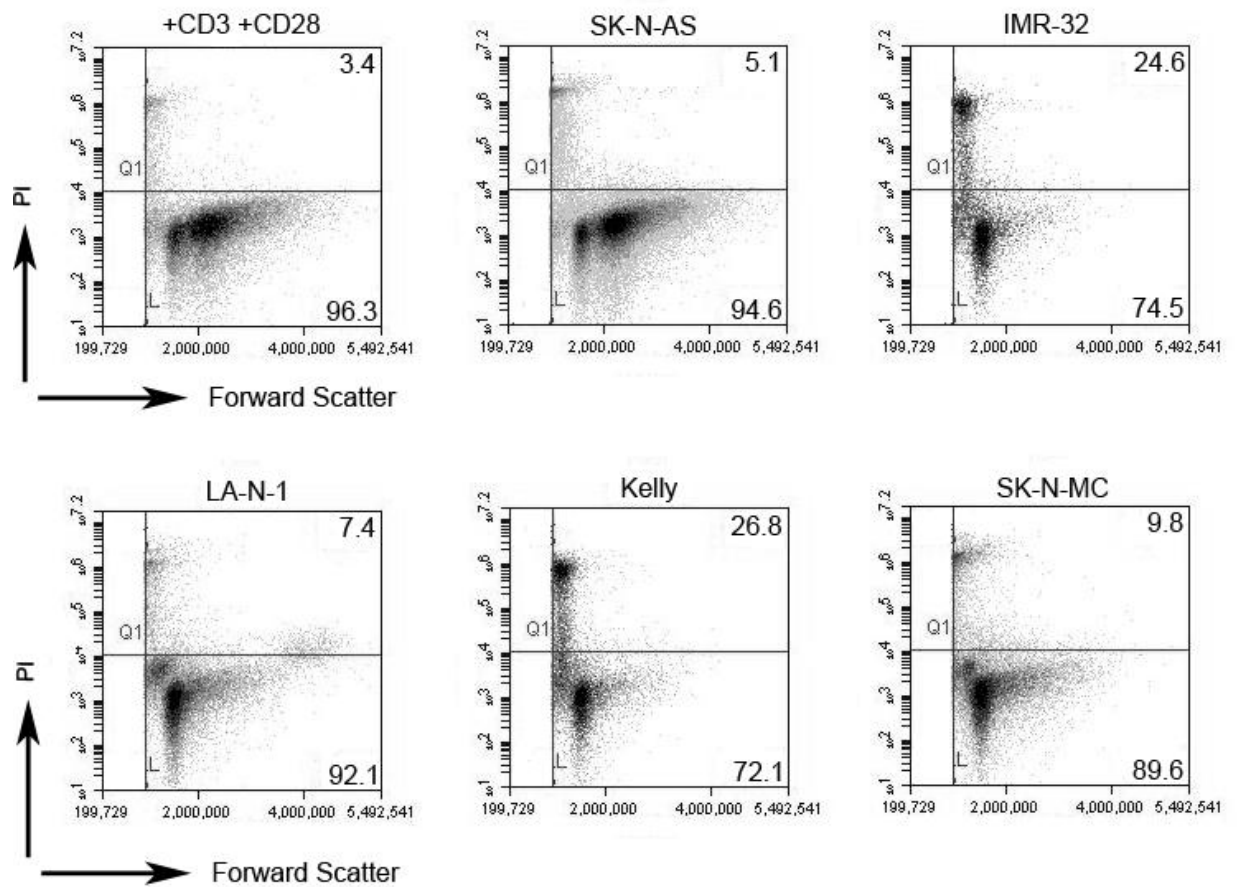


Figure 3.3: Culturing neuroblastoma-derived cell lines with T cells does not induce T cell death. Neuroblastoma derived cell lines were co-cultured with allogeneic T cells from a healthy donor for 96 h. The T cells were then sorted and stained with propidium iodide (PI) to assess cell death. Flow cytometry plots are shown. In each case, the percentage of cells positively stained with PI was less than 26.8% of the total, indicating that T cells are not undergoing wholesale apoptosis in co-culture with neuroblastoma-derived cell lines.

3.1.2 Neuroblastoma-derived cell line suppression of T cell proliferation is dependent on the action of arginase enzymes.

Recent work by this group has highlighted the role of enhanced arginine metabolism by acute myeloid leukaemia (AML) blasts in AML-mediated immunosuppression (Mussai *et al*, 2013). T cell proliferation assays carried out using arginine-depleted medium (Figure 3.4a) highlight the importance of the presence of arginine to T cell proliferation. Suppression of T cell proliferation of greater than 50% was observed when T cells were cultured with as little as 25% arginine depleted medium as a part of the total culture volume. Since suppression of T cell proliferation by neuroblastoma-derived cell lines had already been demonstrated to be likely due to a secreted factor or nutrient depletion, we hypothesized that arginine depletion may also have a role in neuroblastoma-mediated immunosuppression.

L-Arginine is metabolised by two different pathways, mediated by two different enzymes; arginase and nitric oxide synthase (NOS). There exist two isoenzyme forms of arginase in mammals, Arginase type I (ARG1) and Arginase type II (ARG2) which both metabolise arginine into ornithine with the production of urea. ARG1 is expressed in the cytosol of liver cells and forms part of the urea cycle which detoxifies ammonia, and is also produced by MDSC as one of their mechanisms of immune suppression. ARG2 is expressed in the mitochondria of many peripheral tissues, including kidney, small intestine, prostate and mammary gland. NOS converts arginine into citrulline and also produces NO, which is a key intermediate in the production of other reactive nitrogen species (RNS), including peroxynitrite. Mammalian NOS exists in three forms, two constitutively expressed isoforms; endothelial and neuronal NOS, and one inducible isoform, iNOS, which is employed by the immune system to produce RNS as a defence mechanism against invading pathogens.

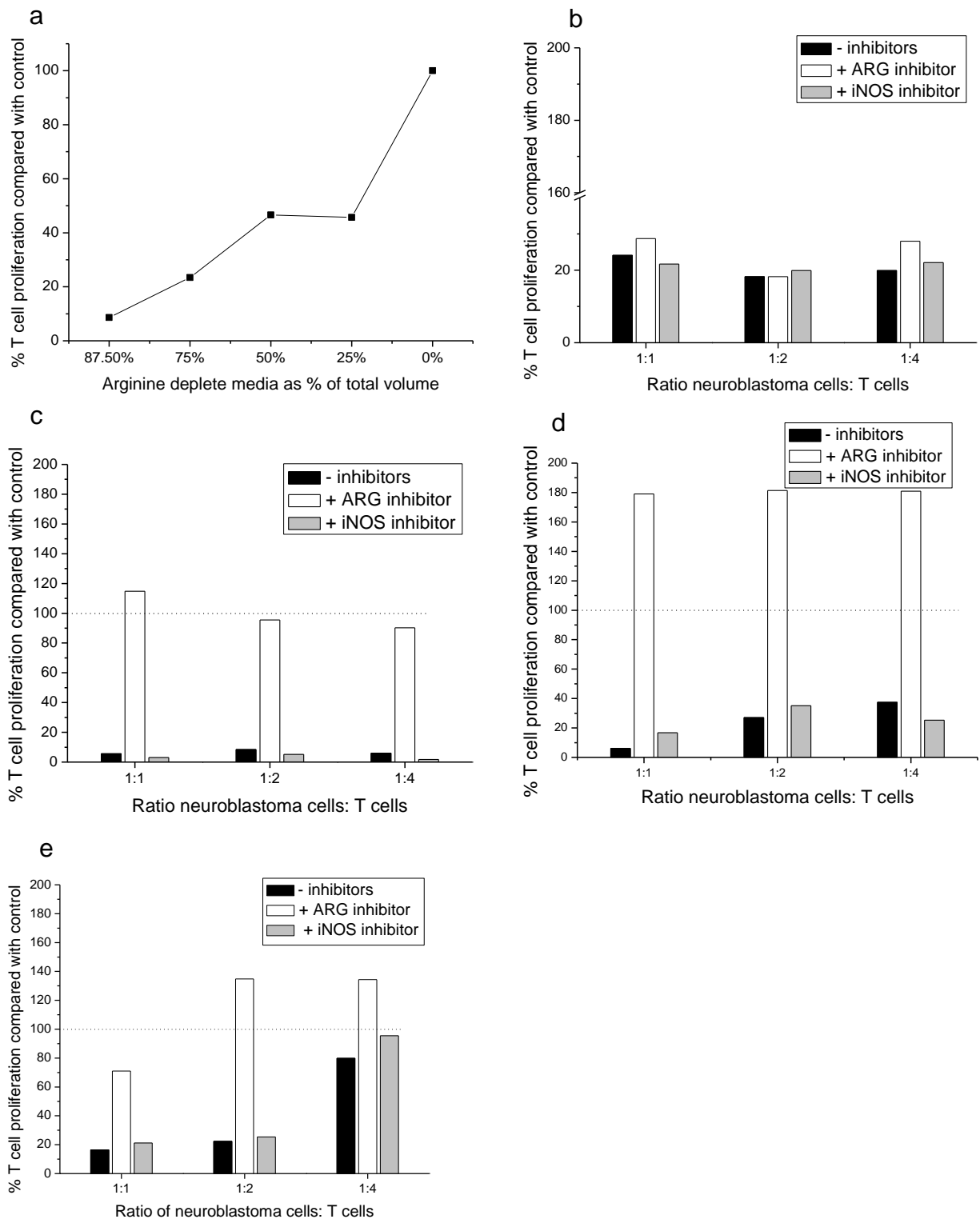


Figure 3.4: Arginase enzyme inhibitor, but not iNOS inhibitor, rescue T cell proliferation when co-cultured with neuroblastoma-derived cell lines. (a) Arginine deplete medium was added to T cell culture medium at a ration varying between 87.5% and 25% total culture volume. T cells cultured in arginine depleted medium exhibited proliferation of less than 50% that of the control of T cells cultured in 100% fresh R10 medium, even at 25% total culture volume.

Neuroblastoma cell lines IMR-32 **(b)** LA-N-1 **(c)** Kelly **(d)** SK-N-MC **(e)** were cultured with allogeneic T cells in a MLR in the presence of the enzyme specific inhibitors for arginase (NOHA) and iNOS (L-NMMA), both added at 0.5 µg/ml. The ratio of neuroblastoma cells: T cells ranged from 1:1 to 1:4. T cell proliferation was measured by [³H]-thymidine incorporation after 4 days. Culture with the arginase enzyme inhibitor restored T cell proliferation in three of the four suppressive cell lines. Culture with the iNOS enzyme inhibitor did not restore T cell proliferation in any of the cell lines. Data are representative of three independent experiments.

To determine whether the metabolism of arginine has a role in neuroblastoma mediated immunosuppression, the T cell proliferation assay was repeated with the addition of either N^ω-hydroxy-L-arginine (NOHA), an inhibitor of both Arginase enzyme isoforms, or L-N^ω-monomethyl arginine (L-NMMA), an inhibitor of iNOS, prior to 96 hour incubation and the addition of [³H]-thymidine. Three ratios of neuroblastoma cells: T cells were used, from 1:1 to 1:4. In the case of the three immunosuppressive neuroblastoma cell lines (LA-N-1 (Figure 3.4c), Kelly (Figure 3.4d) and SK-N-MC (Figure 3.4e), the addition of 0.5 mM Arginase inhibitors fully restored T cell proliferation, while L-NMMA had no effect on T cell proliferation. This is strongly indicative that suppression of T cell proliferation by these three neuroblastoma-derived cell lines is dependent on restricting arginine availability to T cells, thereby rendering the T cells quiescent, and that this depletion of arginine is dependent on tumour cell expression of Arginase.

IMR-32 co-cultures continued to suppress T cell proliferation with both Arginase and iNOS inhibitors included (Figure 3.4b), suggesting the suppression mediated by this cell line is either not based on arginine depletion or the depletion is not mediated by ARG or iNOS. Since neuroblastoma is a cancer predominantly derived from neural cells, it is possible that the neural NOS isoform (nNOS) is expressed by these cells, however, L-NMMA is non-selective for the various isoforms so it would seem likely that nNOS activity is not critical to arginine depletion mediated immunosuppression in any of the cell lines. No restoration of T

cell proliferation was detected in a repeat of the assay using increased doses of both ARG and iNOS inhibitors (data not shown), supporting the hypothesis that IMR-32 mediated suppression is not arginase or iNOS dependent.

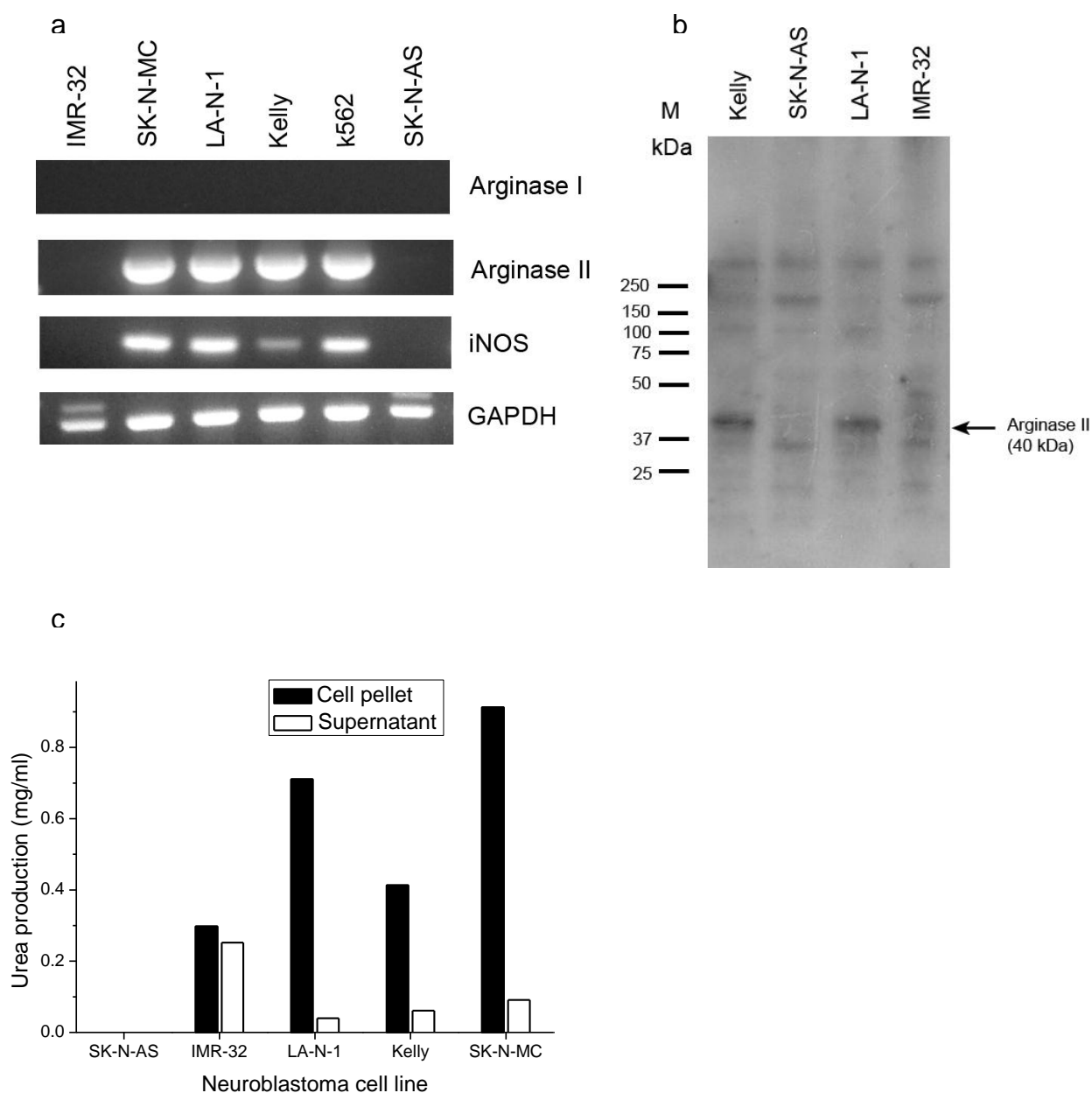


Figure 3.5: Neuroblastoma-derived cell lines that suppress T cell proliferation express active Arginase II. (a) Arginase I, II and iNOS expression in five neuroblastoma cell line lysates determined by RT-PCR. K562 cell line lysate was used as a positive control for Arginase I and iNOS. Three of the five tested neuroblastoma cell lines express Arginase II and iNOS, while the non-suppressive SK-N-AS cell line, as well as the suppressive IMR-32 cell line, do not. None of the cell lines express Arginase I. GAPDH was used to ensure equal loading.

(b) Western blot of neuroblastoma cell line lysates for Arginase II. Two of the cell lines tested (Kelly and LA-N-1) produce bands at the size expected for Arginase II, 40 kDa. **(c)** Whole cell lysates of the neuroblastoma cell lines were tested for the ability to convert arginine into urea using a colorimetric assay. Arginase activity was strong in three of the suppressive cell lines, while SK-N-AS did not display any arginase activity. Arginase activity in cell line supernatants following 96 hour culture was also assessed. In all cases apart from IMR-32, arginase activity in supernatants was barely above the detection limit. This data is representative of three independent experiments.

3.1.3 Suppressive neuroblastoma-derived cell lines express active Arginase II.

We next attempted to prove Arginase expression by neuroblastoma-derived cell lines. Cell line lysates were analysed for ARG1, ARG2 and iNOS mRNA using reverse transcription PCR (Figure 3.5a). None of the cell lines appear to be transcribing the *ARG1* gene as no bands are visible using the primers for this mRNA. With a lack of positive control it is impossible to say with certainty that the primers for Arginase I were working, but the presence of bands corresponding to GAPDH mRNA suggest the PCR protocol worked in all cases. Clear bands are visible for both Arginase II and iNOS mRNA in three of the four suppressive cell lines (LA-N-1, Kelly and SK-N-MC), verified by the use of an acute myeloid leukaemia derived cell line K562 as a positive control for Arginase II and iNOS. This indicates these three cell lines are all transcribing the gene for Arginase II and iNOS while growing in culture, a result consistent with the findings of Mussai and colleagues in the AML setting. A Western blot was then performed on cell line lysates to detect protein expression, using a primary antibody specific for ARG2 (Figure 3.5b). Bands migrating to the expected molecular weight for ARG2 (40 kDa) are observed in both of the two cell lines positive for ARG2 mRNA (Kelly and LA-N-1), confirming that Arginase II is expressed by these cell lines. No band migrating at 40 kDa is observed for IMR-32.

Although iNOS is being transcribed in three of the neuroblastoma cell lines, data from the previous experiment suggests that it is Arginase activity that defines the immunosuppressive phenotype of these cells, since iNOS specific inhibitors did not rescue T cell proliferation. To confirm Arginase activity in both cell lysates and culture supernatants, a colorimetric assay was used to determine urea production following enzyme activation and incubation with arginine. All four suppressive cell lines exhibited Arginase activity in the cell lysates, with urea production ranging from 0.3 mg/mL to 0.92 mg/mL (Figure 3.5c). Significant Arginase activity (0.25 mg/mL) was only detected in the supernatant of IMR-32. Arginase activity in the supernatant is likely a result of secreted Arginase, which has been demonstrated in the case of AML blasts, rather than arginine depletion through intracellular upregulation of Arginase, which may explain the strong suppression of T cell proliferation mediated by IMR-32 derived supernatant (Figure 3.2b). In addition, it is possible that IMR-32 cells are induced to produce and secrete Arginase through the action of cytokines released by T cells during the co-cultured, hence explaining why the IMR-32 cell lysates did not seem to express ARG1 or ARG2 mRNA. However, this fails to explain why arginase inhibitors did not restore T cell proliferation in the assay. There is likely an alternative mechanism involved in observed suppression of T cell proliferation by IMR-32 that likely warrants further investigation.

This data supports the hypothesis that certain neuroblastoma-derived cell lines are capable of directly inhibiting T cell proliferation through the removal of arginine from the T cell microenvironment, a process dependent on tumour expression of Arginase II. To the author's knowledge, this is the first time that this has been demonstrated.

3.2 Neuroblastoma-derived cell line mediated macrophage activation

Besides arginine depletion, several other mechanisms of tumour-mediated immune suppression have been documented, including recruitment and activation of suppressive macrophages to the tumour microenvironment, which in turn dampen T cell-mediated responses to the cancer cells. To investigate whether this mechanism is important in neuroblastoma biology, we set out to determine the level of macrophage activation and polarisation that neuroblastoma-derived cell lines induce *in vitro*, and whether monocytes co-cultured with neuroblastoma cells do indeed adopt an immunosuppressive phenotype.

Monocytes are bone marrow derived leukocytes that circulate in the bloodstream before migrating into tissues and differentiating into dendritic cells and macrophages. They are capable of phagocytic response to pathogen, in part mediated by a pattern recognition receptor CD14, which acts as a co-receptor in the detection of lipopolysaccharide (LPS), a major component of the outer membrane of Gram-negative bacteria. CD14 can be used as a marker for monocytes and monocyte-derived cells, and was used in this study to sort these cells from healthy donor blood. Monocytes and macrophages express a number of unique cell surface receptors other than CD14, including CD11b, one subunit of the heterodimeric integrin $\alpha_M\beta_2$, responsible for regulating cell adhesion and migration. To address the question of whether neuroblastoma has an effect on co-cultured monocytes, we co-cultured neuroblastoma cell lines with monocytes at the ratio of 1:1 for 72 h and then stained for the intracellular expression of CD68. CD68 is expressed in activated macrophages intracellularly on the membrane of lysosomes and endosomes, and tumour associated macrophages expressing CD68 have been linked with poor outcome in several neoplasias, including Hodgkin lymphoma (Tan *et al*, 2012) and basal cell carcinoma (Glaser *et al*, 2011). CD68 expressing cells have been demonstrated to infiltrate neuroblastoma tumour tissue (Apps *et*

al, 2013). In this study, we observed that sorted CD14⁺ cells co-cultured with neuroblastoma-derived cell lines expressed CD68 (Figure 3.6a), with between 53% and 96% of cells analysed staining double positive for CD11b and CD68. This compares with monocytes incubated alone, for which only 17.8% of cells are stained double positive for CD11b and CD68. This demonstrates that macrophages are upregulating CD68 post-incubation with neuroblastoma, suggesting macrophage differentiation and/ or activation is occurring in response to neuroblastoma derived signals.

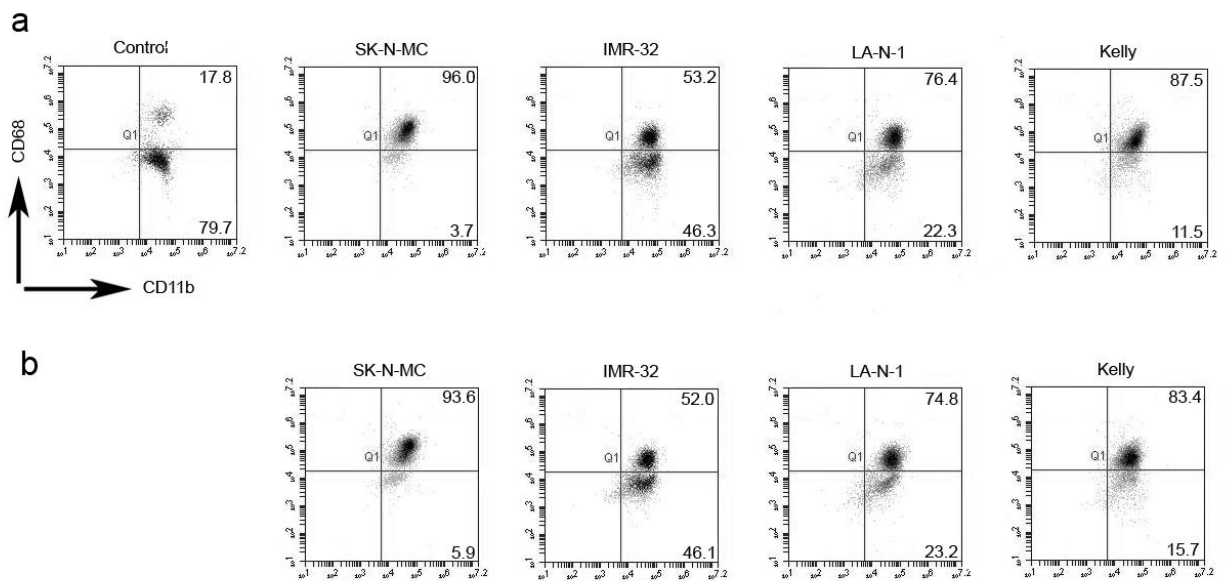


Figure 3.6: Monocytes co-cultured with neuroblastoma-derived cell lines exhibit surface markers of activated macrophages. (a) CD14⁺ cells were sorted from blood of a healthy donor and co-cultured at a ratio of 1:1 with four neuroblastoma-derived cell lines for 96 hours. Flow cytometry plots of cells stained for CD11b and CD68 are shown. CD68 upregulation on CD11b⁺ cells was observed in CD14⁺ cells co-cultured with all four neuroblastoma cell lines, as compared with a control of CD14⁺ cells alone. **(b)** The assay was repeated with the addition of 0.5 µg/ml NOHA and L-NMMA arginase and iNOS inhibitors. No significant difference in the number of CD68⁺ CD11b⁺ cells was observed. This data is representative of two independent experiments.

Recent work by this group has highlighted the role of enhanced arginine metabolism by AML blasts in polarization of healthy monocytes in M2 like phenotype (Mussai *et al*, 2013), and having demonstrated the role of arginine metabolism in the suppression of T cell responses induced by neuroblastoma, tumour expression of arginase as a mechanism of macrophage induction was investigated through addition of arginase and iNOS inhibitors to the cell lines while in culture with the CD14⁺ cells (Figure 3.6b). No significant change in CD68 expression was observed, suggesting that arginine metabolism is not a key mechanism in neuroblastoma mediated macrophage activation.

In order to determine whether the macrophages activated by neuroblastoma inhibit T cell proliferation *in vitro*, CD14⁺ cells were sorted from the harvested neuroblastoma/ CD14⁺ co-culture using antibody coated magnetic beads, irradiated to prevent further proliferation, and then added to a T cell proliferation assay with antibody stimulated T cells as before. A titration was performed with CD14⁺ cells added at varying ratios to the T cells, from 1:1 to 1:8, and T cell proliferation determined by incorporation of [³H]-thymidine (Figure 3.7). All four cell lines that exhibited suppression of T cell proliferation in co-culture also induced a suppressive phenotype in co-cultured macrophages, with T cell proliferation limited to less than 60% of the control population in all cell lines at all ratios. No apparent correlation exists between percentage of cells expressing CD68 as determined by flow cytometry and suppression of T cell proliferation in this assay, but further experiments would be required to confirm this on a statistical basis.

One striking feature of this dataset is the apparent increased proliferation suppression with fewer CD14⁺ cells added to the culture, which is counter-intuitive, as one would expect any suppressive influence of co-cultured monocytes to be greater with a greater number of cells

present. One possible explanation is that the radiation dose was not high enough to arrest proliferation of CD14⁺ cells in the MLR, and therefore [³H]-thymidine incorporated by these cells as well as the T cells leads to a skewing of the data to suggest greater proliferation of T cells when CD14⁺ numbers are higher. However, it is more likely that the macrophages are acting as antigen presenting cells, thereby stimulating the T cells in addition to the anti-CD3 and anti-CD28 stimulation. Higher numbers of antigen presenting macrophages would likely then induce a greater T cell proliferation response, as observed in Figure 3.7.

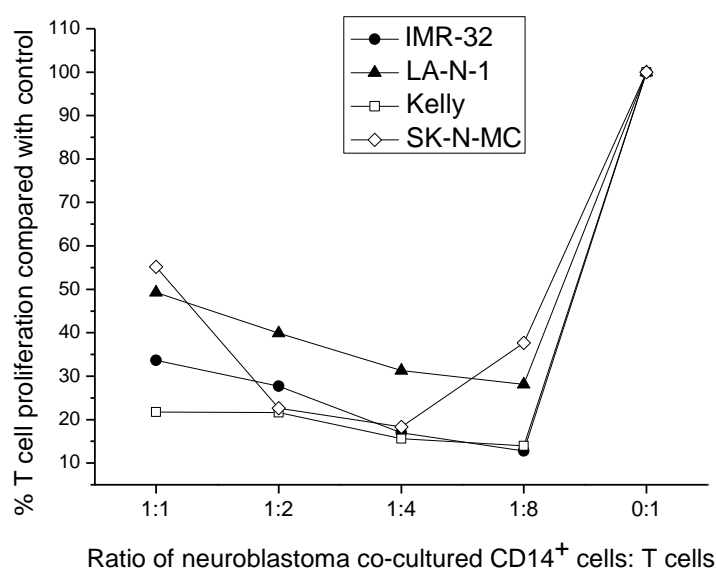


Figure 3.7: Monocytes co-cultured with neuroblastoma-derived cell lines inhibit T cell proliferation *in vitro*. CD14⁺ cells were sorted from blood of a healthy donor and co-cultured at a ratio of 1:1 with four neuroblastoma-derived cell lines for 96 hours. These cells were then sorted again using anti-CD14 magnetic beads and cultured with T cells activated with anti-CD3 and anti-CD28 antibodies at a ratio of between 1:1 and 1:8 in an MLR. T cell proliferation was measured by [³H]-thymidine incorporation after 96 hours. T cell proliferation was inhibited by CD14⁺ cells from co-cultures with all four neuroblastoma cell lines as compared with T cells cultured alone (100% proliferation), and at all four ratios of CD14⁺ cells: T cells.

In addition to CD68, the presence of other macrophage specific markers was also investigated using fluorophore-linked antibody staining in conjunction with flow cytometry. CD206 is a mannose receptor and CD163 a scavenging receptor, both expressed on the surface of M2 polarised macrophages, those usually associated with immunosuppression and tissue remodelling. Observations of initial stains with both these antibodies did not yield any significant apparent increase in surface expression of either. This would suggest that neuroblastoma is not mediating an M2-like phenotype switch in macrophages *in vitro*, although this data is very preliminary and does need confirmation by repeat experiments.

Previous studies have linked several cytokines with the activation of macrophages and induction of an immunosuppressive phenotype (Baay *et al*, 2011). We measured the concentration of IL-1 β , IL-4, IL-6, IL-10, IL-13, TNF- α and GM-CSF in the supernatants of the neuroblastoma derived cell lines that upregulated CD68 expression in monocytes by ELISA. For each cell line, supernatants contained no detectable amount of any of the cytokines (data not shown). This suggests an alternative mechanism is being employed by these cells, perhaps either a cytokine not measured here or a cell: cell contact dependent molecular interaction.

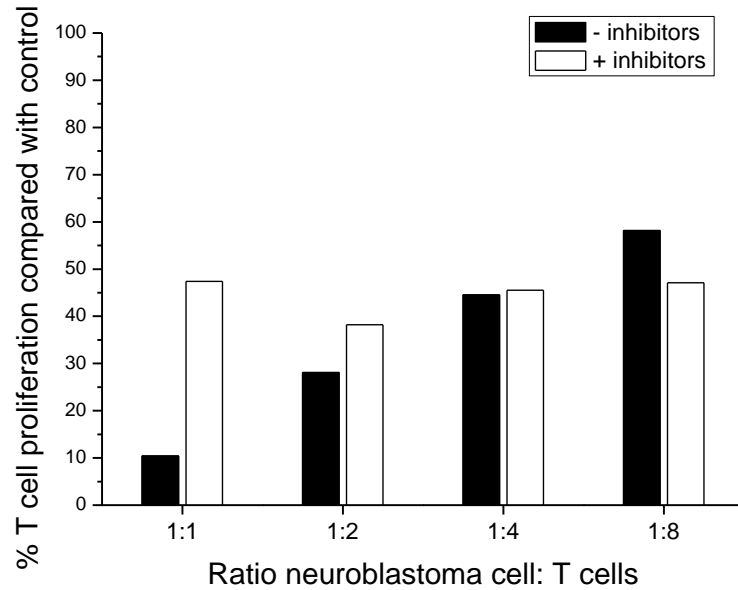
3.3 Neuroblastoma tumour tissue is immunosuppressive and induces macrophage activation ex vivo.

With previous work in this study supporting the hypothesis that neuroblastoma derived cell lines are capable of suppressing T cell proliferation *in vitro*, we set out to determine whether this was also the case using tumour tissue resected from human neuroblastoma patients. Following tissue chopping, digestion and the sorting of diasialoganglioside 2 (GD2)⁺ neuroblastoma cells from the samples by MACS, GD2⁺ cells from two patient samples were

plated in an MLR assay with allogeneic T cells from a healthy donor. As with the cell lines, suppression of T cell proliferation of up to 10% that of the control population was observed in one of the samples at a GD2⁺: T cell ratio of 1:1, while the second sample also suppressed proliferation to around 23% that of the control (Figure 3.8). This result confirms that primary neuroblastoma tumour tissue is indeed capable of suppressing T cell proliferation *ex vivo*. Further to this, when arginase inhibitor (NOHA) was added to the co-culture, T cell proliferation increased five-fold in the case of Tumour 1 at 1:1, and in general increased by around two fold in Tumour 2, constituting a significant restoration of T cell proliferation when arginase activity is prohibited. This supports the viability of using neuroblastoma-derived cell lines as a model of neuroblastoma behaviour *in vivo* and also suggests that arginine depletion may represent a mechanism of immune suppression in primary tumour samples *ex vivo*. In contrast to the cell line experiments, restoration of T cell proliferation to the control level was not observed in these samples, perhaps as a consequence of toxicity of the inhibitor to the cells in the assay.

Flow cytometry analysis of monocytes from a healthy donor co-cultured for 96 hours with GD2⁺ cells isolated from tumour biopsies of neuroblastoma patients revealed a significant fraction of CD11b⁺ cells expressed CD68 compared with the control population (Figure 3.9). In one sample, 64% of monocytes were double positive for CD68 and CD11b, while in the second sample this total rose to over 90%, which suggests that primary neuroblastoma tissue is capable of inducing CD68 expression in co-cultured macrophages. This data is consistent with the CD68⁺ populations observed in CD14⁺ cells co-cultured with neuroblastoma-derived cell lines, and suggests that the cell lines are again representative of their tumour of origin *in vitro*.

Tumour 1



Tumour 2

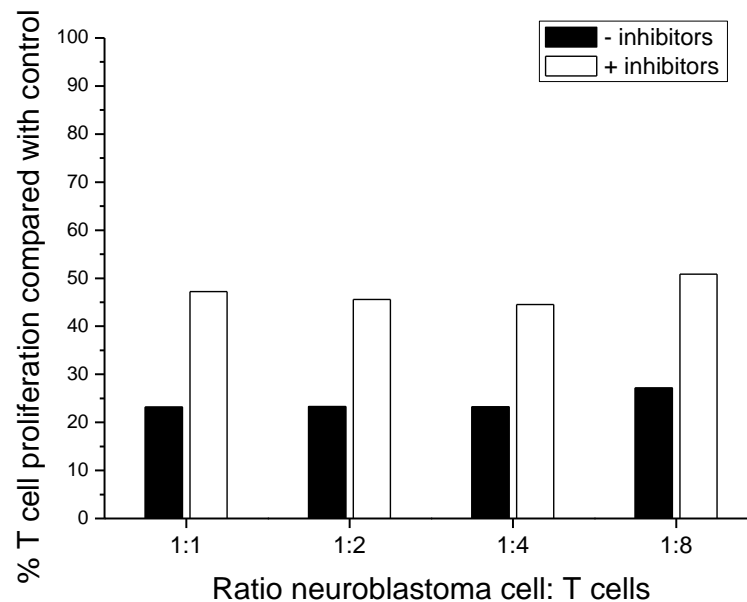


Figure 3.8: Neuroblastoma tissue inhibits allogeneic T cell proliferation in co-culture *in vitro*. Tumour samples from two neuroblastoma patients were MACS sorted for GD2⁺ cells and cultured with allogeneic T cells from a healthy donor in an MLR. The ratio of neuroblastoma cells: T cells ranged from 1:1 to 1:8. T cell proliferation was measured by [³H]-thymidine incorporation after 96 hours. GD2⁺ cells from both tumours suppress T cell proliferation at all ratios investigated to at least 60% that of the control of T cells cultured alone. Addition of arginase inhibitor (NOHA) restores T cell proliferation to around 50% that of the control in all cases.

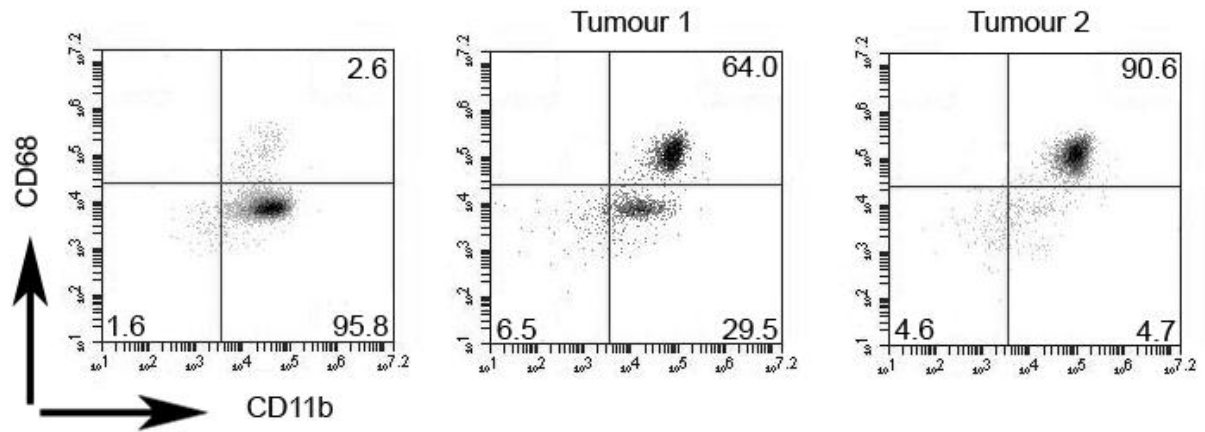


Figure 3.9: Monocytes co-cultured with neuroblastoma tissue express CD68. CD14⁺ cells were sorted from blood of a healthy donor and co-cultured at a ratio of 1:1 with GD2⁺ cells isolated from neuroblastoma patient tissue biopsy samples. Flow cytometry plots of cells stained for CD11b and CD68 are shown. CD68 upregulation on CD11b⁺ cells was observed in CD14⁺ cells co-cultured with GD2⁺ cells from both tumour samples, as compared with a control of CD14⁺ cells alone.

This data, albeit from a limited set of samples, supports the previous results in this study, namely that neuroblastoma is directly suppressive of T cell proliferation via an arginase mediated pathway and that neuroblastoma is capable of inducing an actively immunosuppressive phenotype in co-cultured monocytes. This data also confirms that these findings apply to *ex vivo* primary tissue samples, as well as neuroblastoma-derived cell lines. This is important in demonstrating the potential clinical significance of this research.

DISCUSSION

This study has demonstrated that neuroblastoma-derived cell lines and primary neuroblastoma tissue are capable of suppressing T cell proliferation *in vitro*. This suppression occurs in a contact-independent manner, and T cell proliferation is restored in most cases with the addition of an arginase inhibitor. Three of the four suppressive cell lines expressed active Arginase II, an enzyme responsible for the catabolism of the amino acid arginine into ornithine and urea. This data supports the hypothesis that neuroblastoma is capable of suppressing T cell activity through the depletion of arginine from the microenvironment, a mechanism that has been demonstrated to downregulate T cell expression of the CD3 ζ chain and thereby induce anergy in effector T cells (Raber *et al*, 2012).

Due to the low frequency of new diagnoses and difficulty in obtaining fresh tumour biopsy material, it was decided to use neuroblastoma cell lines as a model of neuroblastoma activity in this investigation. Once proof of concept had been established using these cell lines, the results could be used to inform experimental design on the relatively infrequent and consequently precious human tissue samples. Previous studies conducted using the cell lines selected indicate that they are generally good models of neuroblastoma behaviour *in vivo* (Thiele, 1998), but, as with any data obtained from *in vitro* experiments with cell lines, care must be taken in interpreting the results and any implications for a real world clinical setting. Cell lines are not subjected to the same environmental stresses of their *in vivo* counterparts, growing in hyperoxic conditions and without the interactions of cells *in vivo* with their microenvironment, often leading to non-representative genomic and/ or

proteomic profiles. Not only that, but cell lines in culture sometimes change phenotype with multiple passages, so what begins as a representative phenotype *in vivo* may not be after prolonged culture. Nevertheless, cell lines provide a quick and straightforward way to investigate the biology of neoplastic cells in particular, since they are already immortalised, growing rapidly and without contact-based constraints, allowing large numbers of cells to be cultured quickly for experimentation.

Previous research has uncovered the extent to which tumour cells are capable of influencing the microenvironment in which they proliferate, and the mechanisms employed by these cells in dampening the immune response to enhance their own survival. These mechanisms include secretion of soluble factors, including immunosuppressive cytokines such as IL-6, IL-10 and TGF- β , and other proteins such as PD-L1 and galectin-1, all of which act directly on effector cells such as CTLs or NK cells. Other direct mechanisms include expression of pro-apoptotic ligands such as Fas ligand and TRAIL, which act during cell: cell contact with effector cells, and depletion of critical metabolites such as tryptophan (through the action of indoleamine 2,3-dioxygenase) or glucose. Finally, tumour cells have been demonstrated to interact with other cells in their microenvironment, such as fibroblasts and other stromal cells, macrophages and dendritic cells, plus immature myeloid cells. These interactions often stimulate the target cell to adopt an immunosuppressive phenotype, forming M2 polarised macrophages, MDSC, or expressing immunosuppressive cytokines.

Previous studies have highlighted the ability of neuroblastoma to evade CLT mediated control through several direct mechanisms, including downregulation of HLA class I molecules and costimulatory molecules (Airolidi *et al*, 2003), downregulation of NKG2D

ligands (Raffaghello *et al*, 2004) and upregulation of galectin-1 (Soldati *et al*, 2011) or macrophage migration inhibitory factor (Yan *et al*, 2006). This study expands these known mechanisms to include arginine depletion, dependent on the action of arginase enzymes, and more specifically Arginase II.

Despite myeloid derived suppressor cells (MDSC) having long been established as inactivating T cells through arginine depletion via the action of ARG1, direct suppression of T cell proliferation by cancer cells through arginine depletion has not been widely reported. Studies of prostate cancer cell lines have demonstrated that ARG1 and ARG2 expression in these lines has an immunosuppressive effect (Gannon *et al*, 2010), while ARG2 expression by AML blasts also appears to inhibit T cell proliferation *ex vivo* (Mussai *et al*, 2013). However, AML blasts have a developmental origins similar to that of MDSC, so it is perhaps more likely that they may function in a similar manner. Arginase II activity has been demonstrated to be important in regulating cell growth and T cell activity in murine renal carcinoma cell lines (Tate *et al*, 2008), and although other previous research has focused primarily on the effect of Arginase I activity, this study highlights the potential importance of ARG2 in solid tumours of tissues that constitutively express this isoform, including neuroblastoma. Importantly, this study also describes arginase dependent immunosuppression in neuroblastoma patient tumour samples as well as cell lines, indicating that this is likely to be a clinically relevant process.

It is likely that the increased expression of ARG2 in neuroblastoma derived cell lines observed in this study is due to the increased metabolic requirements of the tumour cells due to their uncontrolled proliferation. Arginase II is involved in the synthesis of several

amino acids, including L-ornithine, L-proline and L-glutamate (Jenkinson *et al*, 1996), and high arginase activity has been correlated with increased proliferation of breast cancer (Singh *et al*, 2000) and colorectal cancer (Buga *et al*, 1998) cell lines. Neuroblastoma cells capable of upregulating their arginine metabolism are more likely to be able to proliferate (Pegg *et al*, 1982), but as an added effect, deplete arginine from their microenvironment and deny it to T cells, which also require comparatively high levels of nutrients to activate and proliferate. Thus, through enhanced synthesis of arginase, these cells receive a double boost to their survival, and therefore it is reasonable to expect that these cells will increase the tumour burden and contribute to aggressive disease.

Interestingly, since arginine has been demonstrated as being essential to the growth of many tumours, including breast cancer and colorectal cancer, one proposed cancer therapy is removal of arginine through recombinant arginase drugs such as pegylated arginine deiminase (ADI Feun *et al*, 2008). This would most likely be administered to patients with an already weakened immune system (i.e. before haematopoietic stem cell transplant) and so the negative effect on patient T cell populations would be negligible compared with the impact on the tumour, but the potential immunosuppressive action of such drugs would need to be assessed if they are to be administered to immuno-competent patients.

Although suppression of T cell proliferation does not appear to be dependent on iNOS activity, since addition of iNOS inhibitor (L-NMMA) did not restore proliferation in the MLR, iNOS is being transcribed in three of the suppressive cell lines. Previous studies have highlighted the interaction of arginase and iNOS in the metabolism of arginine, suggesting that if both enzymes are expressed the production of peroxynitrite in the absence of

arginine induces T cell apoptosis (Bronte *et al*, 2003). Since we have not observed T cell apoptosis in this study, it may be that iNOS is not active, or only active at a low level. Further studies will determine the level of iNOS activity in these cell lines by assaying NO₂⁻ production.

One important limitation of this study is that the neuroblastoma mediated impact on the immune system was defined by suppression of T cell proliferation only. Future work should investigate the impact of neuroblastoma on tumour specific T cell cytotoxicity. Munder and colleagues recently demonstrated the maintenance of tumour antigen specific cytotoxicity of CD8⁺ cells in the absence of arginine *in vitro* (Munder *et al*, 2013). It is therefore important to determine here whether cytotoxicity is impaired or merely proliferation, although clearly the potential total killing will be reduced if the T cells are prevented from proliferating. This could be done by using T cells specific for neuroblastoma-specific antigens, such as GD2, NY-ESO or MAGEA1, and work on this is currently underway in our group. The preliminary data obtained in this study suggests that the T cells are entering an anergic state, neither undergoing apoptosis nor becoming Tregs, but it would be useful in terms of generating potential therapies to confirm this by determining whether the T cells could be reactivated following co-culture with the neuroblastoma cell lines. In addition, the physiological relevance of arginine depletion in the tumour microenvironment needs to be assessed *in vivo*. This would not be straightforward, however, since either depleting arginine or knocking out arginase activity would have an effect not only on potential T cell activity but also on the tumour itself. This also has implications for any prospective therapy of neuroblastoma or other ARG2 expressing tumours by targeting arginine metabolism. Arginase inhibitors, including the two used in this study, have not entered clinical trials due to concerns about disruption of the metabolically critical urea cycle. One possible route to a therapeutic would be development of an antibody or siRNA that can specifically target ARG2, which is not involved in the urea cycle.

Cancers are genomically and phenotypically heterogeneous, even within a single tumour, and neuroblastoma is no exception (Speleman *et al*, 2011). Accordingly, one may expect cell lines developed from neuroblastoma samples to exhibit varying phenotypes, depending on their source. Results from this study support this hypothesis, and highlight the potential variability of neuroblastoma biology from patient to patient. SK-N-AS is the only cell line tested that is negative for N-myc amplification, and exhibited very little suppression on T cell proliferation, and no detectable arginase expression by RT-PCR or activity. IMR-32 strongly suppressed T cell proliferation but this suppression does not appear to be dependent on arginase activity. It is possible that with different primers for ARG1 transcription of this enzyme may be detected in IMR-32, as arginase activity was observed in IMR-32 pellets and supernatant. Likewise, it is possible that addition of a stronger arginase inhibitor, such as nor-NOHA, would restore T cell proliferation in MLRs with this cell line. This work needs to be carried out to confirm whether IMR-32 suppression is truly independent of arginase activity, but from this data it seems that another mechanism may be at work in this cell line, perhaps galectin-1 or MIF upregulation, which could be investigated in further studies. The remaining cell lines (LA-N-1, Kelly and SK-N-MC) and the two patient tumour samples all exhibited arginase dependent suppression of T cell proliferation, suggesting this mechanism is employed in some but not all neuroblastoma tumours.

This study has demonstrated that neuroblastoma-derived cell lines and primary neuroblastoma tissue induce monocyte differentiation in co-culture to a CD68⁺ macrophage phenotype, which is typically associated with tumour associated macrophages (TAMs). This builds on previous research which highlighted the accumulation of CD68⁺ macrophages in neuroblastoma by immunohistochemical staining (Apps *et al*, 2013) and suggests that these TAMs may be activated once in the tumour microenvironment. We also determined that

these macrophages are capable of suppressing T cell proliferation, suggesting a second mechanism by which neuroblastoma may create an immunosuppressive tumour microenvironment, inhibiting the normal cytotoxic T cell response to antigen or stress ligand that may be presented by the neuroblastoma cells themselves. Previous studies have associated CD68⁺ activated macrophages with disease progression in hepatocellular carcinoma (Budhu *et al*, 2006), highlighting that the potential immunosuppressive activity of these cells has a clinical relevance, and therefore further investigation of this mechanism may be justified. Continuation of this work may involve assessment of CD68⁺ cell association with neuroblastoma xenografts in immunodeficient mice, but the analysis of human tumour sample and high level of CD68⁺ CD11b⁺ cells observed suggests this is reflective of *in vivo* conditions. More tumour samples need to be analysed before any conclusions can be drawn from this data however.

Morandi and colleagues also found that neuroblastoma cell lines are capable of activating monocytes and inducing differentiation into CD68⁺ macrophages (Morandi *et al*, 2007). They ruled out TGF- β , IL-10 or soluble GD2 as mediating factors in this activation, and our results confirm this, without identifying an alternative candidate. Cell line supernatants were negative for several cytokines attributed with macrophage activation and M2 polarisation, including IL-1 β , IL-4, IL-6, IL-10, IL-13, TNF- α and GM-CSF, suggesting none of these as being important in neuroblastoma mediated macrophage activation.

The glycosaminoglycan hyaluronan, a major component of the extracellular matrix, can be secreted by tumour cells and has been attributed with macrophage activation (Kuang *et al*, 2007). M-CSF is another possibility (Bottazzi, 1990) although this cytokine is mainly linked

with proliferation of macrophages rather than activation. It is possible that co-culture of the neuroblastoma cells with monocytes triggers production of an activating cytokine by the neuroblastoma cells and that since this experiment conducted on cell line supernatants alone, these cytokines would not be detected. Repeat of the ELISA on supernatant from a co-culture may help identify the cytokines involved.

Although they were immunosuppressive, monocytes co-cultured with neuroblastoma cell lines did not display markers of M2 macrophage polarisation (CD206 and CD163), and monocyte activation was arginase-independent, as arginase inhibitors had no effect on CD68 expression. This contrasts with a previous study by members of this group which determined that AML blasts are capable of activating monocytes and polarising them to an M2-like phenotype (Mussai *et al*, 2013). This polarisation was dependent on arginase activity. Further exploration of potential neuroblastoma mediated M2-like polarisation of monocytes is warranted however, since the data obtained during this study was preliminary and therefore inconclusive.

Overall this study has identified a novel immunosuppressive mechanism in neuroblastoma, which may have implications for treatment of this important childhood disease.

REFERENCES

- Airolidi I, Lualdi S, Bruno S, Raffaghello L, Occhino M, Gambini C, Pistoia V, Corrias MV. 2003. Expression of costimulatory molecules in human neuroblastoma. Evidence that CD40+ neuroblastoma cells undergo apoptosis following interaction with CD40L. *Br J Cancer*. 88(10):1527-36
- Antony PA, Piccirillo CA, Akpinarli A, Finkelstein SE, Speiss PJ, Surman DR, Palmer DC, Chan CC, Klebanoff CA, Overwijk WW, Rosenberg SA, Restifo NP. 2005. CD8+ T cell immunity against a tumor/self-antigen is augmented by CD4+ T helper cells and hindered by naturally occurring Tregulatory cells. *J Immunol*. 174 (5):2591-601
- Apps JR, Hasan F, Campus O, Behjati S, Jacques TS, J Sebire N, Anderson J. 2013. The immune environment of paediatric solid malignancies: evidence from an immunohistochemical study of clinical cases. *Fetal Pediatr Pathol*. 32 (4):298-307
- Asgharzadeh S, Salo JA, Ji L, Oberthuer A, Fischer M, Berthold F, Hadjidanil M, Liu CW, Metelitsa LS, Pique-Regi R, Wakamatsu P, Villablanca JG, Kreissman SG, Matthay KK, Shimada H, London WB, Spoto R, Seeger RC. Clinical significance of tumor-associated inflammatory cells in metastatic neuroblastoma. *J Clin Oncol*. 30 (28):3525-32
- Baay M, Brouwer A, Pauwels P, Peeters M, Lardon F. 2011. Tumor cells and tumor-associated macrophages: secreted proteins as potential targets for therapy. *Clin Dev Immunol*. 565187
- Bailey C, Negus R, Morris A, Ziprin P, Goldin R, Allavena P, Peck D, Darzi A. 2007. Chemokine expression is associated with the accumulation of tumour associated macrophages (TAMs) and progression in human colorectal cancer. *Clin Exp Metastasis*. 24 (2):121-30
- Biswas SK, Chittechath M, Shalova IN, Lim JY. 2012. Macrophage polarization and plasticity in health and disease. *Immunol Res*. 53 (1-3) 11-24
- Biswas SK, Mantovani A. 2010. Macrophage plasticity and interaction with lymphocyte subsets: cancer as a paradigm. *Nat Immunol*. 11 (10):889-96
- Biswas SK, Mantovani A. 2012. Orchestration of metabolism by macrophages. *Cell Metab*. 15 (4) 432-7
- Bottazzi B, Erba E, Nobili N, Fazioli F, Rambaldi A, Mantovani A. 1990. A paracrine circuit in the regulation of the proliferation of macrophages infiltrating murine sarcomas. *J Immunol*. 144 (6):2409-12
- Brandacher G, Perathoner A, Ladurner R, Schneeberger S, Obrist P, Winkler C, Werner ER, Werner-Felmayer G, Weiss HG, Göbel G, Margreiter R, Königsrainer A, Fuchs D, Amberger A.

2006. Prognostic value of indoleamine 2,3-dioxygenase expression in colorectal cancer: effect on tumor-infiltrating T cells. *Clin Cancer Res.* 12 (4):1144-51

Bronte V, Serafini P, Mazzoni A, Segal DM, Zanovello P. 2003. L-arginine metabolism in myeloid cells controls T-lymphocyte functions. *Trends Immunol.* 24 (6):302-6

Budhu A, Wang XW. 2006. The role of cytokines in hepatocellular carcinoma. *J Leukoc Biol.* 80(6):1197-213

Buga GM, Wei LH, Bauer PM, Fukuto JM, Ignarro LJ. 1998. NG-hydroxy-L-arginine and nitric oxide inhibit Caco-2 tumor cell proliferation by distinct mechanisms. *Am J Physiol.* 275 (4 Pt 2):R1256-64

Carr EL, Kelman A, Wu GS, Gopaul R, Senkevitch E, Aghvanyan A, Turay AM, Frauwirth KA. 2010. Glutamine uptake and metabolism are coordinately regulated by ERK/MAPK during T lymphocyte activation. *J Immunol.* 185 (2) 1037-44

Carvalho L. 1973. Spontaneous regression of an untreated neuroblastoma. *Br J Ophthalmol.* 57 (11):832-5

Cham CM, Driessens G, O'Keefe JP, Gajewski TF. 2008. Glucose deprivation inhibits multiple key gene expression events and effector functions in CD8+ T cells. *Eur J Immunol.* 38 (9) 2438-50

Chappert P, Schwartz RH. 2010. Induction of T cell anergy: integration of environmental cues and infectious tolerance. *Curr Opin Immunol.* 22 (5) 552-9

Chen W, Jin W, Hardegen N, Lei KJ, Li L, Marinos N, McGrady G, Wahl SM. 2003. Conversion of peripheral CD4+CD25- naive T cells to CD4+CD25+ regulatory T cells by TGF-beta induction of transcription factor Foxp3. *J Exp Med.* 98 (12) 1875-86

Choi BS, Martinez-Falero IC, Corset C, Munder M, Modolell M, Müller I, Kropf P. 2009. Differential impact of L-arginine deprivation on the activation and effector functions of T cells and macrophages. *J Leukoc Biol.* 85 (2):268-77

Cobbold SP, Adams E, Farquhar CA, Nolan KF, Howie D, Lui KO, Fairchild PJ, Mellor AL, Ron D, Waldmann H. 2009. Infectious tolerance via the consumption of essential amino acids and mTOR signaling. *Proc Natl Acad Sci U S A.* 106 (29) 12055-60

Coughlin CM, Fleming MD, Carroll RG, Pawel BR, Hogarty MD, Shan X, Vance BA, Cohen JN, Jairaj S, Lord EM, Wexler MH, Danet-Desnoyers GA, Pinkus JL, Pinkus GS, Maris JM, Grupp SA, Vonderheide RH. 2006. Immunosurveillance and survivin-specific T-cell immunity in children with high-risk neuroblastoma. *J Clin Oncol.* 24 (36):5725-34

Curiel TJ, Coukos G, Zou L, Alvarez X, Cheng P, Mottram P, Evdemon-Hogan M, Conejo-Garcia JR, Zhang L, Burow M, Zhu Y, Wei S, Kryczek I, Daniel B, Gordon A, Myers L, Lackner A, Disis ML, Knutson KL, Chen L, Zou W. 2004. Specific recruitment of regulatory T cells in ovarian carcinoma fosters immune privilege and predicts reduced survival. *Nat Med.* 10 (9):942-9

Doedens AL, Stockmann C, Rubinstein MP, Liao D, Zhang N, DeNardo DG, Coussens LM, Karin M, Goldrath AW, Johnson RS. 2010. Macrophage expression of hypoxia-inducible factor-1 alpha suppresses T-cell function and promotes tumor progression. *Cancer Res.* 70 (19):7465-75

Fallarino F, Grohmann U, You S, McGrath BC, Cavener DR, Vacca C, Orabona C, Bianchi R, Belladonna ML, Volpi C, Santamaria P, Fioretti MC, Puccetti P. 2006. The combined effects of tryptophan starvation and tryptophan catabolites down-regulate T cell receptor zeta-chain and induce a regulatory phenotype in naive T cells. *J Immunol.* 176 (11):6752-61

Fest S, Huebener N, Bleeke M, Durmus T, Stermann A, Woehler A, Baykan B, Zenclussen AC, Michalsky E, Jaeger IS, Preissner R, Hohn O, Weixler S, Gaedicke G, Lode HN. 2009. Survivin minigene DNA vaccination is effective against neuroblastoma. *Int J Cancer.* 125 (1):104-14

Feun L, You M, Wu CJ, Kuo MT, Wangpaichitr M, Spector S, Savaraj N. 2008. Arginine deprivation as a targeted therapy for cancer. *Curr Pharm Des.* (11):1049-57

Fischer K, Hoffmann P, Voelkl S, Meidenbauer N, Ammer J, Edinger M, Gottfried E, Schwarz S, Rothe G, Hoves S, Renner K, Timischl B, Mackensen A, Kunz-Schughart L, Andreesen R, Krause SW, Kreutz M. 2007. Inhibitory effect of tumor cell-derived lactic acid on human T cells. *Blood.* 109 (9):3812-9

Fontenot JD, Gavin MA, Rudensky AY. 2003. Foxp3 programs the development and function of CD4+CD25+ regulatory T cells. *Nat Immunol.* 4 (4) 330-6

Fox CJ, Hammerman PS, Thompson CB. 2005. Fuel feeds function: energy metabolism and the T-cell response. *Nat Rev Immunol.* 5 (11) 844-52

Gabrilovich DI, Nagaraj S. 2009. Myeloid-derived suppressor cells as regulators of the immune system. *Nat Rev Immunol.* 9 (3):162-74

Gabrilovich DI, Ostrand-Rosenberg S, Bronte V. 2012. Coordinated regulation of myeloid cells by tumours. *Nat Rev Immunol.* 12 (4):253-68

Galon J, Costes A, Sanchez-Cabo F, Kirilovsky A, Mlecnik B, Lagorce-Pagès C, Tosolini M, Camus M, Berger A, Wind P, Zinzindohoué F, Bruneval P, Cugnenc PH, Trajanoski Z, Fridman WH, Pagès F. 2006. Type, density, and location of immune cells within human colorectal tumors predict clinical outcome. *Science.* 313 (5795) 1960-4

Gannon PO, Godin-Ethier J, Hassler M, Delvoye N, Aversa M, Poisson AO, Péant B, Alam Fahmy M, Saad F, Lapointe R, Mes-Masson AM. 2010. Androgen-regulated expression of arginase 1, arginase 2 and interleukin-8 in human prostate cancer. *PLoS One.* 11;5(8)

Glaser R, Andridge R, Yang EV, Shana'ah AY, Di Gregorio M, Chen M, Johnson SL, De Renne LA, Lambert DR, Jewell SD, Bechtel MA, Hearne DW, Herron JB, Kiecolt-Glaser JK. 2011. Tumor site immune markers associated with risk for subsequent basal cell carcinomas. *PLoS One.* 6 (9)

Gong D, Shi W, Yi SJ, Chen H, Groffen J, Heisterkamp N. 2012. TGF β signaling plays a critical role in promoting alternative macrophage activation. *BMC Immunol.* 15 13:31

Gordon S. 2003. Alternative activation of macrophages. *Nat Rev Immunol.* 3 (1) 23-35

Görgün GT, Whitehill G, Anderson JL, Hideshima T, Maguire C, Laubach J, Raje N, Munshi NC, Richardson PG, Anderson KC. 2013. Tumor-promoting immune-suppressive myeloid-derived suppressor cells in the multiple myeloma microenvironment in humans. *Blood.* 121 (15):2975-87

Gowda M, Godder K, Kmiecik M, Worschech A, Ascierto ML, Wang E, Marincola FM, Manjili MH. 2011. Distinct signatures of the immune responses in low risk versus high risk neuroblastoma. *J Transl Med.* 9:170

Hanahan D, Weinberg RA. 2000. The hallmarks of cancer. *Cell.* 100 (1) 57-70

Hellström I, Hellström KE, Pierce GE, Yang JP. 1968. Cellular and humoral immunity to different types of human neoplasms. *Nature.* 220 (5174):1352-4

Huang B, Pan PY, Li Q, Sato AI, Levy DE, Bromberg J, Divino CM, Chen SH. 2006. Gr1+CD115+ immature myeloid suppressor cells mediate the development of tumor-induced T regulatory cells and T-cell anergy in tumor-bearing host. *Cancer Res.* 66 (2):1123-31

Jenkinson CP, Grody WW, Cederbaum SD. 1996. Comparative properties of arginases. *Comp Biochem Physiol B Biochem Mol Biol.* 114 (1):107-32

Kappler JW, Roehm N, Marrack P. 1987. T cell tolerance by clonal elimination in the thymus. *Cell.* 49 (2) 273-80.

Kelly PM, Davison RS, Bliss E, McGee JO. 1988. Macrophages in human breast disease: a quantitative immunohistochemical study. *Br J Cancer.* 57 (2):174-7

Kessenbrock K, Plaks V, Werb Z. 2010. Matrix metalloproteinases: regulators of the tumor microenvironment. *Cell.* 141 (1):52-67

Kuang DM, Wu Y, Chen N, Cheng J, Zhuang SM, Zheng L. 2007. Tumor-derived hyaluronan induces formation of immunosuppressive macrophages through transient early activation of monocytes. *Blood.* 110 (2):587-95

Kuang DM, Zhao Q, Peng C, Xu J, Zhang JP, Wu C, Zheng L. 2009. Activated monocytes in peritumoral stroma of hepatocellular carcinoma foster immune privilege and disease progression through PD-L1. *J Exp Med.* 206 (6):1327-37

Kurahara H, Shinchi H, Mataka Y, Maemura K, Noma H, Kubo F, Sakoda M, Ueno S, Natsugoe S, Takao S. 2011. Significance of M2-polarized tumor-associated macrophage in pancreatic cancer. *J Surg Res.* 167 (2):e211-9

Laurence A, Tato CM, Davidson TS, Kanno Y, Chen Z, Yao Z, Blank RB, Meylan F, Siegel R, Hennighausen L, Shevach EM, O'Shea JJ. 2007. Interleukin-2 signaling via STAT5 constrains T helper 17 cell generation. *Immunity.* 26 (3) 371-81

Lechner MG, Liebertz DJ, Epstein AL. 2010. Characterization of cytokine-induced myeloid-derived suppressor cells from normal human peripheral blood mononuclear cells. *J Immunol.* 185 (4):2273-84

Levrero M. 2006. Viral hepatitis and liver cancer: the case of hepatitis C. *Oncogene.* 25 (27):3834-47

Lin WW, Karin M. 2007. A cytokine-mediated link between innate immunity, inflammation, and cancer. *J Clin Invest.* 117 (5):1175-83

Liu D, Song L, Wei J, Courtney AN, Gao X, Marinova E, Guo L, Heczey A, Asgharzadeh S, Kim E, Dotti G, Metelitsa LS. 2012. IL-15 protects NKT cells from inhibition by tumor-associated macrophages and enhances antimetastatic activity. *J Clin Invest.* 122 (6):2221-33

Liu GY, Fairchild PJ, Smith RM, Prowle JR, Kioussis D, Wraith DC. 1995. Low avidity recognition of self-antigen by T cells permits escape from central tolerance. *Immunity.* 1995 3 (4) 407-15.

Liyanage UK, Moore TT, Joo HG, Tanaka Y, Herrmann V, Doherty G, Drebin JA, Strasberg SM, Eberlein TJ, Goedegebuure PS, Linehan DC. 2002. Prevalence of regulatory T cells is increased in peripheral blood and tumor microenvironment of patients with pancreas or breast adenocarcinoma. *J Immunol.* 169 (5):2756-61

Luigiano C, Ferrara F, Fagoonee S, Fabbri C, Cennamo V, Virgilio C, Bassi M, Favara C, Morace C, Consolo P, Pellicano R. 2012. Is *Helicobacter pylori* the infectious target to prevent gastric cancer? An interdisciplinary point of view. *Infect Disord Drug Targets.* 12 (5):340-5

Mahmoud SM, Paish EC, Powe DG, Macmillan RD, Grainge MJ, Lee AH, Ellis IO, Green AR. 2011. Tumor-infiltrating CD8+ lymphocytes predict clinical outcome in breast cancer. *J Clin Oncol.* 29 (15) 1949-55

Mellor AL, Munn D, Chandler P, Keskin D, Johnson T, Marshall B, Jhaver K, Baban B. 2003. Tryptophan catabolism and T cell responses. *Adv Exp Med Biol.* 527 27-35

Morandi F, Levreri I, Bocca P, Galleni B, Raffaghello L, Ferrone S, Prigione I, Pistoia V. 2007. Human neuroblastoma cells trigger an immunosuppressive program in monocytes by stimulating soluble HLA-G release. *Cancer Res.* 67 (13):6433-41

Mosser DM, Edwards JP. 2008. Exploring the full spectrum of macrophage activation. *Nat Rev Immunol.* 8 (12) 958-69

Munder M, Engelhardt M, Knies D, Medenhoff S, Wabnitz G, Luckner-Minden C, Feldmeyer N, Voss RH, Kropf P, Müller I, Conradi R, Samstag Y, Theobald M, Ho AD, Goldschmidt H, Hundemer M. 2013. Cytotoxicity of tumor antigen specific human T cells is unimpaired by arginine depletion. *PLoS One.* 23;8(5)

Murali AK, Mehrotra S. 2011. Apoptosis - an Ubiquitous T cell Immunomodulator. *J Clin Cell Immunol.* 10;S3:2

Mussai F, De Santo C, Abu-Dayyeh I, Booth S, Quek L, McEwen-Smith RM, Qureshi A, Dazzi F, Vyas P, Cerundolo V. 2013. Acute myeloid leukaemia creates an arginase-dependent immunosuppressive microenvironment. *Blood*. [Epub ahead of print]

Nagaraj S, Gupta K, Pisarev V, Kinarsky L, Sherman S, Kang L, Herber DL, Schneck J, Gabrilovich DI. 2007. Altered recognition of antigen is a mechanism of CD8⁺ T cell tolerance in cancer. *Nat Med*. 13 (7):828-35

North RJ, Bursucker I. 1984. Generation and decay of the immune response to a progressive fibrosarcoma. I. Ly-1+2⁻ suppressor T cells down-regulate the generation of Ly-1-2⁺ effector T cells. *J Exp Med*. 159 (5):1295-311

Oble DA, Loewe R, Yu P, Mihm MC Jr. 2009. Focus on TILs: prognostic significance of tumor infiltrating lymphocytes in human melanoma. *Cancer Immun*. 2;9:3

Onizuka S, Tawara I, Shimizu J, Sakaguchi S, Fujita T, Nakayama E. 1999. Tumor rejection by in vivo administration of anti-CD25 (interleukin-2 receptor alpha) monoclonal antibody. *Cancer Res*. 59 (13):3128-33

Pegg AE, McCann PP. 1982. Polyamine metabolism and function. *Am J Physiol*. 243 (5):C212-21

Perrone G, Ruffini PA, Catalano V, Spino C, Santini D, Muretto P, Spoto C, Zingaretti C, Sisti V, Alessandrini P, Giordani P, Cicetti A, D'Emidio S, Morini S, Ruzzo A, Magnani M, Tonini G, Rabitti C, Graziano F. 2008. Intratumoural FOXP3-positive regulatory T cells are associated with adverse prognosis in radically resected gastric cancer. *Eur J Cancer*. 44 (13):1875-82

Powell JD, Delgoffe GM. 2010. The mammalian target of rapamycin: linking T cell differentiation, function, and metabolism. *Immunity*. 33 (3) 301-11

Pyonteck SM, Gadea BB, Wang HW, Gocheva V, Hunter KE, Tang LH, Joyce JA. 2012. Deficiency of the macrophage growth factor CSF-1 disrupts pancreatic neuroendocrine tumor development. *Oncogene*. 31 (11):1459-67

Raber P, Ochoa AC, Rodríguez PC. 2012. Metabolism of L-arginine by myeloid-derived suppressor cells in cancer: mechanisms of T cell suppression and therapeutic perspectives. *Immunol Invest*. 41 (6-7):614-34

Rabinovich GA, Gabrilovich D, Sotomayor EM. 2007. Immunosuppressive strategies that are mediated by tumor cells. *Annu Rev Immunol*. 25 267-96

Raffaghello L, Prigione I, Airolidi I, Camoriano M, Levreri I, Gambini C, Pende D, Steinle A, Ferrone S, Pistoia V. 2004. Downregulation and/or release of NKG2D ligands as immune evasion strategy of human neuroblastoma. *Neoplasia*. 6 (5):558-68

Read S, Malmström V, Powrie F. 2000. Cytotoxic T lymphocyte-associated antigen 4 plays an essential role in the function of CD25(+)CD4(+) regulatory cells that control intestinal inflammation. *J Exp Med*. 192 (2) 295-302

Ruffell B, Affara NI, Coussens LM. 2012. Differential macrophage programming in the tumor microenvironment. *Trends Immunol.* 33 (3):119-26

Sakaguchi S, Yamaguchi T, Nomura T, Ono M. 2008. Regulatory T cells and immune tolerance. *Cell.* 133 (5) 775-87

Santilli G, Piotrowska I, Cantilena S, Chayka O, D'Alicarnasso M, Morgenstern DA, Himoudi N, Pearson K, Anderson J, Thrasher AJ, Sala A. 2013. Polyphenol E enhances the antitumor immune response in neuroblastoma by inactivating myeloid suppressor cells. *Clin Cancer Res.* 19 (5):1116-25

Schreiber RD, Old LJ, Smyth MJ. 2011. Cancer immunoediting: integrating immunity's roles in cancer suppression and promotion. *Science.* 331 (6024) 1565-70

Schwartz RH. 2003. T cell anergy. *Annu Rev Immunol.* 2003 21:305-34

Shimizu J, Yamazaki S, Takahashi T, Ishida Y, Sakaguchi S. 2002. Stimulation of CD25(+)CD4(+) regulatory T cells through GITR breaks immunological self-tolerance. *Nat Immunol.* 3 (2) 135-42

Singer K, Gottfried E, Kreutz M, Mackensen A. 2011. Suppression of T-cell responses by tumor metabolites. *Cancer Immunol Immunother.* 60 (3):425-31

Singh R, Pervin S, Karimi A, Cederbaum S, Chaudhuri G. 2000. Arginase activity in human breast cancer cell lines: N(omega)-hydroxy-L-arginine selectively inhibits cell proliferation and induces apoptosis in MDA-MB-468 cells. *Cancer Res.* 60 (12):3305-12

Soldati R, Berger E, Zenclussen AC, Jorch G, Lode HN, Salatino M, Rabinovich GA, Fest S. 2012. Neuroblastoma triggers an immunoevasive program involving galectin-1-dependent modulation of T cell and dendritic cell compartments. *Int J Cancer.* 131 (5):1131-41

Speleman F, De Preter K, Vandesompele J. 2011. Neuroblastoma genetics and phenotype: a tale of heterogeneity. *Semin Cancer Biol.* 21 (4):238-44

Steidl C, Lee T, Shah SP, Farinha P, Han G, Nayar T, Delaney A, Jones SJ, Iqbal J, Weisenburger DD, Bast MA, Rosenwald A, Muller-Hermelink HK, Rimsza LM, Campo E, Delabie J, Brazier RM, Cook JR, Tubbs RR, Jaffe ES, Lenz G, Connors JM, Staudt LM, Chan WC, Gascoyne RD. 2010. Tumor-associated macrophages and survival in classic Hodgkin's lymphoma. *N Engl J Med.* 362 (10):875-85

Stockmann C, Doedens A, Weidemann A, Zhang N, Takeda N, Greenberg JI, Cheresch DA, Johnson RS. 2008. Deletion of vascular endothelial growth factor in myeloid cells accelerates tumorigenesis. *Nature.* 456 (7223):814-8

Takada K, Jameson SC. 2009. Naive T cell homeostasis: from awareness of space to a sense of place. *Nat Rev Immunol.* 9 (12) 823-32

Takahashi T, Kuniyasu Y, Toda M, Sakaguchi N, Itoh M, Iwata M, Shimizu J, Sakaguchi S. 1998. Immunologic self-tolerance maintained by CD25+CD4+ naturally anergic and suppressive T

cells: induction of autoimmune disease by breaking their anergic/suppressive state. *Int Immunol.* 10 (12) 1969-80

Tan KL, Scott DW, Hong F, Kahl BS, Fisher RI, Bartlett NL, Advani RH, Buckstein R, Rimsza LM, Connors JM, Steidl C, Gordon LI, Horning SJ, Gascoyne RD. 2012. Tumor-associated macrophages predict inferior outcomes in classic Hodgkin lymphoma: a correlative study from the E2496 Intergroup trial. *Blood.* 120 (16):3280-7

Tang X. 2013. Tumor-associated macrophages as potential diagnostic and prognostic biomarkers in breast cancer. *Cancer Lett.* 332 (1):3-10

Tate DJ Jr, Vonderhaar DJ, Caldas YA, Metoyer T, Patterson JR 4th, Aviles DH, Zea AH. 2008. Effect of arginase II on L-arginine depletion and cell growth in murine cell lines of renal cell carcinoma. *J Hematol Oncol.* 25;1:14

Thiele CJ. 1998. Neuroblastoma: In (Ed.) Masters, J. Human Cell Culture. Lancaster, UK: Kluwer Academic Publishers, Vol 1, p 21-53

Vakkila J, Jaffe R, Michelow M, Lotze MT. 2006. Pediatric cancers are infiltrated predominantly by macrophages and contain a paucity of dendritic cells: a major nosologic difference with adult tumors. *Clin Cancer Res.* 12 (7 Pt 1):2049-54

von Boehmer H. 2005. Mechanisms of suppression by suppressor T cells. *Nat Immunol.* 6 (4) 338-44

Wang W, Lau R, Yu D, Zhu W, Korman A, Weber J. 2009. PD1 blockade reverses the suppression of melanoma antigen-specific CTL by CD4+ CD25(Hi) regulatory T cells. *Int Immunol.* 21 (9) 1065-77

Warburg O. 1961. [On the facultative anaerobiosis of cancer cells and its use in chemotherapy]. *Munch Med Wochenschr.* 103:2504-6

Whiteside TL. 2012. What are regulatory T cells (Treg) regulating in cancer and why? *Semin Cancer Biol.* 22 (4):327-34

Wing K, Sakaguchi S. 2010. Regulatory T cells exert checks and balances on self tolerance and autoimmunity. *Nat Immunol.* 11 (1) 7-13

Wu ZL, Schwartz E, Seeger R, Ladisch S. 1986. Expression of GD2 ganglioside by untreated primary human neuroblastomas. *Cancer Res.* 46 (1):440-3

Wyckoff J, Wang W, Lin EY, Wang Y, Pixley F, Stanley ER, Graf T, Pollard JW, Segall J, Condeelis J. 2004. A paracrine loop between tumor cells and macrophages is required for tumor cell migration in mammary tumors. *Cancer Res.* 64 (19):7022-9

Yan X, Orentas RJ, Johnson BD. 2006. Tumor-derived macrophage migration inhibitory factor (MIF) inhibits T lymphocyte activation. *Cytokine.* 33 (4):188-98